

***United Nations Institute for Training and Research***

***Explorations in Geographic Information Systems Technology***

***Volume 6***

***Applications in Hazard Assessment  
and Management***

Edited by  
**Srinivas Emani**

Clark Labs

Clark University, Worcester, MA 01610 USA

© 1996, 2001, 2005, 2007, 2009 UNITAR

Palais des Nations

CH-1211 Geneva 10, Switzerland

# ***Introduction***

Recent years have exposed the vulnerability of developed and developing countries alike to natural hazards. In Japan, an earthquake in the city of Kobe in January, 1995, claimed 5,000 lives and more than \$100 billion in damages. In the United States, floods in the midwestern states in 1993 and in the state of California in 1995 resulted in losses of billions of dollars. In India, more than 9,000 people were killed and 10,000 injured in 1993 from an earthquake in the state of Maharashtra. Examples of many memorable as well as less known disasters since the beginning of the decade could easily fill this page. The natural hazards that have been the sources of these disasters have ranged from floods, earthquakes, and coastal storms to drought, mudslides, volcanoes, and forest fires. Equally wide ranging have been the associated social, economic, and biophysical impacts, with ripple effects extending to national and at times even international levels.

Alongside this threat posed by natural hazards are the adverse effects of technological applications. Bhopal, Chernobyl, and Exxon Valdez continue to evoke memories of lives lost and ecosystems devastated as a result of technological disasters. Routine releases of pollutants into air and water continue to undermine human and ecological health in developing countries. Millions around the world are exposed to pesticides and hazardous chemicals, many of them unknowingly.

This growing vulnerability to hazards and the increasing magnitude of socioeconomic impacts associated with disasters have resulted in numerous national and international efforts to assess and manage hazards regardless of their origin. For example, the United States Federal Emergency Management Agency (FEMA) is in the process of introducing a national mitigation strategy to reduce the impacts of natural hazards. At the international level, the United Nations has declared the 1990s as the International Decade for Natural Disaster Reduction.

An important component of these efforts, whether at an international, national, or local level, is the role of information technology. Geographic Information Systems (GIS), in particular, have much to offer for both research and practice in hazard assessment and management. This role stems from the capabilities of GIS to integrate data of different types and from different sources, analyze the data, and present the results in a timely and appropriate manner for both researchers and practitioners. GIS also provide artificial environments within which to simulate processes of the natural environment, thus allowing their use for predicting hazards and their impacts.

This workbook, the sixth in a series on explorations of GIS technology, focuses on the role of GIS in hazard assessment and management. It is divided into two parts. The first part consists of a review paper which summarizes GIS applications in this subject area and discusses the potential role of GIS in hazard management. The second part consists of a set of tutorial exercises on the use of GIS in hazard assessment and management. The tutorial exercises include both natural and technological hazards. They cover a range of themes in hazards including exposure assessment, vulnerability, all-hazards assessment, and disaster mitigation. The GIS techniques used in the exercises range from simple database queries to the use of complex models. The exercises have been written such that the novice to GIS as well as the expert can work with them. All the exercises have been developed for use with IDRISI, although conversion of the exercises and data sets to other GIS systems may be possible.

The workbook would not have been possible without the help and support from many colleagues. Much of the credit for the quality of the exercises in the workbook goes to Michele Fulk, whose comments and suggestions have been invaluable. Yelena Ogneva-Himmelberger and Weigen Jin, along with Daniel Levine at the Oak Ridge National Laboratory, spent many hours developing the nonpoint pollution exercise. Assaf Anyamba and Mahadevan Ramachandran developed the exercise on time series analysis as an early warning tool for drought disaster mitigation. Michele Fulk developed the exercise on using remote sensing to assess the great midwest floods of 1993 in the United States. The exercises were tested by Stephanie Hulina, Peter Kyem, Kevin St. Martin, Siobhan Murray, and James Toledano. Many improvements to the review paper were made as a result of comments by Ron Eastman, Steve Gold, Jeanne Kasperson, Roger Kasperson, Daniel Levine, and Sam Ratick.

The workbook was also peer-reviewed by the following individuals:

Tammy Beaty, Oak Ridge National Laboratory, Oak Ridge, Tennessee

Jeanne X. Kasperson, The George Perkins Marsh Institute, Clark University, Worcester, Massachusetts

Samuel J. Ratick, Graduate School of Geography, Clark University, Worcester, Massachusetts

Daniel Levine, Oak Ridge National Laboratory, Oak Ridge, Tennessee

The series on explorations of GIS technology on which this workbook is based has been supported by the United Nations Institute for Training and Research (UNITAR), Geneva. Nassrine Azimi and Steve Gold at UNITAR in particular have provided much enthusiastic support for the series.

In closing, thanks to my wife, Marcia, for her support and encouragement in the completion of this workbook.

Srinivas Emani, January 1996

## ***Exercises***

In the exercises that follow, we will explore the application of GIS technology in hazard assessment and management. A mix of natural and technological hazards have been selected for this purpose. The natural hazards include extreme storms, floods, earthquakes, and drought. The technological hazards include hazardous materials transportation, and nonpoint source pollution. One complex hazard, accelerated sea-level rise, is also included. The themes in hazard assessment and management covered by the exercises include among others, all-hazards assessment, vulnerability, exposure assessment, and early warning for disaster mitigation. The hazards and themes selected were to some extent dependent on the availability of data sets. For example, a search was conducted for data sets on GIS applications in hazardous waste site characterization. Although a number of such data sets were identified, most of these data sets were considered confidential by the researchers and practitioners who compiled the data. Thus no data were available for an exercise on this subject.

The exercises have been organized to reflect both simple and complex GIS techniques. The exercises in the beginning of the workbook (Exercises 1 through 3) provide an introduction to some of the fundamental techniques for displaying and analyzing maps. Exercises in the later part (Exercises 4 and 5) rely on advanced techniques for analysis and modeling. The last two exercises of the workbook (Exercises 6 and 7) focus on the use of remote sensing data with GIS for hazard assessment. Exercise 6 provides an introduction to this subject, whereas Exercise 7 covers a more complex study on the use of remote sensing techniques as an early warning tool for drought hazard mitigation. Most of the techniques used in these exercises are similar to those in the applications summarized in the review paper and include, among others, reclassification, overlay, proximity analysis, and empirical and process modeling.

# **Revision Notes**

## **January 1998**

We are pleased to present the Windows version of Volume 6 of the UNITAR Workbook Series, Applications in Hazard Assessment and Management. The workbook is written for use with Version 2.0 of IDRISI for Windows. We chose to convert the workbook to this latest version of IDRISI for Windows as we believe that most users have either upgraded to Version 2.0, or will be doing so in the near future. We thank Rhonda Davis for testing the tutorial exercises in the workbook.

Srinivas Emani and Michele Fulk, Editors

January 1998

## **August 2001**

This workbook was revised to be compatible with Idrisi32 Release 2 GIS software and for distribution in electronic format. The content of the volume is the same as that of the previous version, except that specific instructions for the exercises are compatible with Idrisi32 Release 2 rather than older versions. In addition, minor editorial revisions have been made. The editor would like to thank Kiran Batchu, Laurie Canavan, Michele Fulk, Kelly O'Connor, Nick Pieri, and Takashi Tada for their valuable assistance.

Amy Nelson, Revision Editor

August, 2001

## **April 2005**

This volume was revised in April 2005 to be compatible for use with the IDRISI Kilimanjaro GIS and Image Processing software and for distribution in electronic format. The content of the volume is exactly the same as that of the previous version, except that specific instructions for the exercises are given for IDRISI Kilimanjaro rather than older versions. In addition, minor editorial revisions have been made.

## **February 2007**

This volume was revised in February 2007 to be compatible for use with the IDRISI Andes GIS and Image Processing software and for distribution in electronic format. The content of the volume is exactly the same as that of the previous version, except that specific instructions for the exercises are given for IDRISI Andes rather than older versions. In addition, minor editorial revisions have been made.

## **April 2009**

This volume was revised in April 2009 to be compatible for use with the IDRISI Taiga GIS and Image Processing software and for distribution in electronic format. The content of the volume is exactly the same as that of the previous version, except that specific instructions for the exercises are given for IDRISI Taiga rather than older versions. In addition, minor editorial revisions have been made.

# ***GIS Applications in Hazard Assessment and Management: A Review***

**by Srinivas Emani**

## ***Introduction***

Recent years have exposed the vulnerability of developed and developing countries alike to natural hazards. In Japan, an earthquake in the city of Kobe in January, 1995, claimed 5,000 lives and more than \$100 billion in damages. In the United States, floods in the midwestern states in 1993 and in the state of California in 1995 resulted in losses of billions of dollars. In India, more than 9,000 people were killed and 10,000 injured in 1993 from an earthquake in the state of Maharashtra. Examples of many memorable as well as less known disasters since the beginning of the decade could easily fill this page. The natural hazards that have been the sources of these disasters have ranged from floods, earthquakes, and coastal storms to drought, mudslides, volcanoes, and forest fires. Equally wide ranging have been the associated social, economic, and biophysical impacts, with ripple effects extending to national and at times even international levels.

Alongside this threat posed by natural hazards are the adverse effects of technological applications. Bhopal, Chernobyl, and Exxon Valdez continue to evoke memories of lives lost and ecosystems devastated as a result of technological disasters. Routine releases of pollutants into air and water continue to undermine human and ecological health in developing countries. Millions around the world are exposed to pesticides and hazardous chemicals, many of them unknowingly.

This growing vulnerability to hazards and the increasing magnitude of socioeconomic impacts associated with disasters have resulted in numerous national and international efforts to assess and manage hazards regardless of their origin. For example, in the United States the Federal Emergency Management Agency (FEMA) is in the process of introducing a national mitigation strategy to reduce the impacts of natural hazards. At the international level, the United Nations has declared the 1990s as the International Decade for Natural Disaster Reduction.

An important component of these efforts, whether at an international, national, or local level, is the role of information technology (Alexander 1991; Gatrell and Vincent 1992). Geographic Information Systems (GIS), in particular, have much to offer for both research and practice in hazard assessment and management. This role stems from the capabilities of GIS to integrate data of different types and from different sources, analyze the data, and present the results in a timely and appropriate manner for both researchers and practitioners. GIS also provide artificial environments within which to simulate processes of the natural environment, thus allowing their use for predicting hazards and their impacts.

The objective of this paper is to review and discuss the role of GIS in hazard assessment and management. The paper is organized along the following lines. To set the stage, the first section provides an overview of concepts and frameworks in the field of hazard management. The second and third sections review the applications of GIS technology in hazard assessment and management. In the second section, a review of applications is conducted by hazard and covers hazards such as earthquakes, extreme storms, hazardous waste facilities, and surface-water contamination. The third section focuses on two institutional uses of GIS for hazards research, the first by the United States Environmental Protection Agency (USEPA) and the second by the International Institute for Applied Systems Analysis (IIASA). The fourth and final section of the paper uses the findings of the review sections to discuss the nature of the applications and identify themes for further research.

## ***Concepts and Frameworks***

The field of hazard assessment and management is associated with an extensive literature spawning a wide range of disciplines including geography, sociology, toxicology, psychology, economics, and engineering. To do justice to this vast literature is a daunting task for a book, let alone a section of a review paper. Nonetheless, an overview of the key concepts and terms in the field guides the discussion of the GIS applications reviewed in this paper. The overview first defines and differentiates the concepts of hazard, risk, and disaster and then presents frameworks associated with each concept.

## Concepts

A *hazard* is a "threat to humans and what they value" (Kates, Hohenemser, and Kaspersen 1985:21). The threat may originate from natural sources (for example, earthquakes and hurricanes), technological sources (a chemical facility or a hazardous waste site), or a combination of the two (when an earthquake triggers an accident in a nuclear power plant).<sup>1</sup> A *disaster*, on the other hand, is "an event, natural or man-made, sudden or progressive, which impacts with such severity that the affected community has to respond by exceptional measures" (ADB 1991: 3). A disaster is thus the realization of a hazard with such damages to people and property in the affected community that the normal functioning of the community is disrupted. Well-known disasters include the African drought of the mid 1980s, the Bhopal accident, the Chernobyl accident, the earthquake in Kobe (Japan), and Hurricane Andrew in Florida (United States). *Risk* is the "possibility of suffering harm from a hazard" (Cohrrsen and Covello 1989:1). This simple definition relates risk to hazard and identifies two important components of risk: probability (possibility), and consequences (harm).<sup>2</sup> The literature on risk also distinguishes between two constructs of risk: technical, and social.

The *technical* construct of risk involves quantification of the probability that a hazard will be realized and the magnitude of consequences associated with the hazard. For example, the risk of 100 people dying in a year from exposure to a toxic chemical released from a chemical facility might be one in a million (expressed as  $1 \times 10^{-6}$ ). The technical definition of risk is the basis of some classic engineering-oriented risk assessment studies such as the Canvey Island study in the United Kingdom (HSE 1978), the Rijnmond study in the Netherlands (CECA 1982), and the reactor safety study in the United States (Nuclear Regulatory Commission 1975).<sup>3</sup> It has also been adopted in epidemiological and toxicological studies. For example, the toxicological approach has sought to extrapolate the adverse health effects of chemicals from laboratory experiments on animals such as rats and mice to humans (Cohrrsen and Covello 1989). The findings from these experiments are presented in terms of the magnitude of the dose received or administered and the probability of an adverse health effect (such as increased risk of cancer).

Risk as a *social* construct is conceptualized according to the social science paradigm that is adopted in the research. For example, psychologists focus on the individual and use psychometric scaling techniques to gather data from lay people on judgments about risk, and qualitative characteristics of the risk, such as whether the risk is voluntary or involuntary, its catastrophic potential, and the impact of the risk on future generations (Fischhoff et al. 1978; Slovic 1987). Studies adopting this paradigm have shown that lay people conceptualize risk in a qualitative, multidimensional manner as opposed to the narrow, quantitative definition adopted by scientists. Anthropologists, on the other hand, have defined risk perceptions as products of worldviews and cultural biases arising from membership in different cultural groups (Rayner 1986; Rayner and Cantor 1987; Thompson 1980).<sup>4</sup>

## Frameworks

To facilitate assessment and management efforts, frameworks have been proposed for the concepts of risk, hazard, and disaster. In the case of *risk*, for example, a popular but controversial framework for the assessment and management of human health risks was proposed by the U.S. National Research Council (NRC) (NRC 1983). In this framework, *risk assessment* is "the characterization of the potential adverse health effects of human exposures to environmental hazards"

---

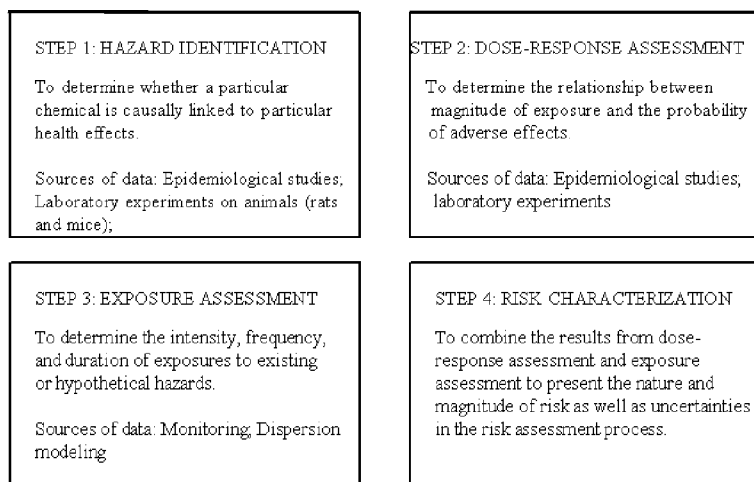
1. Hazards may also originate from social causes, as for example in the case of ethnic violence. These types of social hazards are not considered in this paper.

2. Risk can also be related to the concept of disaster. For example, risk is "the probability that a disaster will occur" (ADB 1991: 4).

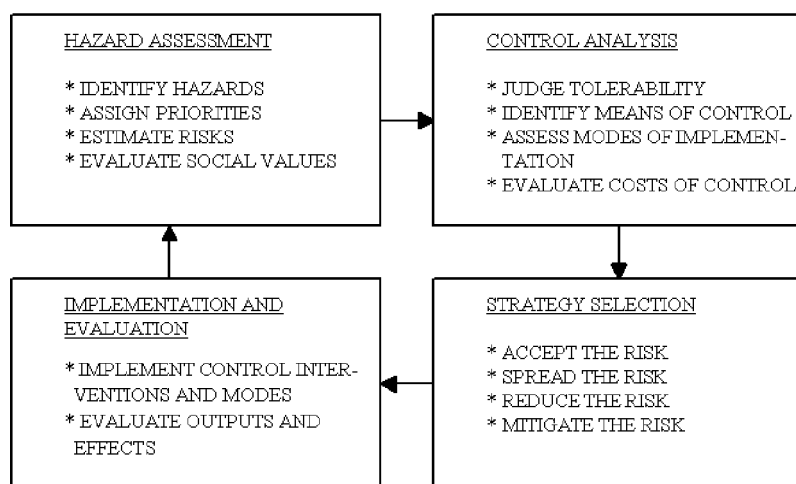
3. Applications of the technical definition of risk to natural hazards can be found in Emmi and Horton (1995) and Petak and Atkisson (1982).

4. These technical and social constructs of risk can also be found in the literature on natural hazards and disasters.

(NRC 1983: 18). *Risk management* is defined as "the process of weighing policy alternatives and selecting the most appropriate regulatory action, integrating the results of risk assessment with engineering data and with social, economic, and political concerns to reach a decision" (NRC 1983: 3). The process of risk assessment is further subdivided into four steps illustrated in Figure 1. NRC (1983: 7) argued for a "clear and conceptual distinction between assessment of risks and consideration of risk management alternatives". This separation has been accepted in principle by agencies such as the EPA (Russell and Gruber 1987). Others, however, have criticized NRC's conceptual distinction between risk assessment and risk management (Hattis and Smith 1987; Freudenburg 1988). For example, Hattis and Smith (1987:93) have argued that "the use of specific types of data, intellectual constructs, estimation or analysis techniques, and terminology necessarily conveys an endorsement of all of these items as appropriate for the problem at hand. Such judgments, however, are both policy-relevant and, coming from a specific expert group, potentially suspect."



In the case of *hazards*, a framework for hazard management was proposed by Kasperson, Kates, and Hohenemser (1985). This framework recognizes four stages in the assessment and management of hazards. Figure 2 illustrates these four stage and the steps involved in each stage.



In the case of *disasters*, several frameworks for management have been proposed using the different temporal stages in a disaster cycle. For example, Quarantelli (1992: 115-116) distinguished among the following four stages in the planning and management process:

1. Mitigation or prevention. This has to do with long range preimpact activities of structural and/or non-structural nature that tend to be one of three kinds: (a) those that attempt to actually eliminate or reduce the probability of occurrence of a disaster; (b) those that are designed to reduce the effects of a disaster; and (c) those that help to redistribute the costs of disaster planning and disasters.
2. Preparedness. This has to do with preimpact activities concerned with preparing for disasters. Preparedness measures are closer to the onset of impact than mitigation ones and tend to be aimed at improving the emergency time response if a disaster were to occur.
3. Response. This has to do with those actions that most closely follow disaster impact.
4. Recovery. This has to do with those disaster-relevant activities that are undertaken after the emergency period is over in an attempt to return to relatively normal functioning.

This paper, in its discussion of the role of GIS in hazard assessment and management, adopts the framework proposed by Kaspersen, Kates, and Hohenemser (1985) (Figure 2). Unlike the NRC framework on risk, this framework does not conceptually distinguish between risk assessment and risk management. The framework is also broad enough to include concepts of disaster planning and management.

## **Review of Applications**

To review the nature of GIS applications in hazard assessment and management, a literature search was conducted in both the GIS and hazards fields. In the GIS field, the search covered proceedings of major conferences, and journals specializing in GIS. The conference proceedings selected for the search were: (1) the annual GIS/LIS conferences held in the United States; (2) the annual European Geographic Information System (EGIS) conferences; and (3) the annual AUTO CARTO conferences held in the United States. The journals consisted of: *Geo Info Systems*, *GIS World*, *The International Journal of Geographical Information Systems*, and *Photogrammetric Engineering and Remote Sensing*. In the hazards field, the search was conducted in the following journals: *International Journal of Risk Analysis*, *International Journal of Mass Emergencies and Disasters*, *Risk Abstracts*, and *Disasters*. The literature from these searches was supplemented by cross-references, chapters in edited volumes in both the GIS and hazards fields, and manuscripts and reports obtained through the research networking process. As illustrated by the bibliography at the end of this paper, a considerable amount of citations were retrieved through these searches.

One additional step was performed to cross-check the findings of this literature search. An on-line bibliographic database, GEOBASE, was searched using relevant key words. GEOBASE consists of more than 500,000 records on worldwide literature in geography and geology. Publications on GIS applications in hazard assessment and management should therefore be indexed in this database. The search in GEOBASE was conducted by hazard as well as by theme, with GIS appearing as one of the key words in all the searches. The results of these searches confirmed most of the references retrieved in the first literature search since the conference proceedings, journals, and edited volumes specializing in GIS are indexed in GEOBASE. The search also provided additional references, many of which were added to the bibliography at the end of this paper.

The literature search shows that applications of GIS technology to hazard assessment and management cover a wide range of hazards as well as themes. Among the hazards addressed by GIS are drought, earthquakes, extreme storms, floods, landslides, noxious and hazardous facilities, surface and ground-water pollution, and hazardous material releases. The themes range from hazard identification and risk assessment to vulnerability analysis, emergency planning, and disaster response and recovery. The review presented in this paper is organized by hazard. For each hazard included in the review, examples are provided illustrating the use of the technology and the themes that have been covered in the applications. It is not claimed that all the themes in the assessment and management of a hazard addressed by GIS technology



are reported here. Rather, the attempt is to illustrate as many different themes as possible from the publications retrieved in the literature search. In addition to hazard-specific applications, applications by two institutions that have considerable experience in applying GIS to hazards research and practice are reviewed: (1) the U.S. Environmental Protection Agency (EPA), and (2) the International Institute for Applied Systems Analysis (IIASA).<sup>5</sup>

The initial review by hazard gives way to the review of institutional applications. The hazards are reviewed in the following (alphabetical) order: drought, earthquakes, extreme storms, flood and inundation hazards, hazardous and noxious waste facilities, hazardous materials, landslides, and surface- and ground-water contamination.

## Drought

In using GIS to assess drought, much of the research has relied upon remotely sensed data and the capabilities of GIS to store and analyze large volumes of such data. An important theme to emerge in this research has been the development of early warning systems for drought (Hellden and Eklundh 1988; Hutchinson 1991). An index of vegetation greenness derived from satellite data, the Normalized Difference Vegetation Index (NDVI)<sup>6</sup>, has been extensively studied for use in early warning systems (Hutchinson 1991).

Hellden and Eklundh (1988) studied the potential of NDVI for early warning and food security monitoring in Ethiopia. NDVI was calculated from the infrared and red bands of imagery captured by the Advanced Very High Resolution Radiometer (AVHRR) instrument aboard the U.S. National Oceanographic and Atmospheric Administration (NOAA) satellites. The data set was made up of: (1) 132 NDVI 15-day maximum value composite images for the period 1981-1986; (2) data for 224 rainfall stations consisting of monthly and annual precipitation records, latitude/longitude coordinates, and elevation data; and (3) agroclimatic (rainfall pattern and length of growing season) and administrative stratification maps of the country. The data on rainfall were used to create annual rainfall anomaly maps for 1982-1985 (the anomalies were expressed as standard deviations from the 1982-1985 mean). Hellden and Eklundh (1988: 18) state that "the spatial distribution of the anomalies, particularly during very dry years, is invaluable information for studies of the relationship between the climatic situation and famine." For example, strong negative anomalies (suggesting the lack of precipitation) were found for the Ethiopian drylands in 1984, a year of severe famine in Ethiopia. To combine the NDVI and precipitation data, Hellden and Eklundh created a five by five pixel window around each rainfall station. The mean NDVI value for each window was selected as the representative NDVI at that station. This data was then used to create annual NDVI anomaly maps for each year from 1982 to 1985 (a detailed discussion of this process is provided in Hellden and Eklundh (1988)). When the NDVI anomaly maps were compared with the rainfall anomaly maps, a strong relationship was found between the two sets of anomalies indicating the potential use of NDVI in an early warning and food security monitoring system.

Eastman and Fulk (1993) used NDVI data at a continental scale in Africa, for the period 1986-1988, to analyze the long-term trend in vegetation patterns and its relationship with the El Nino/Southern Oscillation (ENSO) (see also Anyamba, Eastman, and Fulk 1995). The NDVI was calculated from imagery captured by the AVHRR instrument aboard the NOAA satellites and defined as the maximum value composite among the three NDVI images available for each month. The statistical technique of principal components analysis was used to reduce the 36 NDVI images to a smaller set of 8 component images. Unlike the original images, these component images are uncorrelated with one another but at the same time retain all the information contained in the original images. For example, one component captured vegetation patterns over the three-year period during the summer/winter season whereas another captured the same during by the spring/fall season. More important, two components (Components 7 and 8) were found related to the ENSO events occurring during this three-year period. ENSO warm- phase events result in significantly decreased precipitation in southern Africa and therefore are associated with drought in that part of the region. This was the case in late 1986 and early

---

5. There are other organizations, especially in the consulting sector, which have extensively used GIS technology for hazards research and practice. However, these organizations consider most of their work confidential and have not reported on their experience. Hence such organizations are not covered in this review.

6. A glossary of key terms to this paper is provided at the end of this volume.

1987 and the vegetation patterns (showing lack of vegetation in southern Africa) were captured by both Component 7 and 8. A later study (Anyamba, Eastman, and Fulk 1995) found strong correlations between the two components and an index of ENSO, the Southern Oscillation Index (SOI).

Other studies on the use of GIS in assessing drought include: evaluating the usefulness of NOAA/AVHRR data for estimating vegetation growing periods in Africa and, ultimately, for drought early warning (Henricksen and Durkin 1986); modeling the potential impacts of climate change on the susceptibility of soils in Scotland to drought (Matthews et al. 1994).

## Earthquakes

Two types of applications of GIS technology in earthquake hazard assessment and management are illustrated here: (1) assessing property damage and casualties from a potential earthquake; and (2) analyzing surveys of attitudes and behavior regarding the earthquake hazard.

Emmi and Horton (1993) used GIS to estimate property damages and casualties from a potential earthquake in Salt Lake County, Utah, USA (see also Emmi and Horton 1995; Horton 1993). The GIS was used to capture and store data on: (1) the earthquake hazard defined through the Modified Mercalli Index (MMI) scale; (2) building inventory by use, value, and structural type; and (3) residential and employee population densities. To estimate property damages, damage functions were first derived by statistically fitting polynomials to the Applied Technology Council (ATC)'s tabular data on expected percentage of a structure's value lost during an earthquake (Rojahn 1985). For example, damage functions for two structural types, wood frame and unreinforced masonry, derived in such a manner are (Emmi and Horton 1993):

$$\text{Wood Frame:} \quad \text{Percent Loss} = 27.7 - 9.84(\text{MMI}) + 0.88(\text{MMI}^2)$$

$$\text{Unreinforced Masonry:} \quad \text{Percent Loss} = 428.17 - 162.62(\text{MMI}) + 20.69(\text{MMI}^2) - 0.76(\text{MMI}^3)$$

where MMI is the Modified Mercalli Index value.

Property damages were then estimated by using such functions to combine data on ground shaking intensity with data on building structural types. Similarly, casualty functions were derived by fitting logarithmic functions to tabular data provided by ATC on loss of life and injury as a function of percentage of structure's value lost. To estimate casualties, the data on injuries and deaths derived from the casualty functions were combined with the data on population density. To depict the spatial variation in casualties, Emmi and Horton used the triangular irregular network (TIN). The study found that unreinforced masonry structures are likely to sustain greatest property damage in both the residential and commercial settings of the study area and that injuries in the residential section are concentrated in the north east quadrant of Salt Lake City.

Hodgson and Palm (1992) applied GIS to analyze surveys of homeowners' attitudes and behaviors to the earthquake hazard in California, USA (see also Palm and Hodgson 1992). Two surveys, one in 1989 and the other following the Loma Prieta earthquake also in 1989, gathered data on: (1) behavior (by asking homeowners whether they had purchased earthquake insurance); (2) attitudes (by asking homeowners questions about perceived risk, perceived location of their homes, and perceived damages from a future earthquake); and (3) economic and demographic characteristics. The GIS was used to map the locations of the surveyed homeowners as well as the homeowners who sustained damage during the Loma Prieta earthquake. The Dual Independent Map Encoding (DIME) and Topologically Integrated Geographic Encoding and Referencing (TIGER) street address files were used to geocode the locations. A Global Positioning System (GPS) was not used since it would have been more time consuming given the number of homeowners surveyed (3,400 in the first survey) and the extent of the study area. The GIS was also used to map three variables depicting geophysical risk: (1) the San Andreas fault; (2) the San Andreas fault special study zone (special studies zones are surface fault rupture zones in an earthquake prone area); and (3) a measure of microzonation of potential shaking intensities for the study area. Other maps and analyses produced with the GIS, in conjunction with software such as Statistical Package for the Social Sciences

(SPSS), included: (1) an isopleth map with the surface showing percentage of homeowners who had purchased earthquake insurance; (2) overlays of the map of homeowner locations on the maps of the special study zone and potential shaking intensities; and (3) calculation of euclidean distance from each homeowner's location to the nearest active fault and special studies zone. The study found that the best predictor of behavior (purchase of earthquake insurance) was perceived risk. Other variables, such as the distance to an active fault, were not related to the purchase of insurance. However, the isopleth map of percentage of owners purchasing insurance showed that a greater percentage of people in the San Fernando Valley (the site of a 1971 earthquake) purchased insurance, indicating that experience may be related to purchase of insurance.

Other applications of GIS technology to earthquake hazard assessment include: identifying the cause of a seismic event, that is whether the event was caused by a microearthquake or by a blast in a rock quarry (Byers et al. 1995); sensitivity analysis and accuracy assessment for earthquake risk analysis (Emmi and Horton 1995); and using GIS with Internet to monitor and predict earthquakes (Towers and Gitting 1995).

## Extreme Storms

The term "extreme storms" is used here for both coastal and inland storms, such as hurricanes, typhoons, tornadoes, and blizzards. Two examples of the application of GIS technology to this hazard are provided here: (1) assisting in disaster response and relief operations; and (2) analyzing socioeconomic vulnerability.

GIS was used for disaster response and relief operations in the aftermath of Hurricane Andrew in 1993 in Florida, USA (Corbley 1995; Welebny 1993). Welebny (1993) provides an account of the experiences of one software company, Digital Matrix Services, Inc. (DMS), in offering GIS support services to federal and state agencies involved in disaster response for Hurricane Andrew. For example, the DMS GIS was used to determine the latitude and longitude coordinates for neighborhoods in Homestead City and Florida City, two of the areas devastated by the hurricane. These coordinates allowed the captain of a Goodyear Blimp to use a GPS to position his ship over the neighborhoods in which people were stranded and flash signs in both English and Spanish with instructions on how to get aid. Another task performed with the GIS was to geocode addresses where facilities would be established to provide disaster relief. Once information on the addresses and sites of the facilities was entered by keyboard, the GIS software then searched the ETAK database of the area for a match. Once a match was found, a tag was placed at a location on the street segment reflecting its probable distance from the nearest intersection (Welebny 1993: 46). The appropriate side of the street for the tag was determined by even or odd address number. The kinds of facilities for which this geocoding was carried out included FEMA disaster application centers, Red Cross service centers, tent shelters, and Army field kitchens. Yet another task was to assist the U.S. Army in finding the locations of portable toilets and trash cans used by military units involved in disaster response. As most of the street signs were destroyed during the hurricane, the use of local street maps to plot the locations and then find the toilets and trash cans was not helpful. The Army turned to the DMS GIS for assistance, but collection and storage of data by DMS, Inc. had relied on latitude/longitude coordinates whereas the Army used metric coordinates, obtained through hand-held GPS units, to assign locations to the toilets and trash cans. A projection module in the GIS was therefore used to convert the entire database to the metric system. Records were then created for the locations of all the toilets and trash cans. These records were updated daily to reflect new locations and maps were produced of these locations. The Army personnel used these maps along with their GPS units to find the toilets and trash cans.

Corbley (1995) also discussed the role of GIS in disaster relief and response operations for Hurricane Andrew, but with a focus on a GIS operated by the South Florida Water Management District (SFWMD), which is located in the city of West Palm Beach, Florida. During normal operations, the SFWMD GIS assists in monitoring water quality, assessing water supply, and planning water distribution through a system of canals connecting South Florida to the ocean. In emergencies, the SFWMD GIS assists in relief and response efforts, such as clean-up of debris from canals so that the canals do not clog and exacerbate inland flooding. After Hurricane Andrew, the SFWMD GIS was used for clean-up operations as well as logistics, transportation, and communications among the various agencies involved in disaster response activities. From these applications, Corbley (1995: 41-43) identified several lessons for the use of GIS in disaster response and relief: (1) *Transportation maps are critical* (for routing relief and cleanup crews and locating emergency sites); (2) *GIS should be incorporated into disaster response plans*. For example, the SFWMD GIS now includes a formal system called the Canal and Structure

Tracking System which will facilitate cleanup of debris in canals in the aftermath of a hurricane; (3) *Outside computer models enhance GIS performance*. For example, models such as the Sea, Lake and Overland Surge from Hurricanes (SLOSH) developed by the U.S. National Oceanic and Atmospheric Administration (NOAA) can be used in conjunction with GIS to predict and map areas that are likely to be inundated from storm surge; (4) *Land use maps enhance emergency operations*. For example, landuse maps can be used to locate open spaces that would serve as staging areas for distributing tents, food, and other relief supplies; and (5) *Protecting the GIS*. Rather than a single GIS system located at a headquarters to assist in disaster relief and response efforts, a distributed network of GIS centers, each with a copy of the entire database for the area of concern, is essential in case the GIS at headquarters and more than one other site are destroyed during the disaster.

Emani and colleagues (1993) explored the use of GIS in analyzing vulnerability to extreme storms in the coastal community of Revere, Massachusetts, USA. The extreme storm considered in this study is the *nor'easter* but the methodology is also applicable to other coastal storms such as hurricanes. Following Dow (1993), the study defined vulnerability as the differential susceptibility, in a general sense, among social groups and locations to suffer losses from hazards. Three dimensions of vulnerability were identified: (1) exposure or the likelihood of suffering losses from a hazard; (2) resistance or the ability to withstand the impacts of a hazard; and (3) resilience or the ability to recover from the impacts of a hazard. Each of these dimensions, in turn, is defined through individual factors. For example, exposure to a hazard is determined by the types of landuse (such as residential, industrial, or agricultural) in a community. Similarly, the ability to withstand the impacts of a hazard (resistance) and recover (resilience) are associated with socioeconomic factors such as age, ethnicity, and income. The GIS was used to capture and display individual factors and dimensions of vulnerability. For example, to capture exposure to nor'easters the Flood Insurance Rate Map (FIRM) for Revere was digitized and stored in the GIS. Using the reclassification option in the GIS, only those areas in Revere at risk from a 100-Y flood were easily identified. To capture socioeconomic indicators of vulnerability such as age and income, two types of data from the U.S. Census Bureau were combined with the GIS: (1) block groups created from TIGER/Line files; and (2) attribute socioeconomic data, at the block group level, retrieved from Summary Tape File (STF) 3A. The GIS was also used to combine the different dimensions to produce a composite picture of vulnerability for the community. For example, data on exposure as represented by areas of 100-Y flood were combined with data on age to produce a map showing the spatial distribution of elderly populations in areas at risk from flooding.

Other GIS applications for assessing extreme storms include: a framework for a computer system with a GIS component for simulating losses from hurricanes (Berke et al. 1985); the role of GIS in disaster response and relief following hurricane Andrew (Foresman 1992); and the use of GIS by the insurance industry to analyze and map the distribution of exposures and losses (Langdon and Barnes 1995).

## **Flood and Inundation Hazards**

Two types of GIS applications are illustrated here: (1) in emergency response and damage assessment during a disaster; and (2) in planning and mitigation. GIS was used in conjunction with remotely sensed data for disaster response and damage assessment during the floods of 1993 in the midwest of the United States (Gardner 1994; Speed 1994). Gardner (1994) provides the following account of the use of Landsat satellite imagery with GIS in emergency evacuation of neighborhoods likely to be inundated by the Des Peres river in the city of St. Louis:

Given the rapidly rising waters, and the strain on the already overtaxed emergency services systems, the police reasoned that evacuating everyone would dangerously waste time and resources. They asked the city Community Development Agency (CDA) to produce a map that would show which parcels contained buildings and which of these were in danger of inundation. The analysts at CDA obtained Landsat imagery from the Corps of Engineers and loaded the digital data into their GIS. A digital map showing the normal boundaries of the River Des Peres, parcels, and building locations were electronically superimposed over the satellite imagery. Topographic and elevation data indicated those areas most likely to be subjected to flooding. The current boundaries of the flood waters were extracted from TM data and added to the map. The resulting map clearly showed the police where to concentrate their evacuation efforts. The successful evacuation began within four hours after the CDA received the initial request. No lives were lost.

Landsat imagery were also used with GIS for assessing damages from the midwest floods (Speed 1994). Damages to crops, roads, landfills, municipal water wells, and superfund sites were assessed by overlaying different data layers on the flood images. For example, the analysis identified the number of municipal water wells that were damaged and the number of households that were supplied by these wells which helped prioritize work orders for restoring service (Speed 1994).

Rosenfeld (1994) explored the use of GIS in flood hazard mitigation in Bangladesh, with a focus on education and research activities and technology transfer involving GIS. These activities were sponsored by organizations such the International Geographical Union (IGU), United Nations Development Program (UNDP), and the United States Agency for International Development (USAID). For example, a GIS laboratory at the Bangladesh Space Research and Remote Sensing Agency was sponsored by the USAID. This laboratory allowed researchers to analyze Landsat imagery before and after the 1987 floods to determine the extent of flooding. The IGU helped establish a GIS training facility at the University of Dhaka. In one of the tasks performed for this training facility, Rosenfeld and his colleagues from the University of Dhaka tested the use of a GPS with GIS for data acquisition. The researchers depended extensively on the GPS for locational information while visiting rural areas that were flooded during past events.

In a series of studies, Gornitz and White (1992; 1994) used GIS to assess the physical vulnerability of United States coastlines to accelerated sea-level rise. Two coastal hazards were addressed in these studies: inundation and erosion. From a larger database of 29 variables compiled for the studies, the authors selected seven variables for analyzing vulnerability to the two coastal hazards: (1) mean elevation, (2) local subsidence trend, (3) geology, (4) geomorphology, (5) mean shoreline displacement, (6) maximum wave height, and (7) mean tidal range. These seven variables were selected because of their use in measuring risk to coastlines. High risk coastlines have low relief, high subsidence rates, high erosion rates, and high wave energies (Gornitz, White, and Cushman 1991). The seven variables were reclassified to seven relative risk variables, each of which ranged from 0 to 5 with a 1 indicating a low risk and 5 a high risk from that variable (0 was reserved for missing values). Six indices of vulnerability were compiled and tested with the seven relative risk variables. Of these six indices, two proved to be less sensitive than the others to any errors that might be committed in the classification of the relative risk variables. These indices are:

- (1) the square root of the product mean defined as:

$$CVI1 = [(x_1 * x_2 * x_3 * x_4 * x_5 * x_6 * x_7) / n]^{1/2}$$

- (2) the sum of products defined as:

$$CVI2 = [4x_1 + 4x_2 + 2(x_3 + x_4) + 4x_5 + 2(x_6 + x_7)]$$

where CVI = Coastal Vulnerability Index;  $x_1$  = mean elevation;  $x_2$  = local subsidence rate;  $x_3$  = geology;  $x_4$  = geomorphology;  $x_5$  = mean shoreline displacement;  $x_6$  = maximum wave height; and  $x_7$  = mean tidal range.

A sampling of other studies applying GIS to flood and inundation hazards are: modeling the impacts on coastal wetlands due to inundation as a result of sea-level rise (Lee et al. 1992); using remote sensing data with GIS in estimating the probable maximum flood within a river basin (Mettel 1992); and use of GIS to assist in contingency planning for floods (Bocco, Sanchez, and Riemann 1995).

## Hazardous and Noxious Waste Facilities

GIS technology has been extensively applied to the assessment and management of hazardous and noxious waste facilities.<sup>7</sup> This is not surprising given the amount and diversity of data that are needed to select or characterize a waste facility, and the corresponding ability of a GIS to store and manipulate such data (Estes et al. 1987). Furthermore, the growing

---

7. In this review, waste facilities are distinguished from industrial facilities involved in manufacturing and processing activities (for example, chemical facilities). GIS applications for industrial facilities are considered in the next section on hazardous materials.

interest in the management of waste facilities coincided with the increasing use of GIS in hazards research with the result that the bridging of these two fields was inevitable. Two types of applications stand out: (1) characterization and remediation of waste sites; and (2) selection of sites for waste facilities.

### **Characterization and Remediation of Waste Sites**

One of the first studies to emerge in this area was a demonstration project for the EPA (von Braun 1984; 1986). A spatial data base for a hazardous waste facility was created from a variety of sources such as aerial photographs, maps, and slides. The data layers in the final database included Elevation, Topography, Buildings, Samples, Wastes, Site Roads, and Ponds. The Map Analysis Package (MAP) was used to analyze the data. One type of analysis identified and characterized onsite drainage basins for surface runoff waters (von Braun 1986: 56). To do this, a cartographic model was developed in which the Drainage Basins data layer was first created by combining the Elevation and Ponds data layers. The Drainage Basins data layer was then related with the Samples, Wastes, and Buildings data layers to yield a characterization of each basin. Another type of analysis involved the evaluation of remedial alternatives for storm water control by modification of the input topography. For example, berms, dikes, and pavements were "built" on the topography map to stop site runoff and the new ponds and basins that resulted were identified and quantified (von Braun 1986: 65). This early study has remained one of the few in which different remedial alternatives for a hazardous waste site were simulated and compared within a GIS context.

Moreno and Heyerdahl (1991) demonstrated the remediation of a hazardous waste site through revegetation of adversely affected areas (see also Moreno and Heyerdahl 1992). Three criteria were established for selecting areas for revegetation (Moreno and Heyerdahl (1991: 22): (1) the areas should have experienced serious degradation (need); (2) the soil contamination and physiographic conditions of the area should not significantly impair plant growth (limitations); and (3) the areas should have soil properties and physiographic conditions favorable for plant growth (opportunity). For each of these criteria, data was acquired and integrated within a GIS (the ERDAS GIS system). For example, Landsat Thematic Mapper imagery was used to capture vegetation cover (expressed as density in percent) and vegetation vigor (expressed qualitatively as a range from very vigorous to very feeble). Areas with low density and very feeble vigor were selected as those most in need of revegetation. The site was also divided into soil contamination zones which were sampled for toxic chemicals such as arsenic, lead, and zinc. The concentrations of these toxic chemicals were stored in one attribute table whereas the toxicity thresholds of the same chemicals were stored in a second attribute table. The two attribute tables were then combined with the soil contamination zones to yield a map of limitations to revegetation.

Other studies on waste site characterization and remediation include: use of GIS as a tool for assessing the impacts of Superfund sites on endangered species (Hunter 1986); identification of sites of historical hazardous materials accumulation (Samsel and Colten 1988); a conceptual framework for integrating GIS with remedial investigations and feasibility studies (Bieber 1988); monitoring the proposed high-level radioactive waste repository at Yucca Mountain, Nevada, USA (Carr et al. 1989); and use of GPS and GIS to identify and map radioactive waste sites (Runyon and Hammitt 1994).

### **Selection of Sites for Waste Facilities**

Bagheri and Dios (1990) used GIS to identify potential sites for the disposal of hazardous waste in New Jersey, USA. Data were collected on a number of factors from which four were used to assess the suitability of a site: (1) depth to bedrock; (2) percent slope; (3) depth to ground-water; and (4) soil permeability. The data on each of the four factors were recoded into four categories of suitability: unsatisfactory, marginal, satisfactory, and optimal. Two measures of aggregate suitability were then tested: (1) standard geometric mean; and (2) logistic geometric mean. Areas that ranked highly on both suitability measures were selected as optimal for the potential disposal of hazardous waste.

The use of GIS in selecting a hazardous waste site at the U.S. Army's Rocky Mountain Arsenal in Colorado, USA, was illustrated by Van Zee and Lee (1988). They first identified "data themes" needed for site selection, such as topography, ground-water, bedrock, flood plains, and transportation. After the database was created, several types of analyses including overlay, proximity analysis, and cartographic modeling were used to identify potential sites. For example, an overlay of

topographic contours with ground water contours yielded a depth-to-ground water map. Proximity analysis was performed to determine buffer zones inwards from the boundary of the facility. The cartographic model utilized a set of siting criteria to identify a potential landfill site. The model was run interactively with siting experts and decision makers to test alternatives and trade-offs among the siting criteria. Van Zee and Lee found that decision makers were able to identify and choose among site alternatives in three one-hour computer sessions that might otherwise have taken months using manual cartographic methods.

A study by Carver (1991) integrated GIS and multi-criteria evaluation (MCE) techniques in determining suitable sites for the disposal of low- and intermediate-level radioactive wastes in the United Kingdom. Although traditional GIS techniques such as overlay analysis allow different siting factors to be combined in determining suitable sites, they provide only a deterministic survey of the potential sites based upon one set of objectives (such as those of the technical expert). They do not, for example, allow the incorporation of multiple and conflicting objectives into the site-selection process in order to yield the best compromise sites. Carver illustrates how to achieve this with GIS through the use of three types of MCE techniques (Ideal Point Analysis, Concordance-Discordance Analysis, and Hierarchical Optimization). In order to combine GIS and MCE, algorithms for the three MCE techniques were programmed in FORTRAN 77 and linked with ARC/INFO GIS through Arc Macro Language (AML). A set of hypothetical criteria were identified for evaluating sites such as: hydrogeological environment; population density; proximity to conservation areas; proximity to existing nuclear installation; and landuse type. Different participants in the siting process will have different weights regarding the importance of these criteria. For example, environmentalists will likely regard proximity to conservation areas as more important than proximity to an existing nuclear installation. To capture these weights, a 7-point scale was used with 7 indicating very important and 1 indicating unimportant. Hypothetical weights on this 7-point scale were developed for each criteria for three types of participants: nuclear industry; general public; and environmentalists. These weights were used with the MCE algorithms and the GIS to identify and map best compromise sites for each weighting scheme as well as for each type of MCE technique. From these compromise sites, the most suitable sites were identified on the basis of coincidence and robustness.

Other studies in this application area include: role of GIS in selecting sites for solid and hazardous waste landfills (Jensen and Christensen 1986; Richason and Johnson 1988); combining GIS with multi-criteria decision-making techniques for identifying waste disposal sites in Lombardy, Italy (Peckham 1993); use of GIS by the U.S. Department of Energy (DOE) to evaluate potential impacts from the siting of a landfill at DOE's Savannah River Site in South Carolina (Stewart, Martin, and Jennetta 1993).

## **Hazardous Materials**

Two types of GIS applications can be found on the assessment and management of hazardous materials: (1) mapping the social and demographic characteristics of populations living in proximity to industrial facilities storing or releasing hazardous materials. This type of application falls under the theme of *environmental equity and justice*<sup>8</sup>; and (2) assessing the risk from transporting hazardous materials.

## **Environmental Equity and Justice**

McMaster and Johnson (1987) used a GIS to assess the vulnerability of a community, Santa Monica, California, USA, to hazardous materials. A data base of Santa Monica, captured in grid cells of 100-meter resolution, was developed for variables such as transportation networks, ethnicity, population density, age structures, landuse, and institutions. To determine the population at risk, the actual number of hazards per grid cell was used instead of the types of hazards in each cell. The

---

8. This theme has also been addressed in the case of hazardous and noxious waste facilities (see for example, Zimmerman (1993)).

study found minority groups (Asians, Blacks, and Hispanics) living in close proximity to the locations of hazardous materials.

Burke (1993) explored the question of whether race was significantly related to environmental hazards when the effects of other important variables such as income were controlled. A case study was conducted in Los Angeles County, California, USA, with the unit of analysis being the census tract. Data on socioeconomic and demographic characteristics at the census tract level were obtained from the Summary Tape File. Spatial data on census tracts was obtained through the TIGER/Line files. GIS was used to combine these two sets of data to produce maps of explanatory variables such as race (defined as percentage of minority population) and income (defined as media per capita income). Data on hazardous facilities releasing chemicals into the environment in Los Angeles County were obtained from the Toxic Chemical Release Inventory (TRI) database. GIS was used to integrate the data on census tracts and hazardous facilities through a point-in-polygon operation. This allowed the determination of the number of facilities falling in each census tract. GIS was also used to visualize the spatial relationships between TRI facilities and explanatory variables. For example, TRI facilities were overlaid on a map of percentage of minority population classified into four categories (<27%, 27-55%, 56-88%, >88%). This visual display showed a strong positive association between the two variables---there were fewer TRI facilities in census tracts with less than 27% minority population. Regarding income and the location of TRI facilities, low-income census tracts contained many of the TRI facilities. The study also explored the relationship between TRI facilities and different ethnic groups. For example, most TRI facilities were found to be located in hispanic-dominated census tracts and for a given income level, African-Americans and Hispanics were more likely to live near TRI facilities than Whites and Asians. The study, however, could not conclude whether race or income was a more important variable.

Glickman, Golding, and Hersh (1995) used GIS to assess the relationship between the location of hazardous facilities and the socioeconomic and demographic characteristics of host and nonhost communities in Allegheny County, Pennsylvania, USA. The data on hazardous facilities were obtained from the TRI database for 1990 whereas the socioeconomic and demographic information was obtained from the Summary Tape Files. Rather than adopting one unit of analysis, this study relied on GIS to examine environmental equity for five different units: block groups, census tracts, municipalities, and circles of half-mile and one-mile radius centered on each TRI facility. At the block group level, the study found that the percentage of population that is black (10%) and minority (11%) is slightly lower in the block groups with TRI facilities than in block groups without TRI facilities (percent population black is 11% and minority is 13%). A similar result was obtained at the census tract level. However, the results were reversed at the municipality level where the percent population black and percent population minority is substantially higher when TRI facilities are present (15% and 18% respectively) than when they are not present (6% black and 7% minority). A similar result is obtained but with smaller differences when the circles are used. For example, with the circle of half-mile radius the percent population black when TRI facilities are present is 14% compared to 11% when TRI facilities are not present. Thus, different results were obtained for different units of analysis. The authors suggest that if proximity is of concern then the circle might be the best unit of analysis to explore environmental equity. The authors conclude that the advantage of using GIS in environmental equity analysis is that it allows the user to define and create an appropriate unit of analysis for the problem at hand rather than rely on pre-existing census units such as block groups or census tracts.

Other studies on this subject include: combining TRI data ranked by amount and toxicity with data on population density at the county level in the southeastern United States (Stockwell et al. 1993); exploring the role of different geographical scales and zoning schemes on environmental equity analysis (Sui and Giardino 1995).

## **Hazardous Materials Transportation**

Lepofsky, Abkowitz, and Cheng (1995) discussed the role of GIS in managing hazardous materials transportation accidents (see also Abkowitz, Cheng, and Lepofsky 1990). Five GIS application areas are identified and examples from the state of California, USA, are provided for each area: (1) risk assessment; (2) routing and scheduling; (3) emergency preparedness; (4) evacuation planning; and (5) incident management. In the case of risk assessment, for example, the likelihood of an accident's occurring on a stretch of a highway ( $9.72 \times 10^{-6}$ ) was multiplied by the total population residing in a five-mile buffer zone of the stretch (105,211) to yield a risk value (1.023). The likelihood of the accident was determined from historical data on accident rates. The total population living in the five-mile buffer zone was determined by using the



GIS to overlay census data on the buffer zone and then calculating the number of people falling in the zone.

Chakraborty and Armstrong (1995) used GIS to estimate population characteristics of areas in Des Moines, Iowa, USA, likely to be affected by a hypothetical hazardous materials transportation accident involving the release of chlorine into the air. The dispersion of chlorine following the accident was modeled with a software, ALOHA (Areal Locations of Hazardous Atmospheres). ALOHA uses data on the conditions at the accident site (such as the name of the city, type of buildings in the vicinity of the site), quantity and properties of the chemical released, and atmospheric conditions (such as wind speed, wind direction, and relative humidity) in determining the concentration of the chemical downwind of the accident site. This result is displayed in the form of a plume "footprint". In the Des Moines study, Chakraborty and Armstrong created such a footprint using hypothetical data (for example, release of 200 gallons of chlorine with wind at 13 knots from the west). The footprint was then overlaid on a map of the street network for the city with the origin of the footprint being the accident location. Next, census block groups falling within the footprint were determined by overlaying a map of the block groups on the footprint. Finally, population characteristics (percentage of White population, percentage of Black population, household income, and others) were estimated by assuming that population was uniformly distributed in each block group. If a block group fell partially within the plume footprint, then the population characteristics were adjusted according to the proportion of the area of the block group falling in the footprint. When repeated for 50 randomly selected locations in the city, the analysis showed that the areas likely to be affected by a hazardous material transportation accident had a higher concentration of minorities and lower household incomes than the city as a whole. Other applications on hazardous materials transportation are: the role of GIS in hazardous waste transportation (Brainard, Lovett, and Parfitt 1994); and using GIS for route characterization and risk assessment for radioactive waste materials transportation assessment (Souleyrette and Sathisan 1994).

## **Landslides and Geomorphological Hazards**

Two types of applications can be found on this subject: (1) the role of GIS in portraying and analyzing landslides and geomorphological hazards; and (2) linking GIS with physical and socioeconomic models for assessing impacts.

Brabb (1987) discussed the use of a GIS in analyzing and portraying geologic hazard maps for San Mateo County, California, USA. The tasks of this GIS project were: (1) building the GIS database (DEMs, hydrography, transportation, landuse, etc.); (2) manipulating the GIS data base (for example, combining the dip map, slope map, and landslide inventory to determine the relationship between over-dip slopes and landslide distribution); (3) applications of GIS data (for example, develop a system for releasing GIS data to decision makers and landuse planners); and (4) training. The use of GIS yielded several new topics of research relating quantitative morphology with hazardous geologic processes. For example, landscapes formed by different landslide processes were quantified in numeric terms for comparison.

Soeters and van Westen (1994) addressed the role of GIS and remote sensing in landslide hazard assessment with a focus on the issue of scale in analysis. The authors identify four types of scale in such assessments: (1) national scale (<1:1,000,000); (2) regional scale (1:100,000); (3) medium scale (1:25,000-1:50,000); and (4) large scale (1:5,000-1:15,000). Different GIS techniques for landslide hazard assessment are applicable at different scales. For example, at the national scale GIS can be used for an inventory on the distribution and classification of landslides. At the medium scale, on the other hand, GIS can be used for statistical analysis in which the importance of different factors contributing to landslides can be calculated through bivariate and multivariate statistical analyses. The authors also discuss issues of accuracy in the hazard assessment. At the national scale, for example, errors in interpretation of remotely sensed data can affect the accuracy of the landslide inventory process.

Pearson and colleagues (1991; 1992) linked GIS with spatial models and expert systems in assessing and mapping landslides. The approach adopted was to develop a system of physical, socioeconomic, and statistical models linked through a user friendly interface. For example, the physical module incorporated a DEM from which slopes were derived. The statistical model was used to assess uncertainties in the parameters of the physical module through Monte Carlo simulations. The system of models was embedded within the framework of expert systems. An interface between ARC/INFO and an expert system *Nexpert Object* was developed and applied to landslide hazard assessment in Cyprus.

Other applications using GIS in landslide and geomorphological hazard assessment are: developing a technique for risk assessment of landslide hazards in India with factors such as lithology, landuse, and azimuth direction (Gupta and Joshi 1990); a training package on using GIS for landslide hazard assessment (van Westen et al. 1992); and developing landslide hazard zonation maps in Colombia using factors such as bedrock and surficial geology, topography, landuse, and climate (Mejia-Navarro and Wohl 1994).

## **Surface- and Ground-water Contamination**

GIS has been extensively used for assessing surface- and ground-water contamination because of the ease with which data and models pertaining to physical phenomena and processes can be integrated with a GIS. Several applications of each type are illustrated below.

### **Surface-water Contamination**

In assessing surface-water contamination, numerous applications have addressed the role of GIS in modeling nonpoint sources of pollution. Examples are provided here of some of the models used and steps adopted in the modeling process.

Levine and colleagues (1993) used GIS to develop, test, and calibrate a model for nonpoint source pollution in twelve watersheds of the Lake Ray Roberts Drainage Basin in Texas, USA. The study focused on the delivery of two types of pollutants: (1) sediments, or soil particles, and (2) nutrients (for example, nitrogen and phosphorus). Three types of data were captured in a raster GIS, IDRISI, for each watershed in the study area: soils; landuse; and elevation. The data on elevation was used to create three additional variables for nonpoint pollution modeling: slopes in a watershed; direction of flow of water and pollutants (through a cell); and length of flow of water and pollutants. The modeling process, based upon empirical models, consisted of five steps, all of which were implemented in the GIS:

1. Sediment and nutrient detachment. In this step, the amount of sediments and nutrients available for transport by water was calculated from data on soils, landuse, and topographic conditions. To calculate the amount of sediments available for transport, the Universal Soil Loss Equation (USLE) was used. To calculate the amount of nutrients available for transport, empirically derived export coefficients for each nutrient were assigned to the landuse data.
2. Overland flow delivery process. Since not all the sediments and nutrients available for transport by water are transported, this step calculated the proportion of pollutants in a cell that was available for transport using data on surface conditions, such as soil permeability, slope, and vegetation density. The calculations were based on nonlinear statistical models which were generated from a database on surface conditions compiled from a body of literature known as vegetation filter-strip studies. These nonlinear models were implemented in the GIS and the proportions of pollutants thus calculated were called *cell delivery ratios*.
3. Stream network delineation. This step delineated the network of temporary and permanent streams that form in a watershed after a storm. A program was developed that counted the number of cells that flow into any one cell based on the direction of flow in each cell. Once the image showing the number of cells flowing into each cell was created, a threshold was applied to delineate the stream network. This network consisted of both permanent streams and temporary drainage channels, the latter being a result of storm activity.
4. Total flow path delivery ratios. In this step, the part of the pollutant load that actually reaches the outlet of a watershed and hence contributes to the final pollutant loading was calculated. The farther a cell is from a stream the smaller will be its contribution to the final pollutant loading as the portion of initial sediments and nutrients carried out of the cell will be trapped in each consecutive cell on the way to the stream. This process was modeled in this step and the results called *total flow path delivery ratios*.
5. Total annual nutrient and sediment loadings. This step involved the calculation of the total mass of pollutants reaching the watershed outlet. First, the results from step 1 and step 4 were combined. Then the total mass of

pollutants was calculated by summing over the values of all the cells in a watershed.

Kim and Ventura (1993) focused on urban nonpoint pollution generated as a result of storm runoff and sewer overflow from residential and commercial landuses in the southern part of Milwaukee County, Wisconsin, USA (see also Harris et al 1991). The first step in the project was to develop a GIS coverage of current landuse in the study area, for which three sources were used: a hard copy plot of landuse purchased from the Southeastern Wisconsin Regional Planning Commission; U.S.G.S. Digital Line Graph (DLG) to delineate street and railroad networks; and aerial photographs. The second step was to delineate storm sewer sub-basins. To do this, a coverage of storm sewer pipes in the study area was generated by digitizing maps provided by local municipalities. Urban storm water regulations formulated by EPA were used in selecting the pipes to be digitized; for example, the minimum diameter of pipes digitized in residential areas was 36 inches. A hierarchical process was applied to the coverage of storm sewer pipes for delineating the sub-basins. Major watershed boundaries were delineated first, sub-watershed boundaries next and individual sewer sub-basin boundaries the last. The third step was to model nonpoint pollution using an empirical model developed by the Wisconsin Department of Natural Resources called SLAMM - Source Loading and Management Model. Six pollutants were modeled with SLAMM: cadmium, copper, lead, phosphorus, sediments, and zinc. For each pollutant, the model estimated the pollutant loadings from each polygon in the landuse coverage. These pollutant loadings were stored as a GIS coverage and used for calculating the total and per acreage pollutant loadings (in pounds per acre per year) at the sub-watershed and watershed levels. The final step in the study was to evaluate the use of a wet pond as a best management practice (BMP) for reducing sediment loadings in receiving waters. Potential sites for such a pond were identified using the landuse and sub-basin coverages and one site selected to achieve a 90% reduction in sediment loadings.

Sivertun and colleagues (1988) illustrated the use of a GIS in identifying critical areas of nonpoint source water pollution (critical areas are areas where the potential contribution of pollutants to the receiving waters is significantly higher than other areas). Four data layers were used in the determination of nonpoint pollution critical areas: soils; slope; landuse; and water-course (which was obtained from river density and closeness to surface water). These four data layers were combined through the following equation to obtain the final data layer:

$$P = ((K*S*W)/4)*L$$

where P = final data layer; K= soils data layer; S = Slope data layer; W = water-course; and L = landuse

The critical areas were identified as pixels with values 255 or greater in the final data layer. The area and percentage of the critical areas were also calculated with the GIS.

Other studies using GIS in nonpoint source pollution include: assessing the effectiveness of wet detention basins as a means of reducing nonpoint pollution (Atkinson 1988); using a model, the Water Resources Evaluation of Nonpoint Sivilcultural Sources (WRENSS), developed by the U.S. Department of Agriculture Forest Service and EPA for assessing nonpoint pollution (James and Hewitt 1992); using the Areal Nonpoint Source Watershed Environment Response Simulation (ANSWERS) model to simulate runoff and soil erosion (De Roo 1993); and developing an index for ranking watersheds according to their agricultural nonpoint pollution potential (Mertz 1993).

## Ground-water Contamination

In using GIS to assess ground-water contamination, numerous studies have relied on an empirical model called DRASTIC.<sup>9</sup> DRASTIC is an acronym for seven hydrogeological factors: Depth to water (D), net Recharge (R), Aquifer media (A), Soil media (S), Topography (T), Impact of the vadose zone (I), and hydraulic Conductivity (C). These seven factors permit assessment of ground water pollution potential in most hydrogeological settings in the United States and data are also generally available for the factors (Evans and Myers 1990).

---

9. DRASTIC was developed jointly by EPA and the American Well Water Association. It is used primarily for regional level assessments of ground water contamination.

Evans and Myers (1990) applied the DRASTIC model to an area in the southeastern section of Delaware, USA. The seven factors comprising the DRASTIC model were captured as data layers in a GIS. To each factor, a rating and a weight were applied. Ratings are applied to the values or categories associated with a factor, as shown below for the factor "depth to ground-water":

Range (feet)	Rating
0-5	10
5-15	9
15-30	7
30-50	5
50-75	3
75-100	2
100 +	1

Weights are assigned to each factor based upon the relative importance of the factor in DRASTIC. For example, depth to ground water is the most important and is assigned a weight of 5 followed by net recharge which is assigned a weight of 4 and so on. The DRASTIC model was then operationalized in the following manner to produce a map of pollution potential:

$$\text{Pollution Potential} = D_r D_w + S_r S_w + T_r T_w + C_r C_w$$

where D, S, T, and C refer to the factors, "r" is the rating associated with each factor, and "w" the weight associated with each factor.

The remaining three factors in DRASTIC, R, A, and I, were not used in this application as they were uniform for the study area. A hazard assessment was then performed on the pollution potential map by combining it with data layers on landuse/land cover and septic system density. This hazard assessment resulted in a qualitative determination of the potential for ground-water pollution. For example, it was found that 17% of the land area in the study region had "low" hazard potential, 34% had "medium", and 49% a "high" hazard potential. More than 50% of the areal extent of two landuse/land cover types associated with ground-water pollution --- agriculture and waste disposal --- occurred in areas predicted by DRASTIC to be high hazard areas.

Padgett (1992) used DRASTIC to assess the vulnerability of ground-water in Florida, USA, to hazardous materials transportation accidents. The study was conducted at two levels: county, and local. First DRASTIC scores were calculated for each county in Florida. These scores were then combined with data on per capita water use and number of crashes per 1,000 drivers to derive a spill risk factor for each county. This spill risk factor was used to rank counties from most to least risky for transportation accidents. At the local level, alternative routes for transporting hazardous materials within a county were evaluated by combining data on the length of a route, spill risk factor, and information about the aquifer. Indices were derived for different routes and the one posing least risk to ground-water was identified.

Other studies that have adopted the DRASTIC model in a GIS context include those by Griner (1989) and Hatchitt and Maddox (1993).

## ***Institutional Applications***

### **United States Environmental Protection Agency (EPA)**

The United States Environmental Protection Agency (EPA) has used GIS for more than a decade in monitoring, characterizing, and managing technological hazards. In addition to the ten regional offices of the agency, several research laboratories such as the Environmental Monitoring Systems Laboratory (EMSL) in Las Vegas, and the Environmental Research Laboratory in Corvallis, Oregon are involved in GIS-related research. A 1989 review of the implementation of GIS within four of the regional offices and several research laboratories found the focus of GIS applications to be ground water pollution followed by hazardous waste sites (EPA 1989). Even the application area of hazardous waste sites emphasized the potential for ground-water contamination from the sites.

Some examples of the GIS applications found in this review were (EPA 1989: II-3 to II-8):

Ground-water mapping (identify wellhead protection areas; map and prioritize water supplies at risk; map potential contamination sources).

Superfund site support (characterize extent of site problems; identify contamination migration routes and populations/locations at risk).

Radon evaluation (examine predictive value of selected variables for high radon readings; identify populations at risk and prioritize high-risk radon areas; identify rural areas and private wells at risk).

Air pollution exposure assessment (determine optimal locations for air quality monitors; identify and locate pollution sources).

A second review, in the form of a telephone survey of all the regional offices, was conducted by Rejeski and Kapuscinski (1990). The key findings of this survey were:

many regions expressed concern over data availability, comparability, and transferability.

many regions expressed confusion over what type of risk modeling to do with GIS and how to go about doing it.

many regions expressed concern over uncertainty in the data and how to communicate it.

Since the beginning of this decade, the EPA has embarked on an ambitious program, the Environmental Monitoring and Assessment Program (EMAP), which will use GIS to characterize ecological resources and assess environmental problems at a national level (Jones 1990; Norton and Slonecker 1990a; 1990b). The main objectives of the EMAP program are: (1) to estimate status and trends in the condition of the Nation's ecological resources, in defined regions and with known accuracy; (2) to seek associations between human-induced stresses and adverse effects on ecological condition; and (3) to provide periodic statistical summaries and interpretive reports on ecological condition to the Administration and the public (Norton and Slonecker 1990a). Some of the analyses envisaged with this GIS are proximity, overlay, buffering, network, and surface modeling and contouring.

### **Advanced Computer Applications (ACA), IIASA**

Since 1985, the Advanced Computer Applications (ACA) group at the International Institute for Applied Systems Analysis (IIASA), Laxenburg, Austria, has used GIS in combination with decision support systems, expert systems, and computer models to analyze hazards (Fedra 1989; IIASA 1992). One of the first projects undertaken by this group was to develop computer-based tools for the assessment and regulation of industrial risks for the Commission of the European Communities Joint Research Center in Ispra, Italy (Fedra 1989). The set of tools developed by ACA was the Ispra Risk Management Support (IRMS) system, an integrated system consisting of several databases, simulation and optimization models, and decision support tools. Among the databases available within this system are: geographical data for Europe (political boundaries, major settlements, transportation networks, water bodies, and industrial plant locations); a hazardous chemicals database (including hazardous substances and attributes such as LD50); and chemical storage facilities (Fedra 1989).

The simulation and optimization models in the IRMS system define the lifecycle of hazardous substances and include models for the industrial production sector, production distribution sector, waste management, and hazardous substances transportation. For example, once the beginning and end points of the hazardous substance to be transported are specified on a graphics interface of the hazardous substances transportation model, it will generate a set of alternate routes and evaluate these routes on the basis of transportation costs and risk estimates for alternative vehicle types (Fedra 1989: 255). A multi-criteria discrete optimization model can then be used to compare and select among the routes by specifying decision criteria and setting constraints based on these criteria.

A second set of projects in which ACA has used GIS involves air quality modeling and management in several developed and developing countries (China, India, Poland, and Austria) (IIASA 1992). In China, an air quality model developed for the Shanxi province includes a multi-criteria optimization model to balance production capacities, a Gaussian air pollution model derived from the Industrial Source Complex (ISC) model, and an expert system to identify feasible locations for industrial activities (IIASA 1992: 8). In the North Bohemian region (between Prague and Dresden) of Central Europe, data on vegetation, soils and pattern of landuse, population distribution, meteorology, and point and area sources of air pollution are combined in a GIS context to simulate short-term pollution episodes and long-term patterns of air pollution. In this application, the Gaussian dispersion model was replaced by a more complex model that reflected the region's topography and meteorological conditions and which consisted two versions, a local version nested within a regional one.

## **Discussion**

The review sections of this paper provide the reader with a flavor for the nature and type of applications of GIS technology to hazards, both natural and technological. In this section, these applications are discussed within the context of hazard management. The objective is to identify those aspects of hazard assessment and management for which applications of the technology are well developed and those requiring further research. The framework of hazard management depicted in Figure 2 is adopted for this purpose.

## **Hazard Assessment**

Hazard assessment includes the components of hazard identification, risk estimation, hazard prioritization, and social evaluation (Kasperson, Kates, and Hohenemser 1985). Hazard identification deals with the question: *What is the hazard?* For example, epidemiological studies and laboratory experiments on animals constitute two approaches to identifying technological hazards. Risk estimation is the quantification of the likelihood and magnitude of consequences associated with a hazard. It involves several types of assessments: source-release assessment (for example, identifying all the possible releases of toxic chemicals from a hazardous waste site); dose-response assessment (identifying the relationship between the dose received and the adverse effects observed); and exposure assessment (for example, determining the population threatened by a hazard) (Cohrrsen and Covello 1989). Hazard prioritization deals with assigning priorities for managing hazards since society cannot simultaneously deal with all hazards. Social evaluation refers to the differing societal responses to hazards, such as public concern and protest, litigation, and increased regulation.

To date, GIS technology has been extensively applied in hazard identification and in some aspects of risk estimation. The use of overlay and proximity analysis to identify the threat posed by noxious and hazardous waste sites has become routine. The mapping of different levels of risk associated with natural hazards (for example, Modified Mercalli Index scales for earthquake hazard) is fairly common (Emmi and Horton 1993). Numerous applications have demonstrated the advantages of using GIS in epidemiological studies for identifying hazards and conducting dose-response assessments (Stallones et al. 1992; Geschwind et al. 1992). Similarly, the use of GIS in exposure assessment, especially in determining the characteristics of a population threatened by a hazard, is well established. GIS-based exposure assessments for ecological risk have also started emerging (see, for example, Crabtree, McGaughey, and Henriksen 1993; Clifford et al. 1995). In the case of dispersion modeling, studies have been conducted linking GIS with dispersion models to map the downwind concentrations of chemicals and pollutants from both hypothetical and actual sources. Monitoring of hazards, which constitutes an important component of natural hazard assessment, has benefited from the linkages of remote sensing and GIS technologies.

In spite of this progress, some gaps remain in the use of GIS for hazard identification and risk estimation. One gap pertains to the type of risk estimates examined within a GIS context. Almost all the GIS applications rely on risk estimates that are defined on an ordinal scale (for example, low, medium, and high risks). However, the process of risk assessment generally yields a quantitative estimate expressed in terms of probability and consequence. For example, the risk of an individual's dying from exposure to a chemical released from a hazardous facility might be expressed as one in a million. Such expressions of risk have not been analyzed or mapped with GIS except in a few studies (see, for example, Moore 1993). Further research is needed on this topic, in particular the role of GIS in displaying and mapping quantitative estimates of risk. For example, such a map could depict individual risk around hazardous facilities (expressed as one in a million or one in thousand) in the form of *risk isopleths* (Moore 1993). Alternatively, the map could focus societal risk (the likelihood of 100 people dying from a single accident at a hazardous facility), in which case *risk contours* would be the more appropriate form of display. Which spatial "profile" of risk is used depends on the objective of the problem at hand. In the case of emergency planning, for example, the interest would be on mapping societal risk (risk contours) and not individual risk (risk isopleths).

Closely related to the gap of handling quantitative estimates of risk in GIS is the gap in assessing and characterizing uncertainty. In addition to the parametric and modeling uncertainties found in traditional risk assessment, GIS introduces the special problems of locational uncertainty and the propagation of uncertainty through spatial analysis (Rejeski 1993). Although much discussion of uncertainty has occurred in the context of risk assessment as well as in the context of GIS, little research has combined these two approaches to uncertainty. A study by Emmi and Horton (1995) on earthquake risk assessment in Salt Lake County, Utah illustrated how this can be accomplished. Emmi and Horton considered two types of uncertainty: (1) in expected ground-shaking intensities, and (2) in the location of boundaries between earthquake ground shaking intensity zones. In the second type of uncertainty (locational uncertainty), they introduced random perturbations of the boundaries and then used Monte Carlo simulations to assess the effects of the perturbations on risk assessment. They found that the boundaries can vary at random within a 1.5 km wide corridor without violating standards of accuracy for risk assessment. In other words, in this case locational uncertainty did not have a significant effect on the results of the risk assessment. Further studies of this kind are needed to develop analytical as well as technical tools for bridging risk uncertainty with GIS uncertainty.

Relatively little research has been carried out on the remaining two components of hazard assessment, hazard prioritization and social evaluation, although GIS can be applied to these components. Regarding hazard prioritization, one application of GIS is to map areas that are at high risk to certain types of hazards and prioritize those areas for management efforts. For example, coastal areas are at higher risk from hurricanes or typhoons than inland areas. Even in high risk coastal areas, some areas are likely to suffer greater impacts than others. Thus, in addition to risk the vulnerability of these areas must be assessed and mapped. One important advantage of using GIS in these tasks is the ease with which data on biophysical and socioeconomic factors can be captured and integrated in a GIS. Areas that are at high risk and that are also highly vulnerable can be prioritized for hazard management efforts. The component of social evaluation will be addressed in the next section.

## **Control Analysis**

Control Analysis includes the components of judging tolerability of risk, identifying means of control, assessing modes of implementation, and evaluating costs of control (Kasperson, Kates, and Hohenemser 1985). The psychological approach to risk perception mentioned earlier in this paper under definitions of risk (p. 4) has identified a number of qualitative characteristics that influence judgments about tolerability, such as whether the hazard is: voluntary or involuntary; equitable or inequitable; associated with high or low risk to future generations. For example, hazards such as nuclear power which are perceived to be involuntary, inequitable, and have a high risk to future generations are associated with high levels of public concern and conflict as opposed to a hazard such as automobile driving which are perceived to be voluntary, equitable, and with low risk to future generations. This stream of research labeled, *behavioral decision theory*, is descriptive in nature and helps understand how people make decisions about risk. The second component of Control Analysis is identifying the means of controlling the hazard. For example, runoff from a hazardous waste site might be controlled by installing berms and dikes. Sometimes the hazard itself cannot be controlled (for example, in the case of natural hazards such as

earthquakes), in which case the focus of means of control shifts to mitigating the consequences of the hazard through land-use planning and structural modifications of buildings. The third component, assessing modes of implementation, refers to approaches for implementing the control actions that have been identified. For example, in the case of the earthquake hazard, people living in earthquake-prone areas can be informed about measures for mitigating consequences. In the case of a hazardous waste site, regulations can mandate that the site be remediated. The final component, evaluating costs of control, assesses the costs of various means of control and modes of implementation.

Of the applications that address the stage of Control Analysis, the focus of GIS applications has been on identifying the means of controlling the hazard. This is not surprising since GIS provides artificial environments in which physical factors and processes from the real world can be analyzed and simulated. Thus, there has been considerable amount of work on identifying remedial alternatives for hazardous waste sites using GIS (a good illustration of this is provided in the work of von Braun (1984; 1986; 1993). In the case of nonpoint source pollution, GIS has served to identify the sources of pollution as well as feasibility of control options such as wet detention basins (see, for example, Atkinson 1988; Kim and Ventura 1993). Emergency planning and response, especially in the case of natural hazards that cannot be controlled, can and has benefited from the use of GIS (Gardner 1994; Weleby 1993). In some cases, the means of controlling the hazard and the costs of control have been evaluated together with GIS. For example, Lepofsky, Abkowitz, and Cheng (1995) explored the tradeoffs between risk and cost of alternative routes for highway shipments of hazardous materials. They found that the route selected when risk is sole criterion is twice as long as other alternatives and might involve too significant costs to be considered practical for haulers.

Relatively little research using GIS has been conducted on the other two components of Control Analysis, judging tolerability of risk and assessing modes of implementation. Almost all behavioral decision theory applications in risk have been aspatial in nature.<sup>10</sup> However, questions such as *How safe is safe enough?* or *How close is safe enough?* have a strong spatial component and are therefore amenable to analysis by GIS. One of the few studies to address these questions is by Hodgson and Palm (1992). They link GIS with surveys of people's perceptions of earthquake hazard in California to assess the relationship between perceived seriousness of risk, proximity to earthquake faults, and purchase of earthquake insurance. GIS can also play a role in resolving conflicts over risk by facilitating public participation in the risk management process. Again, one of the few studies to address this issue used multicriteria evaluation techniques to identify optimum sites for radioactive waste facilities in the United Kingdom (Carver 1993). These techniques allow the integration of the preferences of different participants in the siting process and may help address and resolve conflicts. Further studies must be conducted on identifying the types of conflicts, the timing in a conflict, the factors that are involved in conflicts (equity, risk-benefit tradeoffs), and the appropriate tools and techniques for facilitating public participation in risk management that can be addressed by GIS technology.<sup>11</sup>

Regarding the component of assessing modes of implementation, the role of GIS might be one of communicating information about the hazard and the appropriate mitigation measures for reducing the consequences of the hazard. As with studies on perceptions of risk, studies on risk communication have been aspatial in nature. Much of risk communication research has focused on messages as a means for communicating risks. The role of maps in communicating risks remains untapped.

## Strategy Selection and Implementation and Evaluation

The strategy selection stage combines the means of controlling the hazard and modes of implementation to arrive at different management strategies, including: risk acceptance, risk spreading (redistributing risk over regions or over social groups), risk reduction, and risk mitigation (disaster relief, insurance). The role of GIS in determining means of control as well as modes of implementation was examined in the previous section. Further research on how these can be combined in a GIS context to facilitate management strategies is needed.

---

10. The same holds true for the prescriptive counterpart of decision making about risk, *decision analysis*.

11. A project initiated at Clark Labs is addressing some of these issues.



In the stage of implementation and evaluation, the different management strategies identified in the strategy selection stage are implemented and evaluated. The literature search did not identify any studies on the use of GIS at the implementation and evaluation stage of hazard management. One possible explanation for this is that the results of GIS applications in the implementation and evaluation stage have yet to be discussed in a public forum, as for example in journals or at conferences. The advantages of using GIS for this stage, however, are clear. For example, data on hazardous facilities such as their location, the type and amount of hazardous substances present at the facilities, and the location and capabilities of emergency and enforcement personnel can be stored in a GIS. Using such data, spatial "effort maps" that illustrate the spatial patterns of implementation and enforcement activities can be constructed to match the severity of risk posed by the facilities.

## Conclusions

The application of GIS technology in hazard assessment and management has proliferated in the last decade. This trend is likely to continue and perhaps even accelerate, for as Gatrell and Vincent (1991: 148) pointed out "few areas of the application of GIS technology are as socially significant or environmentally relevant (Gatrell and Vincent 1991: 148)." Future applications should make an attempt to incorporate more social science perspectives from the risk and hazards fields than has been the case thus far. This clearly requires greater collaboration between social science risk researchers and GIS researchers. Furthermore, as the bibliography at the end of this paper shows, few of the publications on this subject have appeared in journals aimed at risk researchers. To foster dialogue between the two communities, GIS researchers should publish their research and findings in the journals aimed at the risk community and present papers at conferences on risk and hazards. At the same time, risk and hazard researchers should acknowledge and incorporate spatial factors into risk assessment research.

## Acknowledgments

I am grateful to Jeanne Kasperson for her comments on the final version of the paper. I would also like to thank Steve Gold, Ron Eastman, Roger Kasperson, Dan Levine, and Sam Ratick for their comments on draft versions of the paper.

## References

- Abkowitz, M., P.D. Cheng, and M. Lepofsky. 1990. The use of geographic information systems (GIS) in managing hazardous materials shipments. *Transportation Research Record* 1261, 35-43. Washington, D.C.: National Academy of Sciences.
- ADB (Asian Development Bank). 1991. *Disaster mitigation in Asia and the Pacific*. Manila, Philippines: ADB.
- Alexander, D. 1991. Information technology in real-time for monitoring and managing natural disasters. *Progress in Physical Geography* 15(3), 238-260.
- Anyamba, A., J. R. Eastman, and M. Fulk. 1995. NDVI as an indicator of climatic variability. *Proceedings of the ACSM/ASPRS conference*, Volume 3: ASPRS, pp. 714-723. Bethesda, MD: American Congress on Surveying and Mapping, and American Society for Photogrammetry and Remote Sensing.
- Atkinson, S.F. 1988. Nonpoint pollution control site selection planning. *Proceedings, GIS/LIS '88*, Vol. 2, pp. 685-694. Bethesda, MD: American Congress on Surveying and Mapping (ACSM) and American Society for Photogrammetry and Remote Sensing (ASPRS).
- Bagheri, S., and R.A. Dios. 1990. Utilization of geographic information system in selection of hazardous waste disposal site in New Jersey Piedmont Province. *Proceedings, GIS/LIS '90*, Vol. 1, pp. 299-306. Bethesda, MD: American Congress on Surveying and Mapping (ACSM) and American Society for Photogrammetry and Remote Sensing (ASPRS).
- Berke, P., et al. 1985. A computer simulation system for assessment of hurricane hazard impacts on land development. In J.M. Carroll (ed.), *Emergency Planning: Simulation Series* 15(1), 149-154.

- Bieber, A.J. 1988. Remedial investigations/Feasibility studies: an integrated GIS approach. *Proceedings, GIS/LIS '88*, Vol. 2, pp. 704-710. Bethesda, MD: American Congress on Surveying and Mapping (ACSM) and American Society for Photogrammetry and Remote Sensing (ASPRS).
- Bocco, G., R. Sanchez, and H. Riemann. 1995. GIS affects flood planning efforts. *GIS World* 8(2), 58-60.
- Brabb, E.E. 1987. Analyzing and portaying geologic and cartographic information for land-use planning, emergency response, and decision making in San Mateo County, California. *Proceedings, GIS '87*, Vol. 1, pp. 362-374. Bethesda, MD: American Congress on Surveying and Mapping (ACSM) and American Society for Photogrammetry and Remote Sensing (ASPRS).
- Brainard, J., A. Lovett, and J. Parfitt. 1994. Using GIS to investigate waste transportation issues. In D. Green, D. Rix, and J. Cadoux-Hudson (eds.), *Geographic Information 1994: The Yearbook of the Association for Geographic Information*, pp. 82-89. London, UK: Taylor and Francis.
- Byers, B.W., et al. 1995. A GIS link for first order seismic source assessment. *Geo Info Systems* 5(2), 34-37.
- Burke, L.M. 1993. Race and environmental equity: A geographic analysis of Los Angeles. *Geo Info Systems* 3(9), 44-50.
- Carr, J., et al. 1989. Application of a raster based GIS technique to temporal monitoring at Yucca Mountain, Nevada, USA. *Proceedings of the National Conference, Challenges for the 1990s: GIS*, pp. 302-313. Ottawa: Canadian Institute of Surveying and Mapping.
- Carver, S.J. 1991. Integrating multi-criteria evaluation with geographical information systems. *International Journal of Geographic Information Systems* 5(3), 321-339.
- CECA (Central Environmental Control Agency). 1982. *Risk analysis of six potentially hazardous industrial objects in the Rijnmond area, a pilot study. A report to the Rijnmond Public Authority*. Dordrecht, The Netherlands: D. Reidel.
- Chakraborty, J., and M.P. Armstrong. 1994. Estimating the population characteristics of areas affected by hazardous materials accidents. In *Proceedings, GIS/LIS '94*, Vol. 2, pp. 154-163. Bethesda, MD: American Congress on Surveying and Mapping (ACSM) and American Society for Photogrammetry and Remote Sensing (ASPRS).
- Clifford, P.A., et al. 1995. An approach to quantifying spatial components of exposure for ecological risk assessment. *Environmental Toxicology and Chemistry* 14(5), 895-906.
- Cohrrsen, J.J., and V.T. Covello. 1989. *Risk analysis: a guide to principles and methods for analyzing health and environmental risks*. Washington, D.C.: Council on Environmental Quality, Executive Office of the President.
- Corbley, K.P. 1995. South Florida fine-tunes GIS in hurricane's aftermath. *GIS World* 8(9), 40-43.
- Crabtree, C.G., B.D. McGaughey, and E.B. Henriksen. 1994. GIS and remote sensing as tools for conducting ecological risk assessments. *Lake and Reservoir Management* 9(1), 84-87.
- Dangermond, J. 1985. Network allocation modeling for emergency planning. In J.M. Carroll (ed.), *Emergency Planning: Simulation Series* 15(1), 101-106.
- De Roo, A.P.J. 1993. Validation of the ANSWERS catchment model for runoff and soil erosion simulation in catchments in The Netherlands and the United Kingdom. *Proceedings, HydroGIS 93: Application of Geographic Information Systems in Hydrology and Water Resources*, pp. 465-474.
- Douglas, M., and A. Wildavsky. 1982. *Risk and culture*. Berkeley, CA: University of California Press.
- Dow, K. 1993. Exploring differences in our common future(s): The meaning of vulnerability to global environmental change. *Geoforum* 23(3), 417-436.
- Eastman, J.R., and M. Fulk. 1993. Long sequence time series evaluation using standardized principal components. *Photogrammetric Engineering and Remote Sensing* 59(8), 1307-1312.

- Eastman, J.R., P.A.K. Kyem, J. Toledano, and W. Jin. 1993. *GIS and decision making*. Explorations in Geographic Information Systems Technology, Volume 4. Geneva, Switzerland: United Nations Institute for Training and Research (UNITAR).
- Emani, S., et al. 1993. Assessing vulnerability to extreme storm events and sea-level rise using geographic information systems (GIS). *Proceedings, GIS/LIS '93*, Vol. 1, pp. 201-209. Bethesda, MD: American Congress on Surveying and Mapping (ACSM) and American Society for Photogrammetry and Remote Sensing (ASPRS).
- Emmi, P.C., and C. A. Horton. 1993. A GIS-based assessment of earthquake property damage and casualty risk: Salt Lake County, Utah. *Earthquake Spectra* 9(1), 1-10.
- Emmi, P.C., and C.A. Horton. 1995. A Monte Carlo simulation of error propagation in a GIS-based assessment of seismic risk. *International Journal of Geographical Information Systems* 9(4), 447-461.
- EPA (Environmental Protection Agency). 1989. *Geographic information systems: Case Studies of EPA's Implementation*. PM218-B. Washington, D.C.: Administration and Resources Management, United States Environmental Protection Agency.
- Estes, J., et al. 1987. Coordinating hazardous waste management activities using geographical information systems. *International Journal of Geographical Information Systems* 1(4), 359-377.
- Evans, B.M., and W.L. Myers. 1990. A GIS-based approach to evaluating regional groundwater pollution potential with DRASTIC. *Journal of Soil and Water Conservation* 45(2), 242-245.
- Fedra, K. 1989. Computer-based information and decision support systems for management of hazardous substances and industrial risk. In P. Maltezou, A.K. Biswas, and H. Sutter (eds.), *Hazardous waste management*, pp. 242-257. London: Tycooly.
- Fischhoff, B., et al. 1978. How safe is safe enough? A psychometric study of attitudes toward technological risks and benefits. *Policy Sciences* 8, 127-152.
- Fletcher, G. A. 1987. GIS use for hazardous waste site characterization of NAEC Lakehurst, New Jersey. *Proceedings, GIS '87*, Vol. 1, pp. 176-186. Bethesda, MD: American Congress on Surveying and Mapping (ACSM) and American Society for Photogrammetry and Remote Sensing (ASPRS).
- Foresman, T.W. 1987. Present and future role of GIS technology for hazardous waste facility management. *Proceedings, GIS '87*, Vol. 1, pp. 468-475. Bethesda, MD: American Congress on Surveying and Mapping (ACSM) and American Society for Photogrammetry and Remote Sensing (ASPRS).
- Foresman, T.W. 1992. GIS group becomes 'essential personnel' in hurricane Andrews's wake. *GIS World* 6(4), 20, 22.
- Freudenburg, W.R. 1988. Perceived risk, real risk: social science and the art of probabilistic risk assessment. *Science* 242, 44-49.
- Gardner, J.V. 1994. *Landsat and the midwest flood of 1993*. Presented at the Second Thematic Conference on Remote Sensing for Marine and Coastal Environments. New Orleans, LA: 31 January-February 2.
- Gatrell, A.C., and P. Vincent. 1991. Managing natural and technological hazards. In I. Masser, and M. Blakemore (eds.), *Handling Geographic Information*, pp. 148-180. New York: John Wiley and Sons.
- Geschwind, S.A., et al. Risk of congenital malformations associated with proximity to hazardous waste sites. *American Journal of Epidemiology* 135(11), 1197-1207.
- Glickman, T.S., D. Golding, and R. Hersh. 1995. GIS-based environmental equity analysis: a case of TRI facilities in the Pittsburgh area. In G.E.G. Beroggi and W.A. Wallace (eds.), *Computer Supported Risk Management*, pp. 95-114. Dordrecht, The Netherlands: Kluwer.

- Gornitz, V.M., and T.W. White. 1992. *A coastal hazards data base for the U.S. east coast*. ORNL/CDIAC-45. NDP-043A. Oak Ridge, TN: Oak Ridge National Laboratory.
- Gornitz, V.M., and T.W. White. 1994. *A coastal hazards data base for the U.S. gulf coast*. ORNL/CDIAC-60. NDP-043B. Oak Ridge, TN: Oak Ridge National Laboratory.
- Gornitz, V.M., T.W. White, and R.M. Cushman. 1991. Vulnerability of the U.S. to future sea-level rise. In *Proceedings, Coastal Zone '91*, 2354-2368. New York: American Society of Civil Engineers.
- Gould, M.D., et al. 1988. Applying spatial search techniques to chemical emergency management. *Proceedings, GIS/LIS '88*, Vol. 2, pp. 843-851.
- Griner, A.J. 1989. The automation of DRASTIC - A regional model for mapping susceptibility of groundwater contamination. *Proceedings, GIS/LIS '89*, Vol. 2, pp. 679-684. Bethesda, MD: American Congress on Surveying and Mapping (ACSM) and American Society for Photogrammetry and Remote Sensing (ASPRS).
- Gupta, R.P., and B.C. Joshi. 1990. Landslide hazard zoning using the GIS approach - case study from the Ramganga catchment, Himalayas. *Engineering Geology* 28(1-2), 119-131.
- Harris, P.M., et al. 1991. Linking a GIS within urban nonpoint source pollution model. *Proceedings, GIS/LIS '91*, pp. 606-616. Bethesda, MD: American Congress on Surveying and Mapping (ACSM) and American Society for Photogrammetry and Remote Sensing (ASPRS).
- Hatchitt, J., and G.L. Maddox. 1993. Using DRASTIC methods to monitor the quality of Florida's groundwater. *Geo Info Systems* 3(1), 42-45.
- Hattis, D., and J.A. Smith, Jr. 1987. What's wrong with quantitative risk assessment? In R. Almeder and J. Humber (eds.), *Biomedical ethics reviews*, pp. 57-105. Humana Press.
- HSE (Health and Safety Executive). 1978. *Canvey: an investigation of potential hazards from operations in the Canvey Island/Thurrock area*. London, UK: Health and Safety Executive.
- Hellden, U., and L. Eklundh. 1988. *National drought impact monitoring: A NOAA NDVI and precipitation data study of Ethiopia*. Lund Studies in Geography Series C. General, Mathematical and Regional Geography No. 15. Sweden: Lund University Press.
- Henricksen, B.L., and J.W. Durkin. 1986. Growing period and drought and early warning in Africa, using satellite data. *International Journal of Remote Sensing* 7(11), 1583-1608.
- Hodgson, M.E., and R. Palm. 1992. Attitude toward disaster: A GIS design for analyzing human response to earthquake hazards. *Geo Info Systems* 2(7), 41-51.
- Horton, C.A. 1993. *Earthquake risk: a geographic information system based model and sensitivity analysis*. Salt Lake City, UT: University of Utah. Unpublished doctoral dissertation.
- Hunter, D.O. 1986. Geographic information system for assessing sensitive species/Superfund sites: New Jersey pilot project. *Proceedings, GIS '86*, pp. 227-237. Bethesda, MD: American Society for Photogrammetry and Remote Sensing (ASPRS).
- Hutachaoren, M. 1987. Application of geographic information system technology to the analysis of deforestation and associated environmental hazards in Northern Thailand. *Proceedings, GIS '87*, Vol. 2, pp. 509-518. Bethesda, MD: American Congress on Surveying and Mapping (ACSM) and American Society for Photogrammetry and Remote Sensing (ASPRS).
- Hutchinson, C.F. 1991. Uses of satellite data for famine early warning in sub-saharan Africa. *International Journal of Remote Sensing* 12(6), 1405-1421.

- IIASA (International Institute for Applied Systems Analysis). December 1992. *Options*. Laxenburg, Austria: International Institute for Applied Systems Analysis (IIASA).
- James, D.E., and M.J. Hewitt, III. 1992. To save a river: Building a resource decision support system for the Blackfoot river drainage. *Geo Info Systems* 2(10), 37-49.
- Jensen, J.R., and E.J. Christensen. 1986. Solid and hazardous waste disposal site selection using digital geographic information system techniques. *The Science of the Total Environment* 56, 265-276.
- Jones, K. B. 1990. The Environmental Monitoring and Assessment program: An ecological monitoring program for the 1990's and beyond. *Proceedings, GIS/LIS '90*, Vol. 2, pp. 669-681. Bethesda, MD: American Congress on Surveying and Mapping (ACSM) and American Society for Photogrammetry and Remote Sensing (ASPRS).
- Kasperson, R.E., R. W. Kates, and C. Hohenemser. 1985. Hazard management. In R.W. Kates, C. Hohenemser, and J. X. Kasperson (eds.), *Perilous Progress: Managing the Hazards of Technology*, pp. 43-66. Boulder, CO: Westview Press.
- Kates, R.W., C. Hohenemser, and J.X. Kasperson (eds.). 1985. *Perilous Progress: Managing the Hazards of Technology*. Boulder, CO: Westview Press.
- Kim, K., and S. Ventura. 1993. Large-scale modeling of urban nonpoint source pollution using a geographic information system. *Photogrammetric Engineering and Remote Sensing* 59(1), 1539-1544.
- Langdon, D., and S. Barnes. 1995. From pushpins to GIS: Insurance industry turns to digital mapping. *Geo Info Systems* 5(9), 52-54.
- Lee, J.K., et al. 1992. Application of geoprocessing and simulation modeling to estimate impacts of sea-level rise on the northeast coast of Florida. *Photogrammetric Engineering and Remote Sensing* 58(11), 1579-1586.
- Lepofsky, M., M. Abkowitz, and P. Cheng. 1995. Transportation hazard analysis in an integrated GIS environment. In G.E.G. Beroggi, and W.A. Wallace (eds.), *Computer Supported Risk Management*, pp. 115-131. Dordrecht, The Netherlands: Kluwer.
- Levine, D. A., et al. 1993. *A geographic information system approach to modeling nutrient and sediment transport*. Environmental Sciences Division, Publication No. 3993. Oak Ridge, TN: Oak Ridge National Laboratory.
- Matthews, K.B., et al. 1994. Climatic soil moisture deficit - climate and soil data integration in a GIS. *Climatic Change* 28, 273-287.
- McMaster, R., and J. Johnson. 1987. Assessing community vulnerability to hazardous materials with a geographic information system. *Proceedings, AUTO CARTO 8*, pp. 471-480. Bethesda, MD: American Congress on Surveying and Mapping (ACSM) and American Society for Photogrammetry and Remote Sensing (ASPRS).
- Mejia-Navarro, M., and E.E. Wohl. 1994. Geologic hazard and risk evaluation using GIS: Methodology and model applied to Medellin, Colombia. *Bulletin of Association of Engineering Geologists* 31(4), 459-481.
- Mertz, T. 1993. GIS targets agricultural nonpoint pollution. *GIS World* 6(4), 41-43, 46.
- Mettel, C. 1992. GIS and satellite images provide precise calculations of probable maximum flood. *Geo Info Systems* 2(5), 44-48.
- Moore, T.J. 1993. Managing the risks from air toxics. *Geo Info Systems* 3(2), 42-50.
- Moreno, D.D., and L.A. Heyerdahl. 1991. GIS tools for contaminated site remediation: The Bunker Hill Superfund site. *Proceedings, GIS/LIS '91*, Vol. 1, pp. 21-30. Bethesda, MD: American Congress on Surveying and Mapping (ACSM) and American Society for Photogrammetry and Remote Sensing (ASPRS).
- Moreno, D.D., and L.A. Heyerdahl. 1992. GIS helps revegetation efforts at hazardous waste site. *Geo Info Systems* 2(4), 46-51.

- Norton, D.J., and E.T. Slonecker. 1990a. The Environmental Monitoring and Assessment Program's landscape characterization data base: New opportunities in spatial analysis. *Proceedings, GIS/LIS '90*, Vol. 2, pp. 682-690. Bethesda, MD: American Congress on Surveying and Mapping (ACSM) and American Society for Photogrammetry and Remote Sensing (ASPRS).
- Norton, D.J., and E.T. Slonecker. 1990b. The ecological geography of EMAP. *Geo Info Systems* 1(10), 33-43.
- NRC (National Research Council). 1983. *Risk assessment in the federal government: Managing the process*. Washington, D.C.: National Academy Press.
- Nuclear Regulatory Commission. 1975. *Reactor safety study*. WASH-1400. NUREC 75/014. Washington, D.C.: U.S. Nuclear Regulatory Commission.
- Padgett, D.A. 1992. Assessing the safety of transportation routes for hazardous materials. *Geo Info Systems* 2(2), 46-48.
- Palm, R., and M. Hodgson. 1992. *After a California earthquake: attitude and behavior change*. Geography Research Paper No. 233. Chicago: The University of Chicago Press.
- Pearson, E., et al. 1991. Mapping natural hazards with spatial modeling systems. In P. Harts, H.F.L. Ottens, and H.J. Scholten (eds.), *Proceedings, 2nd European Geographic Information Systems (EGIS) Conference, EGIS 91*, Vol. 2, pp. 847-855. Utrecht, The Netherlands: EGIS Foundation, Faculty of Geographical Sciences.
- Pearson, E., et al. 1992. An integrated expert system/GIS approach to modeling and mapping natural hazards. In P. Harts, H.F.L. Ottens, and H.J. Scholten (eds.), *Proceedings, 3rd European Geographic Information Systems (EGIS) Conference, EGIS '92*, Vol. 1. 762-771. Utrecht, The Netherlands: EGIS Foundation, Faculty of Geographical Sciences.
- Peckham, R.J. 1993. Linking GIS and MCDA to manage Lombardy's industrial waste. *Geo Info Systems* 3(6), 46-50.
- Petak, W.J., and A.A. Atkisson. 1982. *Natural hazard risk assessment and public policy: Anticipating the unexpected*. New York: Springer-Verlag.
- Quarantelli, E.L. 1992. *Some aspects of disaster planning in developing countries*. Prepared for the Workshop on Integrated Approach to Disaster Management and Regional Development Planning with People's Participation held in Dhaka, Bangladesh, January 28-February 1, 1990. Reprinted as Article # 247. Delaware: Disaster Research Center, University of Delaware.
- Rayner, S. 1986. Management of radiation hazards in hospitals: plural rationalities in a single institution. *Social Studies of Science* 16, 573-591.
- Rayner, S., and R. Cantor. 1987. How fair is safe enough? The cultural approach to societal technology choice. *Risk Analysis* 7(1), 3-13.
- Rejeski, D., and J. Kapuscinski. 1990. *Risk Modeling with Geographic Information Systems: Approaches and Issues*. Washington, D.C.: U.S. Environmental Protection Agency, National GIS Program (unpublished manuscript).
- Rejeski, D. 1993. GIS and risk: A three culture problem. In D. Goodchild, B.O. Parks, and L.T. Steyaert (eds.), *Environmental Modeling with GIS*, pp. 318-331. New York: Oxford University Press.
- Richason, B.F. III, and J. Johnson. 1988. GIS application in landfill citing processing. In *Proceedings, GIS/LIS '88*, Vol. 2, pp. 695-703. Bethesda, MD: American Congress on Surveying and Mapping (ACSM) and American Society for Photogrammetry and Remote Sensing (ASPRS).
- Rifai, H.S., C.J. Newell, and P.B. Bedient. 1993. GIS enhances water quality modeling. *GIS World* 6(8), 52-55.
- Rojahn, R.L. 1985. *Earthquake damage evaluation data for California, ATC-13*. Redwood City, CA: Applied Technology Council.
- Rosenfeld, C. 1994. Flood hazard reduction: GIS maps survival strategies in Bangladesh. *Geo Info Systems* 4(5), 29-37.

- Runyan, T., and R. Hammitt. 1994. Buried danger: Integrating GIS and GPS to identify radiologically contaminated sites. *Geo Info Systems* 4(2), 28-36.
- Russell, M., and M. Gruber. 1987. Risk assessment in environmental policy-making. *Science* 236, 286-290.
- Samsel, T.B., and C.E. Colten. 1988. Surface hydrology and the accumulation of hazardous materials on the American bottoms, 1890-1990. *Proceedings, GIS/LIS '88*, Vol. 2, pp. 861-866. Bethesda, MD: American Congress on Surveying and Mapping (ACSM) and American Society for Photogrammetry and Remote Sensing (ASPRS).
- Slovic, P. 1987. Perception of risk. *Science* 236, 280-285.
- Sivertun, A., et al. 1988. A GIS method to aid in non-point source critical analysis. *International Journal of Geographical Information Systems* 2(4), 365-378.
- Soeters, R., and C.J. van Westen. 1994. Slope instability: The role of remote sensing and GIS in recognition, analysis, and zonation. In G. Wadge (ed.), *Natural hazards and remote sensing*, pp. 44-50. London: The Royal Society.
- Souleyrette II, R.R., and S.K. Sathisan. 1994. GIS for radioactive materials transportation. *Microcomputers in Civil Engineering* 9(4), 295-303.
- Speed, V. 1994. GIS and satellite imagery take center stage in Mississippi flood relief. *Geo Info Systems* 4, 40-43.
- Stallones, L., J.R. Nuckols, and J.K. Berry. 1992. Surveillance around hazardous waste sites: Geographic information systems and reproductive outcomes. *Environmental Research* 59, 81-92.
- Stewart, J.C., K.L. Martin, and A.R. Jennetta. 1993. U.S. Department of Energy uses GIS to evaluate waste management alternatives. *Geo Info Systems* 3(7), 60-63.
- Stockwell, J., et al. 1993. The U.S. EPA geographic information system for mapping environmental releases of toxic chemical release inventory (TRI) chemicals. *Risk Analysis* 13(2), 155-164.
- Sui, D.Z., and J.R. Giardino. 1995. Applications of GIS in environmental equity analysis: a multi-scale and multi-zoning scheme study for the city of Houston, Texas, USA. In *Proceedings, GIS/LIS '95*, Volume 2, pp. 950-959. Bethesda, MD: American Congress on Surveying and Mapping (ACSM) and American Society for Photogrammetry and Remote Sensing (ASPRS).
- Thompson, M. 1980. *An outline of the cultural theory of risk*. IIASA WP-80-177. Laxenburg, Austria: International Institute for Applied Systems Analysis.
- Towers, A., and B.M. Gittings. 1995. Earthquake monitoring and prediction: A case study of GIS integration using the Internet. in, P.F. Siher (ed.), *Innovations in GIS* 2, pp. 233-244. London, UK: Taylor and Francis.
- van Westen, C.J., et al. 1992. *UNESCO-ITC project on mountain hazard mapping in the Andean environment, using geographical information systems, 2 parts*. Paris: United Nations Educational, Scientific, and Cultural Organization (UNESCO) and Enschede, The Netherlands: International Institute for Aerospace Survey and Earth Sciences.
- Van Zee, C., and J.E. Lee. 1988. Hazardous waste disposal site selection using interactive GIS technology. *Proceedings, AUTO CARTO 9*, pp. 391-396. Bethesda, MD: American Congress on Surveying and Mapping (ACSM) and American Society for Photogrammetry and Remote Sensing (ASPRS).
- Vincent, P., et al. 1988. Emergency planning with geographic information systems. *ESRC Newsletter* 63 (October), 20-23.
- von Braun, M. 1984. *Geographic information systems in the analysis of a hazardous waste site*. EPA 68-03-3210. Cincinnati, Ohio: U.S. Environmental Protection Agency, Hazardous Waste Engineering Research Laboratory.
- von Braun, M. 1986. Use of a geographic information system for site characterization and predictive modeling at the Western Processing Site, Kent, Washington. in *Proceedings of the Geographic Information Systems for Environmental Protection Workshop*, Las Vegas, 22-23 January 1986. Las Vegas: Environmental Research Center.

- von Braun, M. 1993. The use of GIS in assessing exposure and remedial alternatives at Superfund sites. In D. Goodchild, B.O. Parks, and L.T. Steyaert (eds.), *Environmental Modeling with GIS*, pp. 339-347. New York: Oxford University Press.
- Welebny, R.J. 1993. After Andrew I need a map that shows..... *Photogrammetric Engineering and Remote Sensing* 59(1), 45-47, 50-51, 54-56.
- Wilson, J.D. April 1995. Midwest's great floods of '93 spawns new floodplain management actions. *Earth Observation Magazine* 18-22.
- Zeigler, D.J., et al. 1983. *Technological hazards*. Washington, D.C.: American Association of Geographers.
- Zimmerman, R. 1993. Social equity and environmental risk. *Risk Analysis* 13(6), 649-666.



## ***Exercise 1: Mapping and Assessing Natural Hazards in Ecuador, South America***



## Introduction

While natural hazards affect all countries, developing countries are particularly vulnerable to such hazards. In Africa, thousands of lives have been lost to drought and famine. Two earthquakes struck northeast Ecuador in March 1987, causing over 1,000 deaths and damages of about \$1 billion (NRC, 1991). In 1993, an earthquake in the state of Maharashtra, India, claimed over 9,000 lives and injured more than 10,000 (IFRCCS, 1994). To reduce this vulnerability of developing countries to natural hazards, strategies for disaster mitigation and preparedness are being emphasized. Geographic Information Systems (GIS) can play a prominent role in the development and implementation of these strategies (OAS, 1991).

This introductory exercise to the workbook reviews some fundamental techniques in GIS for assessing natural hazards. The exercise is divided into two sections. The first section illustrates the concepts of Boolean maps and Boolean analysis in analyzing data on natural hazards. The second section illustrates the role of GIS in all-hazards assessment. An all-hazards assessment determines the risk to a location from several natural hazards as opposed to a single hazard. The data used in the exercise depict three natural hazards, earthquakes, drought, and soil erosion, for a part of Ecuador, South America.<sup>1</sup>

- a) First, open IDRISI and under the File menu, select IDRISI Explorer. Then select its Projects tab. This option allows you to set the project environment of your file folders. Make sure that the Editor pane is open at the bottom of the form. If you right-click anywhere in the Projects form, you can select to show the Editor. The Editor pane shows the Working and Resource folders. Choose to either create a new project or edit the existing project to include the folder holding the data for this exercise, (e.g., c:\UNITAR\Hazards\Data\Exercise\_1). Please note that this folder must be listed as either the main Working folder or one of the Resource folders. Then open the User Preferences dialog from the File menu and click on the Revert to Defaults button, then click OK. This will turn on the automatic display of module output with legend and title options.
- b) To view the first image, SEISMIC, click on the Display menu and choose DISPLAY Launcher. You could also do this more directly by clicking on the icon with a world map. Click the browse button at the right side of the file input box or double-click in the input box to bring up the pick list. Select the file SEISMIC. Choose the user-defined palette option and select RISK as the palette file from the pick list. Click OK to display the image.<sup>2</sup>

SEISMIC shows areas at different levels of earthquake risk, as defined by the Modified Mercalli Index (MMI), for the part of Ecuador for which data are available. The MMI is an index of ground shaking intensity that relates ground shaking during an earthquake to the effect on people and buildings. In the Index, the levels I to VI represent *low* risk, VII to IX represent *moderate* risk, and X to XII represent *high* risk. The MMI levels in this part of Ecuador range from V to X. The distribution of the levels follows mostly an east to west orientation, with the eastern part at low risk and the central and western parts at moderate to high risk. The coastal regions of the country located in the western part (see the figure on the title page of this chapter) have an MMI level of VIII, placing them at moderate earthquake risk.

- c) Close the image SEISMIC. Open DISPLAY Launcher again and select the image DROUGHT to be displayed. Indicate that you will use a user-defined palette and choose RISK as the palette file. Also indicate that you want to include a legend and a title, then click OK to display the image.

The image DROUGHT shows three areas of drought hazard in Ecuador: Low, Moderate, and High. As with earthquake risk, areas of moderate and high drought hazard are located in the central and western sections of the area captured by the data. Much of the coastal region is associated with moderate drought hazard.

- d) Close the image DROUGHT and display the image EROSION using the Qualitative palette, a title, and a legend.

---

1. These data are part of a larger database generated and published by the Ministry of Agriculture, Ecuador, through a technical cooperation program with the Department of Regional Development and Environment, Organization of American States (OAS).

2. Unless otherwise specified, use the default options for any parameters not specifically mentioned.

The image EROSION shows three areas: 'No Erosion', 'Under Erosion', and 'Potential Erosion'.

## Analyzing Natural Hazards

The analysis of data in a GIS context can range from simple analytical operations such as database query to the use of complex models which simulate phenomena in the natural environment. In this section, some of the simple analytical operations in GIS are reviewed.

One operation that is often carried out in a GIS context is database query by attribute which asks: At which locations is a particular attribute found? In the case of drought hazard in Ecuador, this might be: At which locations is there a high drought hazard? This involves creating a new image from DROUGHT which shows only areas of high drought hazard. In DROUGHT, the value 1 refers to areas of low drought hazard, the value 2 refers to areas of moderate drought hazard, and the value 3 refers to areas of high drought hazard. To retain only the areas of high drought hazard in the new image, we will assign the value 0 to the values 1 and 2 in DROUGHT, and the value 1 to the value 3. This process is called reclassification since it reclassifies the original values into new values. It is carried out in IDRISI with the RECLASS module.

- e) Run the module RECLASS from the GIS Analysis/Database Query menu. Use the default user-defined reclassification option and specify DROUGHT as the input image and HIGHDR as the output image. Assign a new value of 0 to all values ranging from 1 to those just less than 3. Assign a new value of 1 to all values ranging from 3 to those just less than 4. Click OK to run the RECLASS module. IDRISI will display HIGHDR when the module has finished running. HIGHDR is known as a Boolean image since it has only two values, 1 and 0. The value 1 shows areas of high drought hazard and the value 0 shows all the other areas.

There is a second approach to database query by attribute in IDRISI which is used here for finding areas under erosion in Ecuador. Instead of reclassification, we will use the module ASSIGN to *assign* new values to the existing values in EROSION using the identifiers of the features in this image. ASSIGN requires an attribute values file in which the first column contains the existing values in EROSION and the second column contains the new values to be assigned. Any existing values which are not specified are automatically assigned the new value 0. In this case, we will first create with the Edit module an attribute values file with only one row. The first number in this row will be the feature identifier of areas under erosion, which is 2.<sup>3</sup> The second number in the row will be 1, the new value for the areas under erosion. We will then assign the attribute values file to EROSION with the ASSIGN module. The resulting image will be a Boolean image with the value 1 for areas under erosion and 0 elsewhere. Since the remaining two features in EROSION, areas with no erosion and areas with potential erosion, are not specified in the attribute values file, the values for these features in the new image will be automatically set to 0.

- f) Open the module Edit from the GIS Analysis/Database Query menu. Enter the following numbers, separated by one space:

2 1

From the File menu in Edit, choose Save as... Enter the filename UNDER. Save as an Attribute values file and click the Save button. You will be prompted to choose a data type for the new file. Click OK to accept the default option of Integer and Close Edit.

- g) Run ASSIGN from the GIS Analysis/Database Query menu. Specify EROSION as the feature definition image, UNDER as the attribute values file, and UNDER as the output image. The resulting image will be displayed with the Qualitative palette.

Both RECLASS and ASSIGN can often be used in the same situation. However, there are some important distinctions that may guide your choice. With RECLASS, ranges of values may be assigned new values and any values not specifically

---

3. If you would like to confirm this, use Metadata from IDRISI Explorer to view the documentation file for EROSION.

included will remain unchanged. With ASSIGN, each individual value must be specified and any that are not will be automatically assigned the value of 0.

## Boolean Hazard Analysis

We have called GIS-based hazard analysis involving Boolean maps "Boolean hazard analysis". One type of this analysis may involve a compound database query such as: *What are the areas of high drought hazard that are under erosion?* To identify such areas, we need to combine an image of the areas of high drought hazard with an image of areas under erosion. In the last section, we developed these images as HIGHDR and UNDER respectively. Since these are both Boolean images, we will use a mathematical technique called Boolean algebra to combine the images. Boolean algebra is based upon logical operators such as AND and OR. The mathematical operation to invoke the logical operator AND is multiplication, and to invoke the logical operator OR is addition. Since we are interested in areas of high drought hazard *and* areas under erosion, we will use the logical operator AND. We will therefore multiply the two Boolean images HIGHDR and UNDER. The table below shows that multiplication is the mathematical operation with which to invoke the logical operator AND.

First image	Second image	Output image
HIGHDR	UNDER	HIGHDR*UNDER
0	0	0
1	0	0
0	1	0
1	1	1

- h) The OVERLAY module will be used for multiplying HIGHDR and UNDER. Run the module OVERLAY. Specify the first image as HIGHDR, the second image as UNDER, and the output image as BOTHRISK. Select the multiply option (First \* Second). Click OK to run the module. The image will be displayed when the module has finished running.

BOTHRISK is a Boolean image, with the value 1 showing areas of high drought hazard that are under erosion, and the value 0 showing all other areas. The image shows that for this part of Ecuador many of the areas of high drought hazard are also under erosion.

Boolean hazard analysis may also combine Boolean with non-Boolean images. For example, we could identify the types of crops cultivated within the areas of high drought hazard. To address this query, we need an image of crop cultivation and an image of the high drought hazard areas. The image of crop cultivation in this part of Ecuador is called CROPS.

- i) Display CROPS with the Qualitative palette.

CROPS shows the distribution of three types of crops cultivated in Ecuador: strategic crops, export crops, and basic crops. Strategic crops cultivated in Ecuador include cotton, tea, African palms, and hemp. Export crops consist of bananas, cocoa, coffee, and sugar. Basic crops include rice, corn, and wheat.

To find the crops cultivated in high drought hazard areas, we will combine CROPS with HIGHDR using the OVERLAY module and the multiplication option.

- j) Run OVERLAY. Multiply the first image CROPS with the second image HIGHDR. Specify the output image as CROPDR.
- k) Display CROPDR using the Qualitative palette. There are no descriptive legend captions for this image. To update the legend, we will use Metadata in IDRISI Explorer. From the Files tab in IDRISI Explorer, select the

file CROPDR. If the Metadata pane is not in view at the bottom of the form, right-click anywhere in IDRISI Explorer and check that Metadata is selected. Then, scroll through Metadata and double-click on the Categories option in Metadata to update the legend. In the Categories form, click the button Copy from. Pick the file CROPS on the list that appears. The code and caption of the legend will be filled in. Close and save the changes. Redisplay the image.

1. *What are the different types of crops cultivated in the high drought hazard areas?*

## Calculating Area

Almost all GIS include an analytical component for calculating area. For example, one might be interested in finding the area used for different types of crops in the high drought hazard zone. In IDRISI, this can be determined with the AREA module.

- l) Run the module AREA from the GIS Analysis/Database Query menu and specify the input image as CROPDR. Select tabular as the output format and calculate the area in acres. Click OK. The area in acres used for different types of crops in the high drought hazard zone will appear on the screen. The first column of numbers represents the legend categories in the image. The second column shows the area for each legend category. The first three columns in the table below show these results:

Legend category	Crop type	Area in high drought hazard zone (acres)	Total area (acres)
1	(No crops cultivated)	31,553	--
2	Strategic	28,872	
3	Export	15,617	
4	Basic	5,233	

2. *Calculate the total area used for each crop type from CROPS and enter it into the last column in the table above. Which type of crop has the highest proportion of cultivated area in the high drought hazard areas?*

## All-Hazards Assessment

This section illustrates the use of GIS in *all-hazards* assessment. An all-hazards assessment would identify areas in Ecuador that are at risk from multiple hazards as opposed to a single hazard. An all-hazards assessment has several advantages. For example, such an assessment would benefit planners and decision-makers who can recommend a common set of measures for mitigating the impacts from a range of hazards (OAS, 1991; NRC, 1994). Landuse regulations, building codes and standards, and emergency planning and response developed for mitigation purposes can apply to multiple hazards.

A GIS is particularly well suited for all-hazards assessment because of the ease with which it can combine and overlay different types of data on hazards. Since not much research has been carried out in this area, there are no clear guidelines on how to conduct an all-hazards assessment using GIS. OAS (1991: 6-5) has suggested that a simple all-hazards assessment may depict three elements of multiple hazards on one map: location, likelihood of occurrence (or frequency of return period), and severity. Godschalk and Brower (1985) suggest a focus on vulnerability, expressed as the probable damage to resources that would occur from the multiple hazards in a location.

Since data on likelihood of occurrence and vulnerability are not available for the study area, the all-hazards assessment in this exercise will focus on depicting location and severity. The areas depicting these elements are those at high risk from earthquakes, subject to high drought hazard, and are under erosion. The logic of Boolean algebra can be used in the assessment since each of the input images is a Boolean image. The Boolean images for areas of high drought hazard and

areas under erosion were developed and combined in the last section into the Boolean image called BOTHRISK. The Boolean image for areas of high earthquake risk needs to be developed. Recall that the areas of high earthquake risk in Ecuador are those with the value of 6 (depicting an MMI value of X). Therefore, you can use RECLASS to create the Boolean image showing areas of high earthquake risk.

- m) Run RECLASS. Specify the image to be reclassified as SEISMIC. Call the new image HIGHER. Opt for user-defined reclassification and indicate that you wish to:

Assign a new value of: 0

to all values ranging from: 1

to just less than: 6

Continue by indicating that you will:

Assign a new value of: 1

to all values ranging from: 6

to just less than: 7

HIGHER is a Boolean image with the value 1 showing areas of high earthquake risk. There is only one small area in the center of the image that is at high risk to earthquakes.

3. *Describe an approach other than RECLASS to create HIGHER.*

For the all-hazards assessment, we must combine HIGHER and BOTHRISK. This is a Boolean operation involving the logical operator AND. We can therefore use OVERLAY with the multiplication option.

- n) Run OVERLAY and specify that you want to multiply the first image HIGHER with the second image BOTHRISK to create the output image ALLHAZ.

- o) Display ALLHAZ with the Qualitative palette.

The image ALLHAZ shows the area identified by the all-hazards assessment, that is, the area which has high earthquake risk, high drought hazard, and is under erosion. In this case, only a few small areas in Ecuador are shown to be at high risk for all three types of natural hazards.

4. *Assume that planners would like the all-hazards assessment to identify areas of moderate to high (according to the MMI) earthquake hazard, moderate to high drought hazard, and under erosion. Find such areas in Ecuador using the images provided with this exercise.*

5. *What are the different types of crops cultivated in the areas identified in the all-hazard assessment in Question 4? What is the area (in acres) occupied by the crops?*

## Conclusions

This exercise reviewed some of the fundamental techniques in GIS for analyzing data on natural hazards. The concepts of Boolean images and Boolean analysis were introduced as part of this review. The exercise also explored how GIS can be used in all-hazards assessment. Because of its capabilities for combining different types of data, GIS offers exciting opportunities in all-hazards assessment for both researchers and practitioners. For example, guidelines on conducting all-hazards assessment with GIS can be developed by researchers based upon the needs of practitioners.

## References

- Godschalk, D.R., and D.J. Brower. 1985. Mitigation strategies and integrated emergency management. *Public Administration Review* 45 (special edition): 64-71.
- IFRCCS (International Federation of Red Cross and Crescent Societies). 1994. *World disasters report*. Dordrecht, The Netherlands: Kluwer Publishers.
- NRC (National Research Council). 1991. *The March 5, 1987, Ecuador earthquakes: mass wasting and socioeconomic effects*. Washington, D.C.: National Academy Press.
- NRC (National Research Council). 1994. *Facing the challenge: the U.S. national report to the IDNDR World Conference on natural disaster reduction, Yokohama, Japan, May 23-27, 1994*. Washington, D.C.: National Academy Press.
- OAS (Organization of American States). 1991. *Primer on natural hazard management in integrated regional development planning*. Washington, D.C.: Department of Regional Development and Environment, Organization of American States.

## ***Exercise 2: Assessing Socioeconomic Vulnerability to Extreme Storms and Associated Flooding***



Revere Beach, Massachusetts, circa 1920



## Introduction

In this exercise, we will assess socioeconomic vulnerability to a natural hazard at the community level. The hazard under consideration is an extreme storm called the *nor'easter*. Nor'easters affect coastal communities in the eastern part of the United States during the winter months of November to April. They derive their name from the prevailing wind pattern which places the track of the storms North to Northeast along the Atlantic seaboard of the United States. Nor'easters often reach their greatest intensity as they pass through states such as Massachusetts located in the northeastern United States.

The damages to coastal communities from nor'easters occur as a result of high winds, storm surge, and flooding associated with high tides. The impacts include: property damage, loss of business, costs of emergency response and cleanup, injuries, and in some cases even fatalities. Assessing socioeconomic vulnerability to these storms is important since it may help identify strategies for mitigating the impacts of the storms. For example, emergency planning and response activities in coastal communities can be targeted at groups vulnerable to the storms (such as the elderly living in shore-front houses). In this exercise, we focus on assessing the socioeconomic vulnerability of a coastal community, Revere, located just north of the city of Boston in the state of Massachusetts. The methodology adopted in the exercise is drawn from Emani and colleagues (1993).<sup>1</sup>

Vulnerability is defined here as *the differential susceptibility, in a general sense, among social groups and locations to suffer losses from hazards* (Dow, 1993). It is composed of three dimensions: (1) exposure or the likelihood of suffering losses from a hazard; (2) resistance or the ability to withstand the impacts of a hazard; and (3) resilience or the ability to recover from the impacts of a hazard. Each of these dimensions, in turn, are defined through individual factors. For example, exposure to a hazard is determined by the types of landuse (such as residential, industrial, or agricultural) in a community. Similarly, the ability to withstand the impacts of a hazard (resistance) is associated with socioeconomic factors such as age, ethnicity, and income. The elderly and the poor are less likely to be able to withstand the impacts of a hazard as opposed to the younger and the rich (Drabek and Key, 1984). Table 2.1 shows the three dimensions of vulnerability and some of the factors that compose each dimension.

Table 2.1. Dimensions of vulnerability and some component factors

Exposure	Resistance	Resilience
Landuse	Age	Size of housing unit
Lifelines (electricity networks, transportation networks, and so forth)	Income	Income
Flood hazard zones	Ethnicity	Disaster insurance
Elevation	Structural integrity of buildings	Emergency management practices

Both physical factors (for example, flood hazard zones and elevation) as well as socioeconomic factors (for example, age and ethnicity) are included in our definition of vulnerability. The focus of this exercise, however, is on using GIS to assess and map socioeconomic factors of vulnerability. At the same time, the exercise will also illustrate the capability of GIS in developing composite indices of vulnerability to natural hazards at the community level. To develop such composite indi-

---

1. The data used in this exercise were collected as part of a research project, "Assessing Socioeconomic Vulnerability of Coastal Communities to Extreme Storm Events and Sea-level Rise," supported by the Northeast Regional Center of the National Institute for Global Environmental Change (NIGEC), Harvard University. The editor is grateful to Dr. Samuel J. Ratick, Associate Professor at Clark University and Principal Investigator for the project, for donating the data for the exercise.

ces, socioeconomic factors must be combined with physical factors. Therefore, flood hazard zones are included in the exercise to represent the physical component of vulnerability.

The exercise is divided into two sections. The first section focuses on the exposure dimension of vulnerability. In this section, two factors capturing exposure, flood risk zones and landuse, in the community of Revere are described. These two types of data are then combined to produce a map of exposure to nor'easters in Revere. The second section of the exercise focuses on the dimension of resistance. In this section, data from the United States Bureau of Census are used to assess and map socioeconomic factors of vulnerability in Revere. These data are then combined with data on flood hazard zones to yield a composite index of vulnerability to nor'easters for the community.<sup>2</sup>

## ***Exposure to Nor'easters***

### **FEMA Flood Risk Zones**

The risk from flooding associated with extreme storms such as nor'easters has been determined for the community of Revere by the United States Federal Emergency Management Agency (FEMA). As part of its National Flood Insurance Program (NFIP), FEMA has developed a Flood Insurance Rate Map (FIRM) for Revere. The FIRM shows areas at different levels of risk from flooding with a focus on areas at risk from a hundred-year (100-Y) flood (FEMA, 1992). A 100-Y flood is defined as a flood level with a one percent or greater chance of being equaled or exceeded in any given year. The areas at risk from a 100-Y flood are determined through statistical analysis of historical records, topographic surveys, and hydrologic and hydraulic analysis (FEMA, 1992).

- a) Using IDRISI Explorer, change your Working folder to that holding the data for this exercise, (e.g., \UNITAR\Hazards\Data\Exercise\_2).
- b) Use DISPLAY Launcher to view REVFIRM, an image of the flood risk zones in Revere. Select the user-defined palette FIRM and choose to display a legend and title. The image as displayed does not show the location of either the coast or the estuaries in this coastal community. In Composer, choose Add Layer and specify COAST as the vector layer to be added. Use the Uniform White symbol file.

The legend for REVFIRM can be interpreted as follows:

- |   |   |
|---|---|
| A | Areas at risk from 100-Y flood.   |
| B | Areas between 100-Y and 500-Y flood. Risk from flooding is moderate.                            |
| C | Areas at minimal risk.  |
| V | Areas along coast at risk from 100-Y flood with additional risks due to Velocity (wave action). |

As expected, the areas at risk from both a 100-Y flood and wave action (the V areas) fall right on the coastline for Revere. The areas at risk from only a 100-Y flood (the A areas) are in close proximity to the coast and the estuaries. However, not all areas which are proximate to the coast and estuaries are at risk from a 100-Y flood. For example, in the southeastern section of Revere, there is an area of minimal risk (C area) near the coast. This section is at a higher elevation making it less vulnerable to flooding. In general, the areas at minimal risk from flooding are located in the interior of the community and away from the coast.

Both the A and V zones can be considered as areas in Revere at *High* risk to flooding during nor'easters. The B zone is at *Moderate* risk whereas the C zone is at *Minimal* risk. Using this classification, we will assess exposure to flooding associated

---

2. The third dimension of vulnerability, resilience, is not included in the exercise. Many of the factors comprising resistance are also factors of resilience. For other factors, such as disaster insurance and emergency management practices, data are either not available or are in a nonspatial form.

with nor'easters in Revere. To do this, we will first create an image containing the areas in Revere at high risk during nor'easters. Next, we will create an image of three types of landuse in Revere: commercial, industrial, and residential. These three landuses were selected for exposure assessment because they are most clearly associated with the socioeconomic impacts of flooding during nor'easters. Finally, we will combine the two images to determine exposure.

c) Run RECLASS and specify REVFIRM as the image to reclassify. Call the output image HIGHRISK. Specify a new value of 1 for all values ranging from 1 to those just less than 2. Continue by specifying a new value of 0 for the values ranging from 2 to those just less than 4. Specify a new value of 1 for the values ranging from 4 to those just less than 5. Click OK.

d) Display HIGHRISK with the user-defined palette FIRM. Choose Add Layer and specify COAST using the Outline White symbol file.

1. *What kind of image is HIGHRISK? What do the areas with value 1 represent? What do the areas with value 0 represent?*

### Landuse in Revere

e) Display REVLUSE with the Qualitative palette. This is an image of landuse in Revere. Again, use Add Layer and select COAST with the Uniform White symbol file. Then use Cursor Inquiry Mode from the toolbar to explore the different landuses in this community.

2. *What is the dominant landuse in this community? What are the landuses near the coast?*

3. *What are the categories in REVLUSE for the following landuses? Enter the values in the table below.*

Landuse	Category value
Residential	
Commercial	
Industrial	

For assessing exposure, we are interested in residential, commercial, and industrial landuses. To create an image of only these three landuses, we will assign new values to the categories for these landuses in REVLUSE. To do this, we will first use the Edit module to create an attribute values file with the new and old values. Then, we will use the ASSIGN module to assign the values file to REVLUSE. This approach is faster in this case than using RECLASS.

f) Use the module Edit to create a new values file. The first column of numbers in the values file should contain the original category numbers in REVLUSE for the three landuses (from the table above). The second column should contain the new values which need to be assigned to the original categories. Enter the following values, separated by one space, into the new file:

6 1

8 2

9 3

Choose Save As from Edit's File menu. Specify the name of the file as LUSE and the type as an Attribute Values File. Save the file. Accept the default integer data type, and close Edit.

- g) Run the module ASSIGN. Specify REVLUSE as the feature definition image, LUSE as the attribute values file, and LANDUSE as the output image. Click OK.
- h) The legend for LANDUSE needs to be updated. Open Metadata from IDRISI Explorer for the image LANDUSE. Double-click on the Categories option and add three legends. Enter the numbers 1, 2, and 3 for the codes. Change the entry for the Code 1 caption to RESIDENTIAL. Repeat this process to change the second legend category to COMMERCIAL, and the third legend category to INDUSTRIAL. When you are finished, save the change.

LANDUSE shows the patterns of the three landuses in Revere. The other landuses were automatically assigned a value of 0 as they were not specified in the attribute values file. Residential landuse is most subject to exposure followed by commercial landuse.

## Assessing Exposure

We now have two images: HIGHRISK, which shows areas of high risk to flooding, and LANDUSE, which shows the three landuses associated with socioeconomic impacts of flooding. To assess exposure, we will combine these two images. Since HIGHRISK is a Boolean image, we can use the logic of Boolean algebra here. As we are interested in the landuses falling in the high risk areas, we want to use the Boolean AND operator. To invoke this operator, we simply multiply the two images, HIGHRISK and LANDUSE. We will do this using the OVERLAY module.

- i) Run OVERLAY and choose the multiplication option. Specify HIGHRISK as the first image, LANDUSE as the second image, and call the output image EXPOSURE. When finished, display EXPOSURE using the Qualitative palette. You may wish to update the legend categories. To do this, open Metadata and double-click on the Categories option. Choose to copy the legend from another file. Select the image LANDUSE. The legend for EXPOSURE will be updated. Save the changes.

EXPOSURE shows the spatial distribution of the three landuses in the high risk areas. The landuse most exposed to flooding is residential landuse. To verify this, we will calculate the area occupied by the three landuses.

- j) Open the module AREA. Specify EXPOSURE as the input image and select the tabular output in acres.
4. *What is the area (in acres) of residential, commercial, and industrial landuses in Revere exposed to high risk from flooding during nor'easters?*

In this section, the dimension of exposure was analyzed using data on landuse and FEMA flood risk zones. Through the application of the overlay technique, we identified the spatial patterns of three types of landuse in areas at high risk to flooding during nor'easters. We also used a tool in GIS to calculate the area of each landuse that was exposed. This analysis of exposure serves as the first step towards more detailed assessments of socioeconomic vulnerability. In the case of Revere, for example, additional modeling to estimate the impacts of flooding can be conducted in the high risk areas identified by the exposure analysis since the impacts are likely to be the highest in these areas.

## Resistance to Nor'easters

In this section, we will rely on data available from the United States Bureau of Census to assess and map socioeconomic factors of vulnerability. Two types of census data for the community of Revere are available from the Census Bureau. These are *spatial* data on geographic features and *attribute* data on socioeconomic factors. We will describe these data types and their use in IDRISI, then illustrate how the two types of data can be combined to produce maps of resistance.<sup>3</sup> These individual maps of resistance are then combined using an index to produce an overall index of resistance. Finally, the maps of resistance are combined with the map of FEMA flood risk zones to show how the dimensions of exposure and

---

3. These maps are of the individual factors that comprise the dimension of resistance (see Table 2.1). For convenience, we will call these *maps of resistance*.

resistance can be integrated in a GIS-based vulnerability analysis.

## Spatial Data

The Census Bureau has developed a 1:100,000 scale digital cartographic database for the United States called TIGER (Topologically Integrated Geographic Encoding and Referencing System) (Bureau of Census 1991). TIGER contains digital data used to define all the census features in the 1990 decennial census. These digital data include roads, railroads, and streams. In addition, TIGER contains feature names, Federal Information Processing Standard (FIPS) codes for census entities such as census blocks, census tracts, cities and townships, and address ranges and zip codes for streets in urban/metropolitan areas.

For assessing resistance to nor'easters in Revere, we selected a spatial census entity defined by the Census Bureau as a *block group*. A Block Group (BG) is a combination of census blocks within a census tract which have the same first digit in their identifying numbers.<sup>4</sup> For example, Block Group 3 within census tract 1703 is a collection of all the census blocks numbered 301 to 397. In most cases, the number of census blocks within a census tract is far fewer than 97. A block group has from 500 to 1,000 inhabitants. The block group level has been selected (as opposed to the census tract or census block level) since much of the attribute census data for assessing socioeconomic vulnerability is available at this level. For example, data on income is not released at the census block level for reasons of confidentiality and privacy.

The TIGER database does not have FIPS codes for block groups; it only has these codes for census blocks and census tracts. Therefore, in order to create a map of the block groups in Revere, we needed information on census blocks and census tracts in Revere. This data was obtained as an Arc/Info coverage from MassGIS, a statewide GIS agency for Massachusetts, which had extracted the data from TIGER. In Arc/Info, the information on census blocks and census tracts was used to create a field for block groups (since each block group is a collection of census blocks within a census tract with the same first digit in their identifier). The data on block groups was then converted from Arc/Info into IDRISI using the DLG module.

- k) From DISPLAY Launcher, display REVBGRP, the image of block groups in Revere, with the Qualitative palette. From Composer, add the vector layer BGROUPS, a vector file of the boundaries of the block groups, with the Uniform White symbol file.

5. *How many block groups are there in Revere?*

## Attribute Data

The attribute data for the 1990 census have been released by the Census Bureau in the form of Summary Tape Files (STF) (Bureau of Census, 1992b). For the block group level, the data are available in a file called Summary Tape File 3A (STF 3A). STF3A has attribute census data for over 100 variables pertaining to age, income, ethnicity, characteristics of housing units, etc. It is thus a powerful database for assessing socioeconomic vulnerability.

For the purpose of illustration, three attribute census variables have been selected as measuring resistance: (1) *age* (defined as the percentage of people older than 65 years); (2) *ethnicity* (defined as the percentage of people of Hispanic origin<sup>5</sup>); and (3) *poverty* (percentage of people with an annual income of less than \$20,000). People who are older, who are poor, and who are members of an ethnic minority group are less likely to be able to withstand and recover from the impacts of a

---

4. A census tract is a small, relatively permanent statistical subdivision of a county in a metropolitan area or a selected nonmetropolitan county, delineated for the purpose of presenting decennial census (Bureau of Census, 1992a). The boundaries of census tracts are usually major streets, natural features such as rivers, and corporate limits of the local government. A census tract contains between 2,500 and 8,000 inhabitants. A census block, on the other hand, is an area normally bounded on all sides by well-defined features such as streets, roads, streams, and railroad tracks. A census block usually contains about 250 to 500 households.

5. We could have selected people from other ethnic groups in this category (such as those of Asian origin), but chose not to do so for this illustration.

natural hazard (Bolin and Bolton, 1986; Dow, 1993; Drabek and Key, 1984). With nor'easters, for example, power outages are common in coastal communities because of the wind and ice conditions associated with such storms. During such power outages, it is the elderly who tend to be most vulnerable and are often the first to be evacuated to emergency shelters.

Data on these three resistance variables were retrieved from STF3A using a software package called EXTRACT developed by the Census Bureau. The data on population by block group in Revere was also retrieved from STF3A. Each of these data sets was extracted into an ASCII file, and then converted to an IDRISI attribute values file. These values files are called ELDER for number of people by block group older than 65 years, HISP for number of people of Hispanic origin, POOR for number of people with an annual income of less than \$20,000, and POPULAT for population by block group. We will first build an IDRISI database from these four values files, and then we will convert the three resistance variables to percentages by dividing each by the population data.

- l) Open Database Workshop from the Data Entry menu, or click on its toolbar icon. Database Workshop is the attribute database management system in IDRISI. As you can see, it has its own menu system and icon bar. To create the database, first go to the File menu in Database Workshop and choose New. Give the name REVERE as the database to create. Click Save. Now that the database exists, we need to populate it with data.
- m) The first field is typically the identifier field. In this case, the identifiers are the block group numbers. This field allows us to properly match up any attributes we might import with the correct block group, and will also allow us to link the attributes in the database with a spatial display. Records can be entered manually or automatically. We will enter them in automatically using the appropriate values files. From the File menu in Database Workshop choose Import/Table/from External File. Select Files of type Attribute Values files (.avl) and select POPULAT.AVL from the files listed and click Open. After the data is imported, save the database. Two fields are automatically created containing 44 records; an Identifier field containing the unique sequential IDs, and the attribute field Population containing the population by blocks. After import, the table name is POPULAT as well. From the Edit menu, select Rename table and rename the existing table to POPINFO. Save the database. We now need to add the additional fields to hold the attribute files ELDER, HISP, and POOR.
- n) We must first create new fields to hold the new variables. From the Edit menu of Database Workshop, choose Add Field. Choose integer, give the field name ELDER, and then click on OK. Save the database and repeat adding fields HISPANIC and POVERTY. Your database should now contain 5 fields -- the identifier field and four attribute fields, three of which are empty.
- o) To import the values files, use the File menu in Database Workshop and choose Import/Field/from AVL. Select the Attribute values file ELDER, the link field name IDENTIFIERS, and the data field name ELDER. Then click OK and save the database.
- p) Repeat the above procedure to import the values files HISP into the HISPANIC field, and POOR into the POVERTY field. Save the database after each step.

Now that we have imported the basic data values, we can calculate the percentage of the population that falls into each of our three resistance criteria. We will do this using the Database Workshop Calculate function.

- q) Choose Add Field from the Database Workshop Edit menu, and create the new field ELDERLY% with integer data type. (By choosing integer, we choose to automatically round the percentage to the nearest whole number.)
- r) From the Query menu, choose the Calculate Field Values command. This will open the structured query language (SQL) editor box.<sup>6</sup> The beginning of the SQL command is already written. It states that we are going to

---

6. SQL is a language common to many database management software systems. It allows for the creation of new data based on various calculations, as well as selective database query, which we will use later in the exercise.

update the database named REVERE by setting some field equal to some calculation. We will use the Fields tab to enter field names, the Arithmetic tab for arithmetic operators, and the Keypad tab to enter numbers. Click the cursor into the Editor box and enter the rest of the SQL command as follows:

```
SET [ELDERLY%] = [ELDER] / [POPULATION] * 100
```

Click OK, then Yes when warned that the operation will modify the database. The ELDERLY% field now contains the result of the calculation.<sup>7</sup>

- s) Repeat the process to create and fill the fields HISPANIC% and POVERTY%. We may now begin to make queries of the database, again using SQL. For example, we may want to find all the block groups that meet certain conditions. If we were to ask the question "Which block groups have populations with more than 50% of the people older than 65?", we could use SQL to quickly find the answer.
- t) To answer the above question, go to the Database Workshop Query menu and choose Filter Table. Again the SQL Editor comes up, but this time with a beginning which has the SELECT command instead of the CALCULATE command. It states that we will be selecting all the fields (indicated with “\*”) from POPINFO where certain conditions are met. Enter the SQL query as follows. (Use the Logic tab to enter the greater than sign.)

```
SELECT *
```

```
FROM popinfo
```

```
WHERE [ELDERLY%] > 50
```

Click OK. Note that only the one record that meets the condition is now displayed in the database. To return to the full database, choose Remove Filter from the Query menu. Leave the database file open.

Viewing the attributes and query results in the database is useful, but often what we really want to see are the spatial patterns of the data. To do this, we can link our spatial database (the map of block groups) with the attribute database we just created. The key to making this link is having a field in the database that has values that match the feature identifiers of the block groups in the vector file. In this case, the field IDENTIFIERS has block group values 1-44 and these values match the identifiers of the corresponding block group polygons in BGROUPS.

- u) In order to link the database REVERE to the image BGROUPS, we need to do two steps. First, we will make a new Vector Collection with BGROUPS. Second, we will establish a display link with that image. Open Collection Editor from the IDRISI File menu. Then, from Collection Editor's File menu, choose New and in the Files of type box, choose Vector Link files. Give your new file the name REVERE\_COLLECTION. Click Open. Choose BGROUPS for the vector spatial frame file. Choose REVERE as the database file. IDRISI will fill in the other boxes. Then select Save and close the Collection Editor.

From the IDRISI File menu, open DISPLAY Launcher. Choose to display a vector file, and pick the filename BGROUPS. You will see a file listed named REVERE\_COLLECTION in the IDRISI Explorer file list with a folder icon to its left. Click on the folder icon. Each of the images listed corresponds to a different field in the REVERE database. Display the layer in REVERE\_COLLECTION named IDENTIFIERS with the Qualitative symbol file. The block groups in Revere will be displayed.

Return focus to Database Workshop by clicking anywhere in it. You may need to drag the display window to the side to be able to see the Database Workshop window. From its Query menu, choose Establish display link. You

---

7. Enclosing field names in square brackets is *required* only in cases where the field name contains spaces or symbols that have other meanings. However, it is recommended that field names always be enclosed in brackets to avoid parsing errors by the database engine.

will be prompted to enter the name of a vector link file (.vtx). Type REVERE\_COLLECTION. Select as the Vector file BGROUPS and as the Link field name IDENTIFIERS. Then click OK. Once the display link is established, we can display the information in the ELDERLY% field as a map layer. One way to display a linked field is to use DISPLAY Launcher to display a vector layer. Click on the folder icon to the left of REVERE\_COLLECTION. Choose the ELDERLY% layer. Display it with a Quantitative symbol file and click the Equal Interval Autoscale option. You should now see each block group color-coded according to the value in the ELDERLY% field for that block group.

- v) Now display the HISPANIC% field, using the same steps.

Often you will have a field that has values beyond the 0-255 range. Our population field, for example, clearly has values well beyond the range of symbol codes in the symbol file. In such cases, the Autoscale option will be turned on automatically when you display the image.

- w) The Display Current Field as Map Layer icon (second from the right) in the Database Workshop interface is identical to the DISPLAY Launcher icon and can be used in much the same way. Place the cursor in the first row of data in the Population column, and click the Display Current Field as Map Layer icon. Population by block group will be displayed on the screen.

Take some time now to explore the database. You may wish to perform some queries as well. When a query filter is in place, those records meeting the query conditions are displayed in red, and the other records are displayed in black. For reference, you may wish to add a copy of the layer BGROUPS to the display using the standard default symbol file. To make the copy, go to IDRISI Explorer and copy BGROUPS to a new file, such as BGROUPS2.

6. *Assume that emergency evacuation during nor'easters must take into special consideration any block group in which more than a third of the population is elderly (over 65 years of age). Where are such block groups in Revere located with respect to the coast and estuaries (and hence most likely to be at risk)?*

## Mapping and Assessing Resistance

We will now use the spatial data on block groups with the attribute census data to create maps of resistance to nor'easters in Revere. Since there can be many variables that can measure resistance, an overall index of resistance can be created from the different variables. For example, a well known concept for combining different variables is the arithmetic mean. Using the three variables selected in this exercise, this index can be defined as:

$$\text{RESIST} = ([\text{ELDERLY}\%] + [\text{POVERTY}\%] + [\text{HISPANIC}\%]) / 3$$

The calculation of this index is easily accomplished within Database Workshop.

- x) Close all images on the screen. Modify the database once more by adding the field RESIST, which has a data type of Single Precision Real.
- y) Use the Calculate Field Values command in Database Workshop's Query menu to fill RESIST with the average of the three fields as shown above. Be sure to include parentheses around the group of the three fields. Display RESIST by using the Display Current Field as Map Layer icon.

7. *What is the highest value in RESIST? The lowest value?*

The use of an average to combine the three individual resistance images resulted in an overall resistance image in which no area in Revere appears to stand out. That is, it is not clear from RESIST which areas in Revere will be able to withstand the impacts of a nor'easter and which will not. In the display of an individual variable, such as ELDERLY, such areas are clear, as for example, the block group in which 60% of the population was older than 65 years. Clearly, the average is not a useful composite index of resistance if planners must identify areas that must be targeted for emergency response during



a nor'easter. Unfortunately, little research has been carried out on the derivation of indices to produce composite images of resistance (or for that matter composite images of the other dimensions of vulnerability: exposure, and resilience). However, some research has been carried out on creating such indices for physical factors of vulnerability (Gornitz and White, 1994). We will explore these indices in Exercise 3 of this workbook.

## Combining Resistance and Risk

In the displays that we have just created, it is possible that block groups with high values of the variables measuring resistance may not fall in areas of high risk to flooding and wave action. That is, a block group may have a vulnerable population but may not be at risk. To determine this, we must integrate the dimensions of exposure and resistance. In other words, we must combine the images of resistance with the image HIGHRISK, which shows areas in Revere at high risk to flooding and wave action. We will do this for one variable, ELDERLY%.

The image HIGHRISK that we made earlier is not based on the geography of the block groups as is our ELDERLY% data. Because these data sets have different geography, we cannot use Database Workshop to produce the image showing where both a high percentage of elderly people and areas with high risk of flooding coincide. We must perform this operation using an overlay process. We will first need to make a raster image representing the elderly percentage variable in the database, then combine it with the HIGHRISK image.

- z) Select the first row of the ELDERLY% field from the Database Workshop File menu, choose Export/Field/to Raster Image option. Name the output raster image PCT\_ELDERLY. Change the background value to zero and hit OK. Another dialog will appear for the reference parameters for the raster image. We can copy these parameters from an existing file REVBGRP and the necessary parameters will be filled in. Click OK and the raster file will be created and displayed. We now have a raster image that represents the attribute information from the ELDERLY% database field.
- aa) Run OVERLAY and choose the multiplication option. Specify the first image as PCT\_ELDERLY, the second image as HIGHRISK, and the output as ELDRISK. When OVERLAY has finished, display ELDRISK with the Quantitative palette. As before, add the vector layers BGROUPS and COAST on the image with the Outline White symbol file.

The image ELDRISK shows that the block group with the highest percentage (60%) of people older than 65 years falls in the area at high risk to flooding in Revere. Also falling in this high risk area are other block groups that have a high percentage of people older than 65 years. Thus, our analysis shows that many people who are older than 65 years in Revere are at risk to nor'easters.

- 8. *Carry out a similar analysis with the other two fields, HISPANIC% and POVERTY%. Do the resulting images show that these two vulnerable groups are at risk to nor'easters and associated impacts?*

## Conclusions

In this exercise, socioeconomic vulnerability to extreme storms called nor'easters was examined at the community level. The role of GIS in assessing socioeconomic vulnerability was explored by mapping and combining factors for two dimensions of vulnerability: exposure and resistance. The application of spatial and attribute census data from the United States Bureau of Census was illustrated. A similar methodology can be applied to assess vulnerability to other types of extreme storms and in different socioeconomic contexts. For example, one could envision such an analysis for cyclones and associated flooding in Bangladesh or India. More research needs to be carried out on creating composite indices for the different dimensions of vulnerability as well as for vulnerability itself. This is especially significant given the large number of variables for which data are now available and the ease with which these data can be mapped and analyzed in a GIS context.

## References

- Bolin, R., and P. Bolton. 1986. *Race, religion, and ethnicity in disaster recovery*. Program on Environment and Behavior Monograph No. 42. Boulder, CO: Institute of Behavioral Science, University of Colorado.
- Bureau of Census. 1991. *TIGER questions and answers*. Washington, D.C: U.S. Department of Commerce, Bureau of the Census.
- Bureau of Census. 1992a. *Maps and more: your guide to Census Bureau geography*. Washington, D.C: U.S. Department of Commerce, Bureau of the Census.
- Bureau of Census. 1992b. *Summary Tape File 3A*. Washington, D.C: U.S. Department of Commerce, Bureau of the Census.
- Dow, K. 1993. Exploring differences in our common future(s): The meaning of vulnerability to global environmental change. *Geoforum* 23(3): 417-436.
- Drabek, T.E., and W.H. Key. 1984. *Conquering disaster: family recovery and long-term consequences*. New York: Irvington.
- Emani, S., et al. 1993. Assessing vulnerability to extreme storm events and sea-level rise using geographical information systems (GIS). In *Proceedings, GIS/LIS '93*, Volume 1: 201-209. Bethesda, MD: American Congress on Surveying and Mapping (ACSM) and American Society for Photogrammetry and Remote Sensing (ASPRS).
- FEMA (Federal Emergency Management Agency). 1992. *Answers to questions about the National Flood Insurance Program. FIA-2*. Washington, D.C.: Federal Emergency Management Agency (FEMA).
- Gornitz, V.M., and T.W. White. 1994. *A coastal hazards data base for the U.S. gulf coast*. ORNL/CDIAC-60. NDP-043B. Environmental Sciences Division Publication No. 4101. Oak Ridge, TN: Oak Ridge National Laboratory.

### ***Exercise 3: Vulnerability of the Gulf Coast of the United States to Accelerated Sea-level Rise***



Gulf Coast, Alabama

## Introduction

In Exercise 2, we examined socioeconomic vulnerability of coastal communities to extreme storms. In this exercise, we will examine the physical vulnerability of coastal areas to the risks posed by accelerated sea-level rise. Some of the consequences of accelerated sea-level rise are inundation, coastal erosion, increased flooding, and the loss of drylands and wetlands (IPCC, 1992). The social and economic impacts associated with these consequences are considerable. For example, much of the small island nation of Maldives is only 1 to 2 meters above mean sea level (IPCC 1992). A 1-meter sea-level rise would therefore inundate much of the nation. Even in larger nations the impacts of sea-level rise can be high. In the United States, a 1-meter sea-level rise would cost \$270 to \$475 billion as a result of shoreline retreat (Lee and colleagues 1992).

The focus of this exercise will be on assessing vulnerability through physical characteristics of the coastline such as elevation, geology, geomorphology, and tidal range. The first part of the exercise describes the database used and the conversion of the database into IDRISI images. We will convert the text file of the seven relative risk variables into an IDRISI database. Also, we will assign the values of the seven variables in the database, that is the seven fields in the database, to the IDRISI image of the grid cell identifiers to create seven relative risk images. The second and third steps are similar to those carried out in Exercise 2 for combining spatial and attribute data in creating maps of resistance to nor'easters. The second part focuses on assessing vulnerability to two risks associated with sea-level rise: erosion, and inundation. In this section, the option of creating and running *macros* for the vulnerability analysis is illustrated. Macros are useful whenever multiple operations have to be carried out on images. Since the analysis of vulnerability in this exercise is based upon indices involving numerous algebraic operations, macros will be particularly useful for handling the GIS operations. In the final section of the paper, we will illustrate another approach to Map Algebra using the module Image Calculator in IDRISI.

## Data Description

The data we will use in this exercise has been compiled by Gornitz and White (1994) and released by the Oak Ridge National Laboratory in the United States as a numeric data package, NDP043B. The study area in the data package is the Gulf Coast of the United States which extends from the state of Texas to the state of Florida. NDP043B consists of 29 variables which measure two coastal risk factors: (1) erosion, and (2) inundation. The data package also includes the coastline of the Gulf Coast at a 1:2,000,000 scale. The sources of data on the 29 variables and the coastline include agencies such as the National Oceanic and Atmospheric Administration (NOAA), the U.S. Army Corps of Engineers, the U.S. Geological Survey (USGS), and various academic institutions.

The data have been referenced to a latitude/longitude grid of cells that covers the Gulf Coast. Each cell in the grid is  $0.25^\circ$  by  $0.25^\circ$  in size. The grid cell identifiers increase from left to right, bottom to top. The grid origin is the cell with the identifier 1 and has the coordinates,  $100^\circ\text{W}$ ,  $24^\circ\text{N}$ . The bounding coordinates of the study area are:  $100^\circ\text{W}$ ,  $24^\circ\text{N}$ ;  $100^\circ\text{W}$ ,  $32^\circ\text{N}$ ;  $80^\circ\text{W}$ ,  $32^\circ\text{N}$ ; and  $80^\circ\text{W}$ ,  $24^\circ\text{N}$ .

Of the 29 variables in NDP043B, seven variables were selected by Gornitz and White for analyzing the vulnerability of the Gulf Coast to coastal hazards: (1) mean elevation, (2) local subsidence trend, (3) geology, (4) geomorphology, (5) mean shoreline displacement, (6) maximum wave height, and (7) mean tidal range. These seven variables were selected because of their use in measuring risk to coastlines. For example, high risk coastlines have low relief, high subsidence rates, high erosion rates, and high wave energies (Gornitz, White, and Cushman, 1991). The Exercise Details section at the end of the volume provides brief descriptions of the seven variables and the procedures adopted for compiling data for each variable. It also provides additional description of the data compiled for two of the variables, geology and geomorphology.

To simplify the manipulation process in the vulnerability analysis, Gornitz and White reclassified the seven variables to create seven relative risk variables. Each relative risk variable ranges in value from 0 to 5 with 1 indicating *very low* risk to erosion or inundation, and 5 indicating *very high* risk to erosion or inundation. The value 0 represents missing values in the original data. The Exercise Details section shows the tables used in creating the seven relative risk variables from the original variables. The data on the seven relative risk variables have also been included as part of NDP043B. In calculating vulnerability, we will use data on the relative risk variables as opposed to the original variables.

## The Feature Definition Image

We have retrieved from NDP043B a text file containing the identifiers of the cells in the grid that covers the Gulf Coast and converted this to the proper IDRISI image format.

- a) Change your main Working folder IDRISI Explorer to the folder where your exercise data are stored (e.g., UNITAR\Hazards\Data\Exercise\_3). Next, run the module Edit and open the GRID.TXT file.

GRID.TXT is the text file which holds data on the identifiers of the grid cells covering the study area. The file consists of a single column of numbers that represent the identifiers. For example, the first identifier is 2481, the second is 2482, and so on. To convert GRID.TXT to an IDRISI image of the study area, we need information on the number of rows and the number of columns in the image. This can be calculated using information on the referencing system and size of the grid cell as illustrated in Figure 3.1. Remember that the size of the grid cells is  $0.25^\circ$ ; the referencing system is latitude/longitude; and the bounding coordinates of the study area are:  $100^\circ\text{W}$ ,  $24^\circ\text{N}$ ;  $100^\circ\text{W}$ ,  $32^\circ\text{N}$ ;  $80^\circ\text{W}$ ,  $32^\circ\text{N}$ ; and  $80^\circ\text{W}$ ,  $24^\circ\text{N}$ .

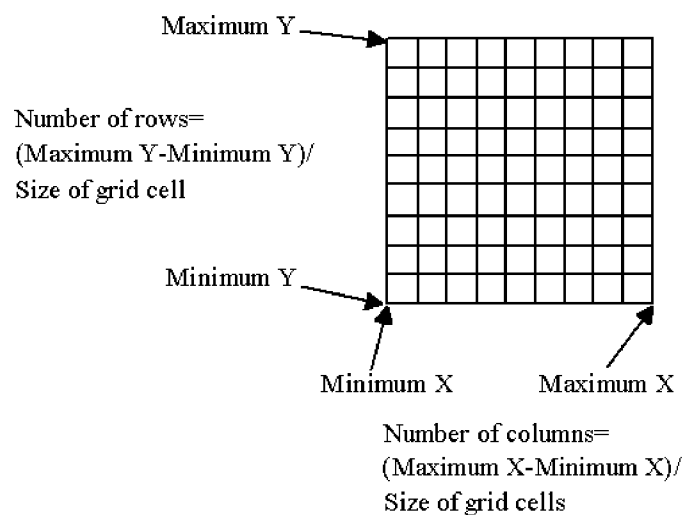


Figure 3.1

1. *What are the number of rows and columns in the image into which GRID.TXT will be imported?*

Now that we have determined the number of rows and columns, we can create the image of grid cell identifiers for the study area. In IDRISI, all images are stored as a single column of numbers. It is the information in the documentation file for an image, particularly the number of rows and columns, that allow the single column of numbers to be displayed and analyzed as an image. We created this documentation file for you.

- b) Use DISPLAY Launcher to view the image GRID with the Quantitative palette. DISPLAY Launcher will invoke autoscaling as the identifiers of the grid cells exceed the range of values for display. Because of autoscaling, adjacent cells are displayed with similar colors although each cell has a unique identifier. The cells can be distinguished from one another by overlaying cell boundaries on the image. To do this, we have provided a vector file called CELLS. Use Add Layer in Composer to overlay CELLS on GRID with the Outline White symbol file. Use Add Layer again to overlay COAST on GRID with the Outline Black symbol file. COAST is the vector file depicting the 1:2,000,000 coastline of the Gulf Coast. Then, with the GRID image highlighted in the Composer window, use Cursor Inquiry Mode to explore the cell identifiers in the image. For example, the first cell in the first row of the image has the identifier 2481, the second cell has the identifier 2482, and so on.

Since the value of each cell in GRID is the identifier of the cell, GRID is the feature definition image covering the study area.

## Creating Relative Risk Images

The next step in data development is to create images of the seven relative risk variables to be used in the vulnerability analysis, which were explained in the Data Description section above.

- c) Use Edit to open the file GCRISK.TXT. Scroll down the file to view more cases.

The first field contains the cell identifiers (these are the same identifiers as in the image GRID). The next seven fields contain the data for the relative risk variables in the order specified above (mean elevation in first field, geology in the second field, and so on). The relative risk scores range from 0 to 5, with 0 indicating missing values, 1 indicating *very low* risk, and 5 indicating *very high* risk. A large number of cells have been assigned a relative risk score of 0 indicating a missing value for the cells for all the seven variables. Many of these cells represent areas which are away from the Gulf Coast, and for such areas data on the relative risk variables were not compiled. In a few cases, data at the Gulf Coast were not available and the cells covering such areas were also assigned the 0 value. This characteristic of the data, common to all the seven variables, will become clear once we create the relative risk images and view them.

After some manipulation, GCRISK.TXT was imported into IDRISI as a database workshop file called RISK. We have provided you with this file and we will use it for creating the relative risk images. To do so, we will use a feature in Database Workshop which will allow us to create raster images from fields linked to the layer CELLS.

- d) Use Database Workshop to open the database called RISK. To link the database to CELLS, you need to create a vector link file (vlx). From the Query menu in Database Workshop, choose the option to Establish display link. Name the vector link file RISK, link it to the vector file CELLS and select IDR\_ID as the link field.
- e) To create the relative risk image for Mean Elevation, from the Database Workshop File menu, choose Export/Field/to Raster Image option. Name the output raster image ELEVATION. Change the background value to zero and hit OK. Another dialog will appear for the reference parameters for the raster image. We can copy these parameters from an existing file: GRID and the necessary parameters will be filled in. Click OK and the raster file will be created and displayed. From Layer Properties in Composer, choose the user-defined palette RISK. We now have a raster image that represents the attribute information from the ELEVATION database field.<sup>1</sup> Use the Add Layer option first to overlay CELLS with the Outline Black symbol file and then again to overlay COAST with the Outline White symbol file. The legend categories show the relative risk values in ELEVATION. Open the documentation file for ELEVATION using Metadata. Double-click the Categories option and choose to copy the legend from another file GEOLOGY. The legend should show: 0 - MISSING, 1 - Very Low Risk, 2 - Low Risk, 3-Moderate Risk, 4 - High Risk, and 5 - Very High Risk. Save the changes.

As the image shows, most of the areas near the Gulf Coast are at high or very high risk to inundation as a result of mean elevation. Also note that the relative risk scores have been captured only for the grid cells in the immediate vicinity of the Gulf Coast. The cells located away from the Gulf Coast have missing values.

The remaining relative risk images for the Gulf Coast have been provided to you. These have been created in the same manner in which ELEVATION was created.

- f) Use DISPLAY Launcher to view GEOLOGY with the user-defined palette RISK. Then, from Composer, use the Add Layer option to first overlay CELLS with the Outline Black symbol file and then overlay COAST with the Outline White symbol file. Because of its geological characteristics, most of the Gulf Coast is at high and very high risk to erosion and inundation.

---

1. The Exercise Details section provides the definitions for this relative risk variable and the other six variables.

- g) Display GEOMORPH with the user-defined palette RISK. In the case of geomorphology, moderate risk areas dominate the Gulf Coast but some very high risk areas also exist.
- h) Display EROSION, the relative risk image for mean shoreline displacement, with the palette RISK. There is a mix of moderate, high, and very high risks to erosion in the Gulf Coast as a result of mean shoreline displacement.
- i) Display SUBSID, the relative risk image for local subsidence rate with the user-defined palette RISK. There appears to be a distinct geographical division of areas in the Gulf Coast for this relative risk variable. The eastern half of the Gulf Coast is at very low risk whereas the western half is at high and very high risk.
- j) Display WVEHGT, the relative risk image for maximum wave height. For this variable, the Gulf Coast consists mostly of low risk areas mixed in with some very low and moderate risk areas.
- k) Display TIDAL, the relative risk image for mean tidal range, with the user-defined palette TIDAL. This variable is characterized by missing values, but where data is available, the Gulf Coast is at low risk from mean tidal range.

These seven relative risk images will be used for calculating the vulnerability of the Gulf Coast to the risks of erosion and inundation. First we will define vulnerability through two indices derived by Gornitz and White. Then we will use macros to calculate vulnerability.

## **Vulnerability Analysis**

In their research on assessing coastal vulnerability (CV), Gornitz, White, and Cushman (1991), and Gornitz and White (1991; 1994) derived and tested six indices of coastal vulnerability (CVIs) based upon the seven relative risk variables. Of these six indices, two proved to be less sensitive than the others to any errors that might be committed in the classification of the relative risk variables. These indices are:

- (1) the square root of the product mean defined as:

$$CVI1 = [(x_1 * x_2 * x_3 * x_4 * x_5 * x_6 * x_7)/n]^{1/2}$$

- (2) the sum of products defined as:

$$CVI2 = [4x_1 + 4x_2 + 2(x_3 + x_4) + 4x_5 + 2(x_6 + x_7)]$$

where:

$x_1, x_2, \dots, \text{and } x_7$  are the images of the relative risk variables for the Gulf Coast, and are defined as:

$x_1$	=	ELEVATION	=	mean elevation
$x_2$	=	SUBSID	=	local subsidence trend
$x_3$	=	GEOLOGY	=	geology
$x_4$	=	GEOMORPH	=	geomorphology
$x_5$	=	EROSION	=	mean shoreline displacement
$x_6$	=	WVEHGT	=	maximum wave height
$x_7$	=	TIDAL	=	mean tidal range

and 'n' is the number of relative risk variables with values greater than 0.

In a GIS context, the set of analytical operations required to calculate these vulnerability indices is called *Map Algebra* since

algebraic operations such as addition, multiplication, and division are performed on maps or images. One could undertake Map Algebra by repeatedly performing the required operations using the appropriate modules. This approach, however, could prove to be tedious if the number of operations is large as is the case with the two vulnerability indices presented above. In IDRISI, there are two approaches for facilitating such repetitive operations. One approach is to create a *macro* for the task. The second approach is to use the module Image Calculator. We will explore the use of macros in this section and Image Calculator in the next.

In IDRISI, macros have an .IML extension and are located in the data directory. A macro consists of a series of lines, each with a module name and the parameters needed to run the module. When a macro is run, each module is executed in turn. To create a macro, the user types the "command line" format for the modules. The module name is followed by an 'x' to indicate that parameters should be taken from the command line. All the parameters are then given in the particular format specified in the IDRISI Help System. For example, the command line parameters when the OVERLAY module is used to multiply two images would be:

```
overlay x 3*image1*image2*output1
```

where 'overlay' is the module being used, 'x' indicates that the command line parameters for the overlay module are being invoked, '3' refers to the option in overlay for multiplication, 'image1' refers to the first image, 'image2' refers to the second image, and 'output1' refers to the output image. The asterisks between parameters are required in IDRISI.

Macro command line parameters for each module can be found in the Help system for that module.

2. *What would be the command line parameters for the following operation: Add ELEVATION and EROSION?*

By using such command line parameters, we will create and run a macro for calculating coastal vulnerability index CVI1, the square root of product mean.

## Calculating CVI1

Using the names of the relative risk images created earlier, CVI1 is defined as:

$$CVI1 = [(elevation * subsid * geology * geomorph * erosion * wvehgt * tidal)/7]^{1/2}$$

As the index is based upon a product calculation, if a grid cell in any one of the seven images holds the value 0, then that grid cell in the final vulnerability image will be 0 and will be considered to have a missing value. To avoid the possibility of a large number of such missing values in the final image, Gornitz and White modified the index as follows (Beaty, 1995):

If a grid cell in all the seven images holds a value greater than 0, then the index will be used as it is. However, if a grid cell in any image holds the value 0, then that grid cell will be reassigned a value 1 so that the product is not 0. But instead of dividing the product by 7 when calculating the index, the product will be divided by 6 as there are six images with values actually greater than 0. Similarly, if the grid cell has a value 0 in two images, then for both images the grid cell will be reassigned a value 1 and the product will be divided by 5 instead of 7. This process is illustrated through the example in Figure 3.2.

ELEVAT	SUBSID	GEOLOGY	GEOMORPH	EROSION	WVEHGT	TIDAL	CVI1	
1 0	4 1	3 5	2 5	5 3	3 5	1 2	7.17	11.18
0 1	0 4	0 5	3 0	2 0	4 5	2 1	3.46	4.47

Figure 3.2

3. *In Figure 3.2, verify the value of CVI1 for each of the four cells.*



We will now proceed to calculate CVI1 through a sequence of steps using macros whenever necessary. In the sequence, we will first calculate the numerator of the index and then the denominator. To calculate the numerator, we must reclassify the value 0 to the value 1 in all the seven images so that the product of the images is not 0. We must then determine the product of the images.

Step 1: Reclassify the value 0 in each of the seven images to the value 1 so that the product of the images is not 0. To do this, we will use the RECLASS module.

- l) Open the module RECLASS. We will be reclassifying an image with a user-defined reclassification. Specify ELEVATION as the input image and call the new image ELEVREC. Assign the new value 1 to old values ranging from 0 to those just less than 1 and click OK. Use DISPLAY Launcher to view ELEVREC with the user-defined palette RISK and a legend. The image shows the value 0 reclassified to the value 1. The risk values ranging from 2 to 5 did not change from the reclassification.

Since this reclassification procedure needs to be repeated for the remaining six relative risk images, we can use a macro here. The command line parameters for RECLASS for the operation just completed is:

```
reclass x i*elevation*elevrec*2*1*0*1*-9999
```

We will use similar command line parameters in the macro for reclassifying the other relative risk images. You can access the command line structure for RECLASS by clicking the Help box in the RECLASS module. You can access information about macro files and their structure by using the Help menu. Go to Help and click on Contents, then click on Search. Type in macro and this will lead you to several choices for macro files.

- m) Open Edit and type the following lines in this file:

```
reclass x I*subsid*subrec*2*1*0*1*-9999
```

```
reclass x I*geology*georec*2*1*0*1*-9999
```

```
reclass x I*geomorph*geomrec*2*1*0*1*-9999
```

```
reclass x I*erosion*erorec*2*1*0*1*-9999
```

```
reclass x I*wveght*wverec*2*1*0*1*-9999
```

```
reclass x I*tidal*tidrec*2*1*0*1*-9999
```

After you have finished typing the lines, save the file by clicking File/Save As. Choose Macro File (.iml) as the file type and STEP1 for the filename, then exit the file.

- n) Go to the File menu and select Run Macro. Specify STEP1 as the macro to run and click Run Macro. IDRISI will indicate each operation as it is completed. If there is an error in a line in the macro, IDRISI will not complete the operation specified in that line. If that happens, use the Edit option to correct the error and run the macro again. After the macro has finished, use IDRISI Explorer to verify that the reclassified images exist in the data directory.

Step 2: Multiply the seven reclassified images to obtain the numerator in CVI1. To do this, we will use the OVERLAY module.

- o) Open the module OVERLAY. Specify ELEVREC as the first image, SUBREC as the second image, and call the output image TMP1. Select the option for multiplying two images and click OK. Use DISPLAY Launcher to view TMP1 with the Quantitative palette and a legend. The lowest value is 1 since we eliminated the 0 values in the first step; the highest value is 25 as both the relative risk variables, elevation and subsidence rate, have relative

risk scores of 5.

Since this step has to be repeated a number of times, we can create a macro to perform the calculation. The command line parameter for the OVERLAY operation we just completed is:

```
overlay x 3*elevrec*subrec*tmp1.
```

We will use similar command line parameters in the macro.

- p) Open Edit and type the following lines in this file:

```
overlay x 3*tmp1*georec*tmp2
```

```
overlay x 3*tmp2*geomrec*tmp3
```

```
overlay x 3*tmp3*erorec*tmp4
```

```
overlay x 3*tmp4*wverec*tmp5
```

```
overlay x 3*tmp5*tiderec*numerat
```

After you have finished typing the lines, save the file as STEP2.IML in the same way as before and then close Edit.

- q) Select Run Macro and specify the file as STEP2 and click Run Macro. After the macro has finished, use DISPLAY Launcher to view NUMERAT with the Quantitative palette and a legend. Use Add Layer from Composer to first overlay CELLS on the image with the default symbol file and then COAST with the default symbol file.

NUMERAT is the image of the numerator in CVI1. The values in the image range from 1 to 11,250. Thus, there is no grid cell in the Gulf Coast which has a relative risk score of 5 in all the seven images as the value for such a grid cell would be 78,125. The files TMP\* created by the macro are temporary files which will be deleted at the end.

Next, we will find the denominator of CVI1, taking into account the modification of the index discussed at the beginning of this section. The denominator is an image in which each cell consists of the number of relative risk images with non-zero values for that cell. For example, if there are five relative risk images with nonzero values for a cell then that cell in the denominator image will have the value 5. To create the denominator image therefore, we will first reclassify the relative risk images to Boolean images with values 0 and 1. Then we will add the Boolean images to find the number of images with nonzero values by grid cell.

Step 3: Reclassify the relative risk images, this time to Boolean images with only two values, 0 or 1.

As this step requires repeated use of the RECLASS module, we can use a macro. Since you already have a macro with the RECLASS module, you should be able to create this one on your own. When reclassifying, specify the same names as you used earlier. For example, ELEVREC for the reclassified elevation image, SUBREC for the reclassified subsidence image, and so on. This will rewrite the earlier images which were created. Specify a new value of 1 for old values ranging from 1 to those just less than 6. Call the macro STEP3.

4. *What are the contents of STEP3?*

- r) Run STEP3. Use DISPLAY Launcher to view ELEVREC with the user-defined palette RISK. All the relative risk scores ranging from 1 to 5 should have been replaced by the value 1. The Boolean images created from the other relative risk images will be similar to this image.

Step 4: Add the Boolean images created above to find the denominator of CVI1.

Again, a macro can be used because of the repeated use of the OVERLAY module for adding the images in this case. Create a macro called STEP4. Call the final image in the macro DIVIDER.

5. *What are the contents of STEP4?*

- s) Run STEP4. After it has finished, use DISPLAY Launcher to view DIVIDER with the Qualitative palette. As there are seven Boolean images, the lowest value is 0 and the highest value is 7.

We now have the numerator and denominator for CVI1. In the next several steps, we will combine these and take the square root of the result to calculate vulnerability.

Step 5: Divide the numerator calculated in Step 2 with the denominator calculated in Step 4. We will use the OVERLAY module for this step.

- t) Open OVERLAY. Specify the first image as NUMERAT, the second image as DIVIDER, and the output image as TMP. Select the option to divide two images and use the division by zero yields zero option. Click OK then view TMP with the Quantitative palette.

A problem with TMP is the large values in the image for the cells with missing values. These large values were calculated as a result of division by 0, since the missing values in the images used in this exercise are represented by the 0 value. Although most GIS software do not recognize division by 0, IDRISI will allow such a division by assigning an arbitrarily large value to the outcome. We will eliminate these large values in the last step.

Step 6: Use the TRANSFORM module to find the square root of TMP.

- u) Run the module TRANSFORM from the GIS Analysis/Mathematical Operators menu. Select the transformation type to be square root. Specify TMP as the input image and call the output SQRROOT. Click OK.

Step 7: Eliminate the large values calculated as a result of division by 0 in TMP. We will do this by masking out the cells with the large values.

- v) Run RECLASS and specify DIVIDER as the image to be reclassified and call the output MASK. Assign a new value of 1 for the old values ranging from 1 to those just less than 8. Click OK. Next, run OVERLAY. Specify the first image as SQRROOT, the second image as MASK, and the output as CVI1. Select the option of multiplying two images. Click OK.
- w) Use DISPLAY Launcher to view CVI1 with the Quantitative palette. Use Add Layer to overlay the vector file CELLS on the image with the Outline White symbol file. Then use Add Layer again to overlay the vector file COAST on the image with the Outline Black symbol file.

6. *What do the higher values in CVI1 represent in terms of the vulnerability of the Gulf Coast to the risks of erosion and inundation?*

Using a histogram of the values in the image CVI1, Gornitz and White (1994) adopted three categories to depict the vulnerability of the Gulf Coast to risks of erosion and inundation: (1) Low Risk (values less than 16 in CVI1); (2) Moderate Risk (values between 16 and 22 in CVI1); and (3) High Risk (values greater than 22 in CVI1). Figure 3.3 shows an area of the Gulf Coast (near the Alabama and Louisiana border) for which this reclassification was carried out.

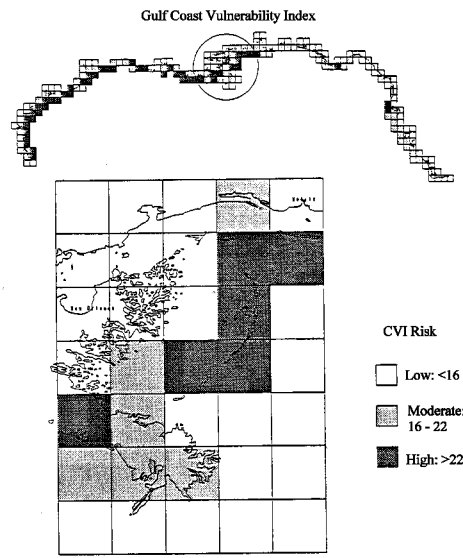


Figure 3.3

- x) Using the appropriate modules in IDRISI and the vulnerability index image CVI1, reproduce the results of Figure 3.3 (Hint: Use RECLASS and DISPLAY Launcher). Call the result CVI1REC.

7. *What steps do you take to obtain this result?*

For illustration, we calculated CVI1 using a series of macros and individual operations. However, all the steps can be entered into one macro file which can be used to calculate CVI1. We have provided this macro to you and it is called CVI1.IML.

- y) To view CVI1, open Edit. Select the option for a macro file and specify the file as CVI1. Click OK to view the file. All the operations performed above are contained in this macro.

## Calculating CVI2

The second coastal vulnerability index is the *sum of products* index. Using the relative risk images used in this exercise, this index can be defined as:

$$\text{CVI2} = 4 * \text{ELEVATION} + 4 * \text{SUBSID} + 2 * (\text{GEOLOGY} + \text{GEOMORPH}) + 4 * \text{EROSION} + 2 * (\text{WVEHGT} + \text{TIDAL})$$

Although a macro can be written for this vulnerability index, it is easier to perform the operations required for this index through the use of Image Calculator. Image Calculator allows two types of operations, mathematical and logical. CVI2 is an example of a mathematical expression since it involves operations such as addition and multiplication. Logical operations involve expressions such as "less than," "not equal to," and Boolean expression such as AND and OR.

- z) Click on the toolbar icon for Image Calculator (the one that looks like a calculator). Enter the name CVI2 for the output image. Place the cursor in the Expression to process input box then click on the value 4 in the numeric box on the left side. This value will be automatically placed in the Expression to process input box. Next click on the multiplication command (\*) in the right column of the operations box. This also will be placed in the Expression to process box after the value 4. Then click on Insert Image and the pick list will appear. Select

the file ELEVATION and the filename will appear in the Expression to process box. Proceed to enter the expression for CVI2 in this manner. Note that for the two operations in which additions are involved (GEOLOGY and GEOMORPH, and WVEHGT and TIDAL) you will need to place parentheses in the appropriate places. After you have finished, save the expression by clicking Save Expression and providing the filename CVI2 for the expression. By saving the expression, you do not have to re-enter the expression in case of a mistake. Next process the expression by clicking on the Process Expression button. When the image autodisplays, you may need to change the palette in Composer.

8. *What is the highest value for CVI2? The lowest value? (If you wish to compare your results, we have provided the answer image with the data set for this exercise. It is called ANS8EX3).*

## Conclusions

Using a coastal hazards data base compiled by Gornitz and White (1994), this exercise examined the vulnerability of the U.S. Gulf Coast to the risks of erosion and inundation. Two indices of vulnerability proposed by Gornitz and White were used: (1) a modified product mean and (2) a sum of products. The analysis using these indices relied on the class of GIS operations called Map Algebra. One section of the exercise illustrated the use of macros to carry out Map Algebra. Another section showed the use of Image Calculator in IDRISI to perform Map Algebra. Image Calculator is well suited for operations that are fewer in number and involve simple mathematical and logical expressions. A macro is more efficient when a large number of operations have to be performed, and some of the operations involve modules which cannot be accessed via Image Calculator.

From a hazards perspective, the definition of vulnerability adopted in the exercise was limited to physical characteristics of the Gulf Coast such as elevation, geology, geomorphology, and erosion. Socioeconomic characteristics, such as the total population living near coastal areas, the number of structures affected by erosion and inundation, and economic impacts associated with loss of property and land, were excluded from the analysis. Nonetheless, the use of indices to combine data on different characteristics of the coast is an important step towards assessing and depicting a composite picture of vulnerability of a place to the potential risks of sea-level rise.

## References

- Beaty, T.W. January 1995. Personal communication.
- Dolan, R., et al. 1989. Patterns of erosion along the Atlantic Coast. In *Proceedings, Coastal Zone '89*, 17-22. New York: American Society of Civil Engineers.
- Gornitz, V.M., and T.W. White. 1994. *A coastal hazards data base for the U.S. gulf coast*. ORNL/CDIAC-60. NDP043B. Environmental Sciences Division Publication No. 4101. Oak Ridge, TN: Oak Ridge National Laboratory.
- Gornitz, V.M. and T.W. White. 1991. The global coastal hazards data base. In *Future climate studies and radioactive waste disposal: Proceedings of the international workshop held at UEA, Norwich*, 1-3 November 1989, 214-224. Norwich, United Kingdom: Climatic Research Unit, School of Environmental Sciences, University of East Anglia.
- Gornitz, V.M., T.W. White, and R.M. Cushman. 1991. Vulnerability of the U.S. to future sea-level rise. In *Proceedings, Coastal Zone '91*, 2354-2368. New York: American Society of Civil Engineers.
- IPCC (Intergovernmental Panel on Climate Change). 1992. *Global climate change and the rising challenge of the sea*. Report of the Coastal Management Subgroup of the Response Strategies Working Group of the Intergovernmental Panel on Climate Change (IPCC).
- Lee, J.K., et al. Application of geoprocessing and simulation modeling to estimate impacts of sea-level rise on the north-east coast of Florida. *Photogrammetric Engineering and Remote Sensing* 58(11): 1579-1586.
- May, S.K., et al. 1983. Erosion of U.S. shorelines. *Earth Observing System* 65: 521-523.

## ***Exercise 4: Estimating Population at Risk from Hazardous Materials Transportation Accidents***



## Introduction

It has been estimated that about 1.5 billion tons of hazardous materials are transported annually in the United States (Abkowitz and Cheng 1988). This transportation resulted in over 8,500 reported accidents in 1990 (USGAO 1991). GIS can play a particularly useful role in assessing and managing the risks associated with these hazardous materials (hazmat) transportation accidents. Some of the GIS capabilities in this area include risk assessment, routing and scheduling, emergency preparedness, and evacuation planning (Abkowitz, Cheng, and Lepofsky 1990).

In this exercise, we will illustrate GIS-based techniques for identifying and estimating the population at risk from hazmat transportation accidents. The objective of the exercise is to estimate the total population at risk from a hypothetical accident involving the release of chlorine into the air.<sup>1</sup> Two GIS-based techniques for population estimation are illustrated in the exercise: (1) the Uniform Density Method of population estimation, and (2) the Land Use Refinement Method of population estimation. We will also explore two approaches to modeling the risk, the first based on the concept of Euclidean modeling and the second based on the concept of dispersion modeling.

The exercise is divided into three sections. In the first section, we will use the concept of Euclidean distance to estimate the population at risk. In the second section, we will use the concept of dispersion to estimate this population. In this section, we will illustrate the use of a software package, ALOHA, for the dispersion modeling. In both of these sections, we will adopt the following steps. First, we will calculate a risk zone in which people are considered to be at risk from the hazmat accident involving the release of chlorine. Then we will estimate the total population falling in the risk zone. The third section of the exercise introduces an IDRISI module called DISPERSE for calculating a dispersion zone.

## Euclidean-Based Population Estimation

### Developing a Euclidean Risk Zone

- a) Change your main Working folder using IDRISI Explorer to be the folder where your exercise data are stored (e.g., UNITAR\Hazards\Data\Exercise\_4). Then, display the image HIGHWAY using the Qualitative palette and a legend.

HIGHWAY is an image of an interstate highway called Interstate 290, or I-290, which passes through Worcester, Massachusetts, USA. The image was created by rasterizing a vector file which is also called HIGHWAY. We will estimate the population at risk in Worcester to a hypothetical accident on I-290 which involves the release of chlorine into the air. To do this, we will first create an image of a risk zone around I-290. A risk zone is the area surrounding a highway or a fixed facility within which the population is at greatest risk from a hazardous materials accident (Zeigler, Johnson, and Brunn 1983). It is analogous to a buffer zone and is specified as a distance around the highway or fixed facility of interest. The distance used for a risk zone in past studies on transportation-related hazardous materials accidents has ranged from half-mile to three miles (Abkowitz and Cheng 1988). Here, we will assume that the risk zone is half-mile. We will use the module BUFFER to create this zone.

- b) Run the module BUFFER from the GIS Analysis/Distance Operators menu. Specify HIGHWAY as the feature image for which to calculate the buffer. Call the output image HALFMILE. Enter the value of 2640 for the buffer width, since a half mile equals 2640 feet. Change the value for buffer zone in the output image to 1. HALFMILE should automatically display with the Qualitative palette.

HALFMILE is a Boolean image with the value 1 representing the risk zone and the value 0 representing the area outside the risk zone. We should note that Euclidean risk modeling assumes that an accident can occur at any point on I-290 and therefore the population of Worcester within a half mile of the entire highway is at risk. This concept of determining the risk zone is different from one in which the site of an accident on I-290 is fixed and the half mile risk zone is calculated for that site, for example as through dispersion modeling, which we explore in the next section.

---

1. Although we selected chlorine for illustrative purposes, the techniques adopted in this exercise can also be applied to other chemicals.

## Estimating Population at Risk: The Uniform Density Method

Now that we have the image HALFMILE for the risk zone, the next step is to estimate the population in Worcester falling in the zone, since this will be the population at risk to a hazardous materials accident on I-290.

- c) Display BLCKGRP, the image of block groups in Worcester, using the Qualitative palette and a legend. Add the vector layer BGROUP with the Outline White symbol file to emphasize the outlines of the block groups. There are 195 block groups in the city. Scroll down the legend to see all of the block groups.

BLCKGRP was created from the U.S. Census Bureau's TIGER/Line database. This database was discussed and used in Exercise 2.

- d) Display the image POPBG with the Quantitative palette. Add the vector layer BGROUP with the default symbol file. Use Cursor Inquiry Mode to explore the values in the image.

POPBG shows the population of Worcester by block group. The population data was retrieved as an attribute values file from the Census Bureau's Summary Tape File (STF) 3A. The values file was then assigned to the block group image BLCKGRP to create POPBG. We will use the two images, BLCKGRP and POPBG, in estimating the population falling in the risk zone.

To estimate the population falling in the risk zone, we will adopt a procedure called the Uniform Density Method for population estimation (Mynar and Hewitt). The Uniform Density Method assumes that the population associated with each block group in Worcester is uniformly distributed throughout the entire block group. Based upon this assumption, population falling in the risk zone is estimated in a five step process.

1. Population density for each block group in Worcester is calculated by dividing the total population of the block group by the area of that block group.
2. The block groups falling in the half-mile risk zone are determined. Some block groups fall entirely in the risk zone, whereas other block groups fall only partially in the risk zone.
3. The area of the block groups falling in the risk zone is calculated. When the entire block group is in the risk zone, the area calculated will be the area of the block group. When only a part of the block group is in the risk zone, the area of the block group will be the area of that part.
4. The population for each block group falling in the risk zone is estimated by combining population density with the area of the block group falling in the risk zone. For example, if population density of a block group is 500 per square mile and its area in the risk zone is 0.7 square miles, then the population of the block group in the risk zone is 350. This is an outcome of the assumption that population is uniformly distributed throughout the block group.
5. The total population falling in the risk zone is calculated by summing up the population of each block group in the risk zone.

We will implement these steps in IDRISI using the data for Worcester. To help clarify the implementation process, we will rely on a type of modeling called cartographic modeling. In cartographic modeling, the steps required to arrive at an end product are sequentially organized. Figure 4.1 illustrates the cartographic model for carrying out the five steps for estimating the population using the Uniform Density Method. Organizing the operations being carried out on the images through such sequential steps helps clarify the steps involved in the GIS analysis.



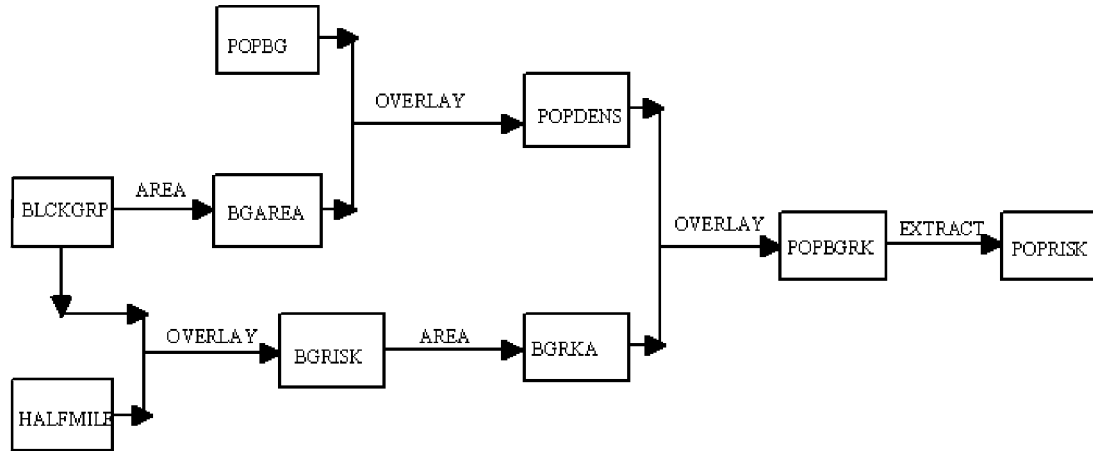


Figure 4.1

- e) Run the module AREA and specify BLCKGRP as the input image. Call the output image BGAREA and select image as the output format. Calculate the area as square miles. Click OK.
- f) BGAREA automatically displays with the Quantitative palette and a legend. All the block groups are black or dark blue! This is because the area of the background pixels has also been calculated and displayed. Since this area has a very high value compared to the block group areas, all these areas are assigned to only a few of the lowest palette colors when autoscaling is used by the display. (Autoscaling is always used when the values are real numbers). Click on Layer Properties in the Composer box. Since the largest block group is less than 2 square miles, enter a new display max of 2 at the bottom of the Layer Properties box and click OK. You can change the display settings in this manner any time a large proportion of your data values fall within a small window of the overall values. Add the vector file BGROUP on this image using the Qualitative symbol file. Then use Cursor Inquiry Mode to explore the values in the different block groups. The value within each block group is the area of that block group in square miles. We can ignore the area of the background pixels as it will be masked out later.

Now that we have the images for population by block group and for area by block group, we can calculate population density.

- g) Run the module OVERLAY and specify the first image as POPBG, the second image as BGAREA, and the output as POPDENS. Choose the overlay option of division (First / Second). Accept the default option for division by zero. Click OK. POPDENS displays automatically. Add the vector file BGROUP with the Outline White symbol file and explore some of the values.

The second step is to determine the block groups falling in the risk zone. As the risk zone image HALFMILE is a Boolean image, this can be achieved by multiplying HALFMILE by the block group image BLCKGRP.

- h) Run OVERLAY again, this time using HALFMILE as the first image, BLCKGRP as the second image, and BGRISK as the output image. Choose the multiplication option. Click OK. Change the palette of BGRISK to be qualitative. Add the vector layer BGROUP with the Outline White symbol file.

The block groups falling in the half-mile risk zone can be seen in the image. Many of the block groups fall only partially in

the risk zone. Note that the portions falling outside the risk zone have the value 0, while those in the risk zone retain the block group identifier. The third step is to determine the area of the block groups that fall in the risk zone.

- i) Run AREA again and specify BGRISK as the input image for which to calculate the area. Specify the name of the output file as BGRKA and choose image as the output format and square miles as the units. Click OK.

The fourth step is to calculate the population for the block groups falling in the risk zone. To do this, we will multiply the population density image POPDENS by the image BGRKA.

- j) Run OVERLAY and specify POPDENS as the first image and BGRKA as the second image. Call the output POPBGRK and choose the multiplication option. Click OK.

The final step is to calculate the total population at risk to a hazardous material accident on I-290. The image POPBGRK captures the population for each block group falling in the risk zone. The values outside of the risk zone are not important. To find the total population falling in the risk zone, we need to extract the population values from this image and then sum the values. We will do this using the EXTRACT module. EXTRACT requires a feature definition image to be used in conjunction with the image from which the values are extracted. The feature definition image we will use is BGRISK since this is the image of features (the block groups) in the half mile risk zone.

- k) Run the module EXTRACT and specify BGRISK as the feature definition image and POPBGRK as the image to be processed. Select the maximum value as the summary type to extract and choose the output type to be a values file. Call the values file POPRISK. Click OK.
- l) Use Edit to edit the values file POPRISK. If you have a spreadsheet or statistical software, import POPRISK into the software as a space-delimited file and calculate the total population. Otherwise, use a calculator to find the total population by summing all the values. Do not include the sum for category 0.

1. *What is the population at risk in Worcester from a hazardous materials accident on I-290, assuming a half mile risk zone, the Euclidean-based risk modeling approach, and the Uniform Density Method of population estimation?*

## Risk Assessment

Thus far, we have considered risk to be synonymous with exposure. A more appropriate definition of risk is that it is a function of the probability or likelihood of an accident and the magnitude of consequences. In the case of risk to human population from hazardous materials transportation accidents, a simple definition of risk is (Lepofsky, Abkowitz, and Cheng 1995):

$$\text{Risk} = \text{Probability of an accident} * \text{Total population exposed}$$

2. *Assume that historical data about hazardous materials accidents on I-290 have indicated the probability of an accident on this highway is  $1.5 \times 10^{-4}$ . What is the risk of a hazardous material accident in a half-mile risk zone around I-290 using the Euclidean modeling approach and uniform density method of population estimation?*

The risk value that is obtained from the question above in and of itself does not have much meaning for risk management. It must be compared with risk values for other hazards that people confront in the half mile risk zone, to the risk posed by other highways in the city or in the region, and to the reduction in risk that is achieved from reducing the probability of an accident. The risk value is also dependent on the spatial extent of the zone, the approach to modeling adopted, and the method of estimating total population. For example, if the spatial extent of the zone is increased the total population at risk increases and the risk value goes up. If the modeling approach is changed, the nature of the risk zone and the population at risk change, and we will get a different risk value.

## Dispersion-Based Population Estimation

In this section, we will adopt a different procedure from Euclidean risk modeling for determining the risk zone for a haz-

ardous material accident on I-290 involving the release of chlorine. The movement of a toxic chemical released into the air from a hazardous materials transportation accident would depend upon forces such as wind direction, wind speed, characteristics of the chemical, and quantity released. When modeled, the shape of the movement, or dispersion, would look plume-like with increasing distance from the site of the accident, since the chemical will dissipate over space and with time. A number of software packages exist which can model such a dispersion plume. One such package is ALOHA (Areal Locations of Hazardous Atmospheres, Version 5.2) developed by the U.S. Environmental Protection Agency (EPA) and the U.S. National Oceanographic and Atmospheric Administration (NOAA) (NOAA and EPA 1995). Since ALOHA is proprietary software, we cannot provide it with this workbook.<sup>2</sup> Instead, we will provide a plume developed in ALOHA for the hypothetical example used in this exercise. First we describe the process through which ALOHA creates the plume.

## Dispersion Modeling with ALOHA

ALOHA requires five types of input for modeling a plume for a chemical released into the atmosphere:

1. Site data. This consists of the city in which the accident has occurred, the type of buildings near the accident site (single story, double story), the surroundings (for example, presence of trees and shrubs), and the time of the accident. In our case, the city is Worcester, the buildings near the accident site are two-storied, the terrain is urban (very few trees and shrubs), and the time of the accident is 1:30 PM.
2. Chemical information. This is information about the chemical for which the plume must be calculated. In our hypothetical example, chlorine is released following the accident. ALOHA extracts information about chlorine from a chemical database that is part of the software. For example, the Immediately Dangerous to Life and Health (IDLH) value for chlorine is 10 parts per million (ppm) and the boiling point is -34.03°C.
3. Atmospheric information. ALOHA requires atmospheric information such as wind direction, wind speed, and relative humidity. For our hypothetical example, we specified a wind direction of 90° (wind is from the west), a wind speed of 12 miles per hour, relative humidity of 50%, and medium cloud cover.
4. Source strength. This pertains to the source of the release (for example, tank, pipe, etc.), the amount released, and the state of the chemical when released (liquid, solid, etc.). Assuming the accident involved a tractor trailer carrying a tank of chlorine, we specified the release to be from a tank, of liquid form, and the amount released to be 100 gallons.
5. Computational formula. ALOHA requires a computational formula for use in dispersion modeling. Two internal options are provided in the software: (1) to use a formula based on the Gaussian distribution; or (2) to let ALOHA decide the formula to be used. We selected the formula based on the Gaussian distribution.

Using these five types of information about the hypothetical accident, ALOHA creates the plume shown in Figure 4.2 below. The darker area in the center of the plume represents the area, as determined by the Gaussian model, in which the IDLH values are 10 ppm. The lines around the darker area represent the larger area that can be potentially covered by the plume because of uncertainty in wind speed and direction. We have imported the plume (as represented by the larger area) as a vector file into IDRISI. We will rasterize the vector file into an IDRISI image so that we can use the plume as the dispersion-based risk zone.

---

2. ALOHA is distributed by the National Safety Council, PO Box 558, Itasca, Illinois 60143, USA.

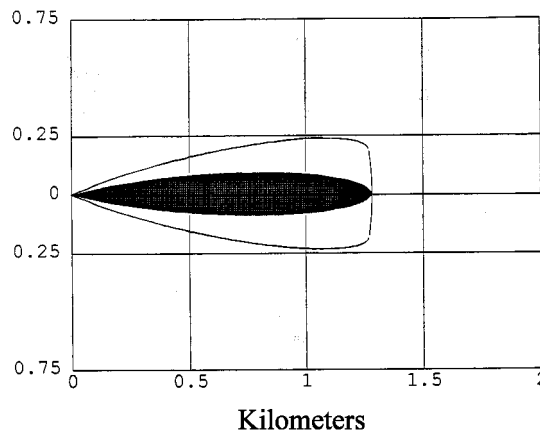


Figure 4.2

### Creating the Dispersion-Based Risk Zone

- m) Display the vector file PLUME with the standard default symbol file. The plume extracted from ALOHA can be seen on the screen. We will convert this vector file into a raster image.
- n) Run INITIAL from the Data Entry menu. Select the option for copying spatial parameters from another image (this is the default option). Specify PLUME as the output image and BLCKGRP as the image from which to copy the parameters. This sets the dimensions and reference system of the new image to be the same as BLCKGRP. Click on OK.
- o) Next run the module RASTERVECTOR from the Reformat menu and specify vector to raster and polygon to raster. Then specify the vector file as PLUME and the image file to be updated also as PLUME.
- p) PLUME should display automatically. Use Add Layer to overlay the vector file PLUME with the Outline White symbol file. Then use Add Layer again to overlay ACCIDENT with the Outline White symbol file. Use Add Layer once more to overlay HIGHWAY with the Outline Black symbol file. The area covered by the plume developed in ALOHA with respect to I-290 and the site of the hypothetical accident can be seen. Zoom into the area if you desire.

PLUME is a Boolean image which shows the dispersion-based risk zone. The next step is to estimate the population in Worcester falling in this zone.

### Estimating Population at Risk: The Landuse Refinement Method

To estimate the population falling in the dispersion-based risk zone, we will adopt a different method than the Uniform Density Method used in the first part of this exercise. The Land Use Refinement Method assumes that the population in a block group is present only in areas of residential landuse as opposed to being uniformly distributed through out the block group (Mynar and Hewitt, n.d.). With the Land Use Refinement Method, we will also illustrate a different approach for calculating the total population at risk which significantly reduces the number of steps involved and which does not require a calculator or separate software to calculate the total population falling in the risk zone.

The steps involved in the Land Use Refinement Method are:

1. Extract residential landuse from all the landuses.
2. Combine data on residential landuse and block groups.
3. Calculate the total area of residential landuse in each block group.
4. Calculate population density in residential areas by combining the population of each block group with the area of residential landuse in each block group.
5. Determine the total population at risk by extracting and summing the population of all areas falling within the risk zone.

The key step is step 3, in which the area of residential landuse in each block group is calculated. Instead of calculating area in square miles as we did in the Uniform Density Method, we will calculate area as the number of cells in the residential areas of each block group. By doing so, population density in step 4 is calculated as population per cell (rather than population per square mile). This allows us to directly extract the total population at risk in the last step.

As in Part A, we will use cartographic modeling to diagram the implementation of the above steps in IDRISI. This model is shown in Figure 4.3

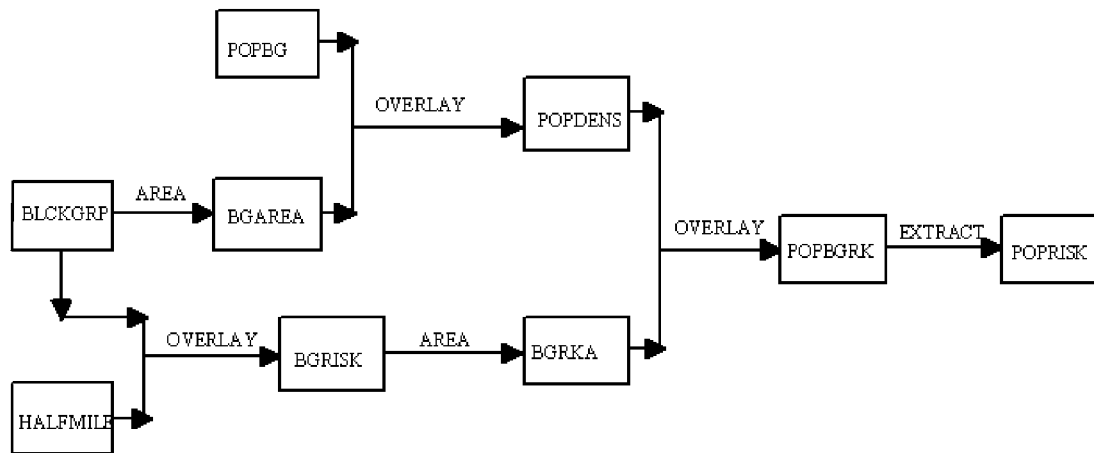


Figure 4.3

We will now carry out the operations identified in the cartographic model displayed above.

- q) Display the image LANDUSE with the Qualitative palette and legend.

LANDUSE is an image of landuse in Worcester derived from U.S. Geological Survey (USGS) Land Use/Land Cover data. In this image, residential landuse is represented by four categories: multi-family lots, less than 1/4 acre lots, 1/4 - 1/2 acre lots, and greater than 1/2 acre lots. We will use these four categories to create an image of residential landuse in Worcester. We will do this by first creating an attribute values file containing the identifiers for these categories and the new value to be assigned to the categories. Then we will assign the values file to LANDUSE.

- r) Use Edit to open a new file. The four categories of residential landuse have the values 10, 11, 12, and 13 in the image LANDUSE. A new value of 1 has to be assigned to these four categories. Enter the following values in the file:

10      1

11	1
12	1
13	1

Save it as a values file named RESID, with an integer data type. Exit the file. Now run ASSIGN and specify LANDUSE as the feature image, RESID as the attribute values file, and RESID as the new image to be created. Display RESID with the Qualitative palette.

RESID is a Boolean image with the value 1 showing all the residential areas in Worcester. We will combine this image with BLCKGRP, the block group image for Worcester. This will allow us to calculate the area of residential landuse in each block group.

- s) Run OVERLAY and specify the first image as BLCKGRP, the second image as RESID, and the output as RESBGRP. Select the option of multiplying two images. Display RESBGRP with the Qualitative palette and a legend. Use Add Layer to overlay the vector file BGROUP on the image with the default symbol file.

The residential landuse falling in each block group in Worcester can be seen. As expected, some block groups do not have any residential landuse.

- t) Run AREA and specify RESBGRP as the image for which to calculate the area. Select the output format to be image and call the output file RESACELL. Calculate the area as cells.

The next step in the landuse refinement method is to find the population density by dividing the population of each group by the area of residential landuse in the block group.

- u) Run OVERLAY and specify the first image as POPBG, the second image as RESACELL, and call the output POPCELL. Select the option of dividing the first image by the second and click OK. Change the palette for POPCELL to the Quantitative palette. The image will be very dark. Change the maximum value display settings in Layer Properties to examine the characteristics of the image.

POPCELL shows the population density in terms of population per cell as opposed to population per square mile. To find the total population falling in the risk zone, we will use EXTRACT to extract the population values from POPCELL using the image of the risk zone, PLUME, as the feature definition image.

- v) Open the module EXTRACT and specify PLUME as the feature definition image and POPCELL as the image to be processed. Select the option of extracting the total (sum) and the output type to be tabular. Click OK.

3. *What is the population at risk in Worcester from a hazardous materials accident on I-290, using the Landuse Refinement Method of population estimation and the dispersion-based risk modeling approach?*

## **The DISPERSE Module in IDRISI**

In this section, we will adopt a different procedure for dispersion modeling from that based on ALOHA. We will use an IDRISI module called DISPERSE. DISPERSE models the movement of phenomena that have no motive force of their own, but which are acted upon by anisotropic forces to disperse them over time. In the case of a transportation-related accident, an example of such a phenomenon is the release of a toxic chemical into the air as a result of the accident. DISPERSE allows us to model this plume-like movement while accommodating the effects of forces such as wind in the case of air dispersion or slope in the case of groundwater pollution.<sup>3</sup>

---

3. For a more detailed description of DISPERSE, refer to the IDRISI Help System.

## Creating a Risk Zone from DISPERSE

To run DISPERSE, we need three images: a source feature image from which distances will be calculated, a force magnitude image which defines the strength of the force acting upon the phenomenon, and a force direction image which specifies the direction in which the force is acting. The source feature image consists of the location of the accident site on I-290. It is from this site or feature that the distance over which the chemical will travel in air is calculated. The force assumed to act on the chemical in dispersing it in the air is *wind*. We will create the force *magnitude* image from the prevailing wind speed for Worcester. We will create a force *direction* image using the prevailing wind direction for Worcester.

- w) Display the image ACCIDENT with the Qualitative palette. This is a rasterized image of the vector file ACCIDENT and shows the site at which the accident has occurred on the highway. This site is just one cell, so you will probably need to zoom in with the Zoom Window tool from the toolbar for a closer look at the site. The image ACCIDENT is the source feature image from which distances will be calculated by DISPERSE.

To create the force magnitude and direction images from this data, we will use the INITIAL module.

- x) Run INITIAL and choose the option of copying spatial parameters from another image. Specify WINDSPD as the name of the image to be created and ACCIDENT as the image from which to copy the parameters. Select output data type to be real (DISPERSE requires a real data type). Next, enter the initial value of the image to be 25 (the prevailing wind speed in Worcester in miles per hour). Click OK.
- y) Run INITIAL again, but this time specify WINDDIR as the name of the image to be created and ACCIDENT as the image from which to copy the parameters. Select output data type to be real, and enter the initial value to be 90 (the direction of the prevailing wind). Click OK.

Now that we have the source feature image, and the force magnitude and direction images, we can run DISPERSE.

- z) Open the module DISPERSE. Specify the source feature image as ACCIDENT, the force magnitude image as WINDSPD, and force direction image as WINDDIR. Next, you must select a source function and are provided with two options: the cosine function or a user-defined file.

The role of the source function is to allow DISPERSE to model the variation in the force (wind speed) as a function of wind direction. For example, if the hypothetical wind direction in Worcester is 90°, then the force would be the maximum in this direction (a wind speed of 25 miles per hour). However, it is unlikely that the gas would travel in a straight line only directly to the east of the spill. There is likely to be some broadening of the plume in directions other than directly east. To model this phenomenon, two source functions, a cosine function and a user-defined function, have been provided as part of the DISPERSE module.<sup>4</sup> We will use the cosine function in this case.

- aa) Select the cosine function with the default value of 2. This value is the exponent used by the cosine function to limit the extent of direction in which the force is considered to act. As the exponent increases, the force (wind speed) acts increasingly in the same direction (in our case, 90°). After some experimentation, we found that an exponent of 2 provides the optimum directional bias for the particular site selected on I-290. Click on the option for maximum distance desired in the output and specify this distance to be 1500 feet. Specify the name of the output image as IDRDISP and click OK. DISPERSE will take some time to create IDRDISP. (Note: In DISPERSE, there is an option to use an isotropic friction surface as well. Such a frictional surface might include, for example, the presence of tall buildings or hills that limit or prevent an air mass from dispersing any further).

The image shows the plume-like shape of distances from the site of the accident on I-290 as calculated by DISPERSE. Since we are interested in creating a risk zone, we must reclassify IDRDISP.

---

4. Both the cosine and the user-defined functions are described in the IDRISI Help System.

- ab) Run RECLASS and specify the input image as IDRDISP and the output image as RISKZONE. Select the user-defined option for reclassification. Specify the new value of 0 for the old values ranging from -1 to those just less than 1 and the new value of 1 for the old values ranging from 1 to those just less than 2000. Click OK.

RISKZONE is a Boolean image which shows the dispersion-based risk zone. Note how the shape of this zone differs from that based on ALOHA.

4. *Using the technique of landuse refinement method for population estimation, estimate the population at risk from the image RISKZONE.*

The approach adopted in using DISPERSE for estimating risk to a hazardous materials transportation accident was limited in its scope. We only considered hypothetical wind speed and direction in our model. We did not take into account the characteristics of the toxic material (chlorine) which affect its rate and extent of dispersion. Similarly, meteorological conditions such as temperature and humidity which influence the dispersion process were not considered. In addition, a user-defined function developed theoretically or empirically might have been employed rather than the default cosine function to model the dispersion. Examples of such user defined functions can be found under discussions of dispersion models (see Withers 1988). ALOHA takes into account some of these factors that DISPERSE does not. However, it fails to incorporate others such as terrain. On the other hand, characteristics of terrain can be easily stored and analyzed with a GIS. Thus there appears to be a need for additional research linking software such as ALOHA with the capabilities of a GIS. Implementing dispersion models entirely within a GIS environment is also possible, as demonstrated by the application of the DISPERSE module in this exercise, and is a topic of further exploration for GIS researchers.

## Conclusions

Two techniques were used in this exercise to estimate the population at risk to a hazardous materials transportation accident. The Uniform Density Method of population estimation assumed that population was uniformly distributed in a block group. The Land Use Refinement Method of population estimation assumed that population in a block group is found only in residential areas. Both techniques were easily implemented in a GIS context. The use of GIS for implementing such techniques of population estimation in combination with other GIS-based techniques for hazard identification and exposure assessment should prove useful for risk assessments of hazardous materials transportation as well as hazardous facilities.

## References

- Abkowitz, M., and P.D. Cheng. 1988. Developing a risk/cost framework for routing truck movements of hazardous materials. *Accident Analysis and Prevention* 20(1): 39-51.
- Abkowitz, M., P.D. Cheng, and M. Lepofsky. 1990. Use of geographic information systems (GIS) in managing hazardous materials shipments. *Transportation Research Record* 1261: 35-43. Washington, D.C.: National Academy of Sciences.
- Lepofsky, M., M. Abkowitz, and P. D. Cheng. 1995. Transportation hazard analysis in an integrated GIS environment. In *Computer Supported Risk Management*, eds. G.E.G. Beroggi, and W.A. Wallace, pp. 115-131. Dordrecht, Netherlands: Kluwer.
- Mynar, F. II, and M. J. Hewitt III. n.d. *Population estimation for risk assessment: A comparison of methods*. Las Vegas, NV: Lockheed Engineering and Sciences Company and Environmental Monitoring Systems Laboratory, U.S. Environmental Protection Agency.
- NOAA (U.S. National Oceanographic and Atmospheric Administration) and EPA (U.S. Environmental Protection Agency). 1995. *Areal Locations of Hazardous Materials (ALOHA), Version 5.2*. Seattle, WA: Hazardous Materials Response and Assessment and Division, NOAA and Washington, D.C.: Chemical Emergency Prevention and Preparedness Office, EPA.
- USGAO (U.S. General Accounting Office). September 1991. *Transportation safety: information strategy needed for hazardous mate-*

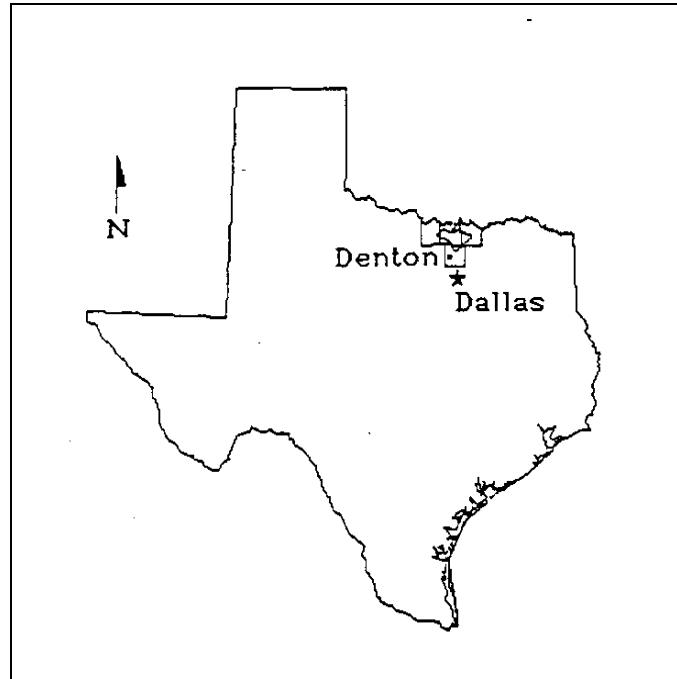


*rials*. Report to the Chair, Subcommittee on Government Activities and Transportation, Committee on Government Operations, House of Representatives. GAO/IMTEC-91-50. Washington, D.C.: United States General Accounting Office.

Withers, J.M. 1988. *Major industrial hazards: their appraisal and control*. New York: Halsted Press.

Zeigler, D., et al. 1983. *Technological hazards*. Washington, D.C.: American Association of Geographers (AAG).

## ***Exercise 5: Nonpoint Source Pollution Modeling***



## Introduction

Nonpoint source pollution results in the degradation of water quality from storm runoff, a process in which pollutants on land are released and transported during rain storms into water bodies. For example, one study reports that more than one billion tons of sediment from agricultural lands are transported into waterways in the United States annually (Mertz 1993). Unlike point sources of pollution such as a factory, nonpoint source pollution originates from multiple locations. In an urban area, it may be produced simultaneously from residential, commercial, and industrial sources. In an agricultural setting, the pollution may occur from different landuses, use of fertilizers, and livestock.

GIS has emerged as a valuable technology for assessing and managing nonpoint source pollution (Atkinson 1988; James and Hewitt 1992; Kim and Ventura 1993; Mertz 1993). Kim and Ventura (1993: 1539) identify several advantages of using GIS for assessing urban nonpoint pollution: (1) street networks captured in a GIS can provide the reference for collecting data on pollutants and delineating storm sewer areas; (2) data on landuse and empirical models for assessing nonpoint pollution can be easily combined within a GIS context; and (3) critical areas contributing significant amounts of pollutants can be identified by aggregating pollutant loadings for major sewer outfalls through overlay analysis. James and Hewitt (1993) illustrate the use of GIS with a model, the Water Resources Evaluation of Nonpoint Sivicultural Sources (WRENSS) model, to assess nonpoint source pollution in the Blackfoot River drainage basin in Montana, USA. At a regional level, Atkinson (1988) found that GIS allows the most feasible sites for controlling nonpoint source pollution to be identified so that planners can focus on such sites and look at more complicated sites in later stages.

In this exercise, we will model nonpoint source pollution and illustrate how the nonpoint pollution delivery process can be estimated using a GIS-based model. The exercise focuses on the delivery of two types of pollutants: (1) sediments, or soil particles, and (2) nutrients, with a focus on nitrogen and phosphorus. Nitrogen and phosphorus were chosen because the data sets available for these pollutants were more complete than for other nutrients. The model adopted was developed, tested, and calibrated on 12 watersheds in the Lake Ray Roberts drainage basin located in north Texas (Levine, et al. 1993).<sup>1</sup> The final product of the model is the annual amount of sediments and the two nutrients, measured in tons, that are lost from the drainage basin per year.

The first section of the exercise describes data on the Lake Ray Roberts drainage basin which will be used for modeling nonpoint source pollution. In the second section, several images are created from the available data for use in the modeling. The third section provides an overview of the steps involved in the modeling process. Because of the complexity of the model, the remainder of the exercise is divided into sections in which each step in the modeling process is comprehensively described and carried out.

## Data Description

From the twelve watersheds in the Lake Ray Roberts drainage basin, we selected the Timber Creek Watershed in Cooke County for illustrating nonpoint source pollution modeling in this exercise. The data on this watershed which we will use are soils, landuse, and elevation. These data layers came from different sources and had different resolutions. They were subsequently resampled to a resolution of 20 meters and compiled into one georeferenced data set (Levine, et al. 1993).

- a) Display TCSOIL with the Qualitative palette and a legend.

The image shows 26 types of soils in the Timber Creek Watershed. The soils map is based on county soil surveys and was compiled by the National Soil Conservation Service. Soil attributes such as mean particle diameter, permeability, and erodibility are important parameters in nonpoint source pollution modeling.

- b) Next display TCLUSE with the Qualitative palette and a legend.

The image shows seven types of landuse in the watershed. Rangeland here refers to natural land cover whereas pasture is

---

1. The data, several programs, and the model used in this exercise were donated by Dr. Daniel Levine of the Environmental Sciences Division at the Oak Ridge National Laboratory, Tennessee, USA.

human-maintained grazing land. The seven landuses were extracted from a classified 1986 Multispectral Scanner (MSS) coverage for the watershed by grouping commercial, residential, and industrial landuses into one category called developed land. The MSS coverage was created by the Center for Remote Sensing and Land Use Analyses at the University of North Texas. Land use defines the amount of nutrients available as well as the surface conditions along the path of flow of pollutants. For example, one would expect more nitrogen to be available in cropland than in developed land.

- c) Display TCDEM, the digital elevation model for the watershed, with the Quantitative palette.

The elevation model was created from contours digitized from 1:24,000 USGS 7.5 minute quadrangle maps. The image shows that elevation is progressively decreasing from the northwest section of the watershed to the southeast indicating the potential direction of flow of pollutants in the watershed. Terrain parameters developed from TCDEM, such as slope, direction of flow, and length of flow play an important role in defining the delivery of pollutants to the watershed outlet.<sup>2</sup>

- d) Display TCMASK with the Qualitative palette. This is a Boolean image showing the extent of the watershed.

The background cells have a value of 0 and the cells within the watershed have a value of 1. This image will be used to mask out the background and extract information about the watershed from the different images created in the modeling process.

In addition to these four images, we will be using a number of attribute values files, macros, and executable files. We will describe these files as we use them in the exercise.

## **Data Development**

In this section, three images for use in the nonpoint pollution model are created. The images pertain to three types of data: (1) slopes in the watershed; (2) the direction of flow of water and pollutants; and (3) the length of flow. We will define each of these data types and create the images for them.

### **Slopes**

Slope gradient is one of the most critical parameters in nonpoint source pollution modeling. It defines the direction and speed of flow of water and pollutants, and affects the capacity of a vegetated surface to retain the pollutants. We will create an image of slopes in the watershed using the digital elevation model, TCDEM.

- e) Run the module SURFACE choose to calculate the slope (this is the default). Specify the name of the input elevation model as TCDEM and call the slope image SLOPES. Select to calculate slopes in percent and click OK. When SURFACE has finished, SLOPES will be displayed. Some of the steeper slopes can be found in the northern sections of the watershed.

### **Direction of Flow**

The direction of flow from a cell is an important element in nonpoint pollution modeling since it determines the direction of flow of water and pollutants. In raster-based models, the direction of flow is usually determined by comparing the elevation of a cell with the elevation of its neighbors. In these models, the number of neighboring cells considered for comparison with a cell as well as the algorithm for calculating direction vary. Some models include all of the eight neighboring cells whereas others include all of the cells except the diagonal cells. Some, such as the aspect option in the IDRISI module SURFACE, calculate direction as an azimuth ranging from 0° to 360° clockwise from north; others specify only eight directions (north, northeast, east, southeast, south, southwest, west, and northwest).

In this exercise, we will use a model in which the elevation in the center cell is compared with the elevations in the eight

---

2. The watershed outlet is the point through which water and pollutants leave the watershed.

surrounding cells. It is assumed that the direction of flow out of a cell corresponds to the direction of maximum elevation drop (Jenson and Domingue 1988). The example below illustrates this model.

Elevation (feet)			Elevation difference (feet)		
807.4	807.8	808.6	1.4	1.8	2.6
806.3	806	807.8	0.3	0	1.8
804.7	804.6	806.8	- 1.3	- 1.4	0.8

In this example, compare the central cell with an elevation of 806 feet to its surrounding cells. Only two cells (to the south and southwest) have lower elevations. Of these two, the cell to the south has the higher elevation drop (1.4 compared to 1.3 for the southwest cell). Thus, the central cell will be assigned a flow direction to the south.

The FLOW module in IDRISI produces the flow direction image from a digital elevation model. It assigns the following values to the eight directions specified:

45 - Northeast	225 - Southwest
90 - East	270 - West
115 - Southeast	315 - Northwest
180 - South	360 - North

Flow directions are assigned in degrees. The table below also illustrates the values and the directions to which they are assigned.

315	360	45
270	--	90
225	180	115

- f) Select the FLOW module. Specify TCDEM as your DEM and DIRECT as the output image. Since this DEM contains no pits, you do not need to perform pit removal. However, since TCDEM has a background value of 0, click the Define background values box and specify 0. Display DIRECT with the Quantitative palette and the autoscale option turned on. Use Cursor Inquiry Mode to explore values in the image. Only eight values, corresponding to the eight flow directions, have been assigned to the cells in the image.
- g) Run HISTO from the GIS Analysis/Statistics menu and specify DIRECT as the input image and click OK.

1. *Which flow direction is predominant?*

## Length of Flow

The length of flow represents the distance that water and pollutants are transported through a cell. For horizontal and vertical flows, the length of flow out of a cell is equal to the resolution of the cell in the image DIRECT. For diagonal flows, the length of flow is the cell resolution multiplied by the square root of 2.

To create an image of the length of flow, we need to assign the length of flow values to each cell in the direction image DIRECT. In our case, cells with flow direction values of 90, 180, 270, 360, representing east, south, west, and north respectively, should be assigned a new value of 20 because these represent horizontal and vertical flows. The cells with

flow direction values of 45, 15, 225, and 315 should be assigned a new value of 28.284, as they represent diagonal flows. An attribute values file with these assignments called LENGTH is included in the data set.

- h) Run the module ASSIGN and specify DIRECT as the feature definition image, LENGTH as the attribute values file, and LENGTH as the new image. Display LENGTH with the Quantitative palette. Use Cursor Inquiry Mode to explore the values in the image. Only three values, 20 for horizontal and vertical flows, 28.284 for diagonal flows, and 0 for background should be represented in the image.

2. *What is the length of flow for horizontal and vertical flows in this data set? For diagonal flows?*

## Modeling

Nonpoint source pollution results in the deterioration of water quality. The degree of deterioration depends on the strength of pollution sources and the delivery process of the pollutants from the source to the receiving waters (Novotny and Chester 1989). Numerous models, empirical as well as theoretical, and ranging from simple to complex, have been created to address these issues. Many of these models, however, lack temporal and spatial dimensions (Levine, et al. 1993). The model discussed in this exercise combines empirical models with spatial parameters affecting the movement of pollutants through the landscape. Before we explore the use of this model, we will introduce some terms and discuss the model in a simplified form.

Consider a watershed with a permanent stream. When a storm occurs, a part of the water from the storm infiltrates through the soil and a part of it is carried down slope as overland flow. As the soil becomes saturated with moisture, more water is carried as overland flow. Moisture content in the soil prior to the storm, the intensity of the storm, its duration, and the permeability of the soil determine the amount of water that is carried as overland flow. Furthermore, soluble sediments and nutrients in the soil detach and dissolve in the water, and are carried away with the water toward the stream. The amount of sediments and nutrients available for transport by water depends on landuse, soil, and topographic conditions. In our model, this is calculated in the first step as "sediment and nutrient detachment". In addition to overland flow, there is also subsurface flow of the infiltrated water. The model does not consider such subsurface flow.

Not all of the available sediments and nutrients in the soil, however, are carried away in the above process. Surface conditions such as soil permeability, slope, and vegetation density define what proportion of sediments and nutrients will be "trapped" in situ and what proportion could be carried away with water. The proportion carried away with water is called the *delivery ratio*. This ratio is calculated for each cell in the watershed in the second step of the model as the "overland flow delivery process".

A third characteristic of the nonpoint pollution delivery process is that during an intense storm, a network of temporary streams is often formed in a watershed. The model used here assumes that the energy of overland flow within these temporary streams is high enough to mobilize and carry away all available sediments and nutrients. This means that the delivery ratio for cells within these temporary streams is 100 (that is, 100% of the available nutrients and sediments will be carried away with water). The network of permanent and temporary streams in a watershed is delineated in the third step of the modeling as "stream network delineation".

The fourth step is determining the path of flow of pollutants from each cell to the watershed outlet. At this stage, we will use the results of step 3 to identify the individual path of water flow from each cell toward the stream network. The length of this path defines the contribution of each cell to the total pollutant load. The further a cell is from the stream the smaller will be its contribution, since a portion of the initial sediments and nutrients carried out of the cell will be trapped in each consecutive cell on the way to the stream. This flow path information is used with results of step 2 to calculate "total flow path delivery ratios" which express the part of available load that actually reaches the stream.

The final step in the model involves calculation of the total mass of sediments and nutrients delivered from each cell in the watershed to the stream. To do this, the initial mass of sediments and nutrients available for transport (determined in step 1) is multiplied by the percent of the mass that actually reaches the stream (from step 4). The total amount of pollutants reaching the watershed outlet is then calculated by summing up the values of all of the cells. The final result of the model will be the "total annual nutrient and sediment loadings" (in tons) leaving the watershed through its outlet.

We will now implement each of these five steps for the Timber Creek watershed.

## **Step 1: Sediment and Nutrient Detachment**

In this section, we will calculate the initial mass of sediments and nutrients available for transport by water flow. When a raindrop impacts the ground, soil particles become suspended and are carried away. Some nutrients borne by the soil particles (such as nitrogen and phosphorus) become dissolved in water. There are theoretical and empirical models that quantify this physical process and the initial mass available for transport. Here, we will use two empirical models, one for calculating the initial mass of sediments, and the other for the initial mass of nutrients.

### **Sediment Detachment**

To calculate the initial mass of sediments available for transport, we will use the Universal Soil Loss Equation (USLE). USLE is one of the most widely used empirical models for this calculation (Wischmeier and Smith 1978). USLE is defined as (Levine et al. 1993: 38):

$$A = RKLSCP$$

where:

$A$  = average annual soil loss per unit area (tons per cell per year),

$R$  = rainfall and runoff factor (tons per hectare),

$K$  = soil erodibility factor,

$L$  = slope length factor,

$S$  = steepness factor,

$C$  = cover and management factor,

$P$  = support practice factor.

Each of these factors is defined below. In the section below we will also describe the data needed to create an image for each factor. The instructions for creating the factor images will be given at the end of this section when we calculate the USLE image.

*R, the rainfall and runoff factor*

This factor (or erosivity index) is an index of how much erosive force the typical storm has on surface soils. In this study, the rainfall and runoff factor  $R$  equals 616 tons/hectare for the entire Timber Creek Watershed. This value was obtained from the Continental isopleth map produced by the U.S. Soil Conservation Service.

*K, the soil erodibility factor*

This factor was obtained from county soil survey tables. This is an empirically-derived index showing how susceptible a soil is to erosion based on soil texture, grain size, permeability, and organic matter content. The higher the value of  $K$ , the more susceptible is the soil to erosion. An attribute values file called SOILK lists the erodibility factor for soils in the Timber Creek Watershed.

- i) Use Edit to open the attribute values file named SOILK. The first column in the file represents the soil type with categories as shown in the soils image TCSOIL. The second column shows the  $K$  factor for each soil type. This values file will be used in the USLE.

*L, the slope length factor*

This factor is calculated using the following formula (Schwab et al. 1981):

$$L = (l/22)^x,$$

where:

$l$  = length of flow across a cell (in meters), and

$x$  = slope factor defined as:

0.5 for slopes > 4%,

0.4 for slopes = 4%,

0.3 for slopes < 4%.

We calculated the length of flow across a cell,  $l$ , as the image LENGTH in the last section. We will use our slope image (SLOPES) to create an image representing  $x$ , the slope factor. To do this, we will first reclassify SLOPES to a new image with three categories: 1 for slopes less than 4%, 2 for slopes equal to 4%, and 3 for slopes greater than 4%. We will then assign the values for the slope factor,  $x$ , to these reclassified categories. To carry out this second task, we have included an attribute values file, SLOPEFAC, to use with the ASSIGN module.

- j) Open the attribute values file SLOPEFAC with Edit. In this file, reclassified values for slopes are assigned the new values for  $x$ , the slope factor.

*S, the slope steepness factor*

This factor is calculated using the following formula (Schwab et al. 1981):

$$S = (0.43 + 0.30s + 0.043s^2) / 6.574,$$

where:

$s$  = percent slope.

We calculated slopes in percent,  $s$ , in creating the image SLOPES, above. This will be used to create the slope steepness factor image.

*C, the cover and management factor*

This factor is assigned on the basis of landuse and land cover. It is an index of how crop management and land cover affect soil erodibility. For example, the index can show whether the management method is conventional tillage in rotation with small grains or whether grazing is mixed with controlled burns. Each results in a different amount of erosion for the same area. The values for determining this index have been empirically derived and are listed in a number of documents and textbooks such as the U.S. Soil Conservation Technical Documents (Levine 1995). The Exercise Details section at the end of this volume lists the values of the cover and management factor for the landuse/land cover found in the Timber Creek Watershed. An attribute values file called COVERFAC was created with these values.

- k) Open the attribute values file COVERFAC with Edit. The left column in the file represents landuse/land cover (the categories are as shown in TCLUSE). The right column shows the C factor for each landuse type. This values file will be used to create the cover factor image.

*P, the support practice factor*

This factor refers to the level of erosion control practices, such as contour planting, terracing, and strip cropping, and is influenced by slope steepness. The value of this factor depends on average slope steepness in the watershed. Since average



slope values in the Timber Creek Watershed range between 2% and 7%, the value of 0.2 was assigned to the entire watershed (Levine et al. 1993).

## USLE

Using the above definitions and formulae, the USLE can be calculated through a series of mathematical operations falling in the class of GIS analytical operations known as Map Algebra. In Exercise 3, we had introduced the use of macros to perform Map Algebra. We will follow the same procedure here and use a macro for solving the USLE. To simplify the task, we have provided a macro called USLE.

- l) Using Edit, open the macro file called USLE.

Lines in the macro beginning with "REM" are remarks that serve to make the file more readable. These remarks have no impact on the computing process. The rest of the lines in the macro represent mathematical operations for solving the USLE. There are five logical parts in this file, the first four of which determine the four factors (K, L, S, C) and the fifth combines the four factors to calculate A, the average annual soil loss per unit area (tons per cell per year). For example, the first line in the macro determines the factor K by assigning the attribute values file SOILK to the soils image TCSOIL. The next four lines determine the slope length factor, L, and so on. A line-by-line explanation of this macro is provided in the Exercise Details section.

- m) Select Run Macro from the File menu. Specify the name of the macro as USLE and click OK. After the macro has finished, open Metadata to view information for the image POTS.

### 3. *What are the minimum and the maximum values in POTS?*

In this section, we employed a widely used empirical model, the Universal Soil Loss Equation (USLE), to calculate the initial mass of sediments available for transport. The use of a macro in IDRISI allowed all the calculations required for implementing USLE to be carried out in one step. Although Image Calculator could have been used for some of the calculations, the mix of analytical operations involved made the macro a more efficient choice.

## Nutrient Detachment

The amount of nutrients available for transport will be calculated using empirically-derived export coefficients for each nutrient. Export coefficients represent the amount of a nutrient (in kilograms) transported from an area (in hectares) per year for each landuse. In this study, they are converted into grams per cell per year to match the spatial resolution of the database. The export coefficients are drawn from tables compiled by Reckhow et al. (1980). The coefficients were selected based on the similarity of soils, rainfall, slopes, and land management characteristics of the Timber Creek watershed to the watersheds in the tables. The export coefficients are provided in the Exercise Details section. We have created two attribute values files of these coefficients. EXPCOEFN and EXPCOEFP are the attribute values files for nitrogen and phosphorus export coefficients, respectively.

- n) Using Edit, open the attribute values file EXPCOEFN and then the attribute values file EXPCOEFP. The first column in both of these files represents the categories for landuse/land cover in the Timber Creek watershed. The second column shows the export coefficients to be assigned to these categories.
- o) Run ASSIGN and specify TCLUSE as the feature definition image, EXPCOEFN as the attribute values file, and POTN as the output image. Display POTN with the Quantitative palette. The image shows the potential load of nitrogen for each cell in the watershed.
- p) Run ASSIGN. Specify TCLUSE as the feature definition image, EXPCOEFP as the attribute values file, and POTP as the output image. The output image shows the potential load of phosphorus for each cell in the watershed.

## Step 2: The Overland Flow Delivery Process

This component of the model "represents the influence of surface conditions, such as soil permeability, slope and vegetation density on the delivery of sediments and nutrients during movement toward a stream channel" (Levine et al. 1993: 4). Models developed in this stage calculate transport (expressed as delivery ratios) of phosphorus, nitrogen, and sediments through each cell in the watershed. The models calculate trapping efficiencies, which are then converted into delivery ratios. Trapping efficiencies show the percent of sediments and nutrients which could be physically "trapped" in a cell. Delivery ratios show the percent that can "escape" from the cell. The sum of the trapping efficiency and the delivery ratio is 100%.

A body of literature known as vegetated filter-strip (VFS) studies describe nutrient- and sediment-trapping efficiencies of a vegetated surface as a function of vegetation, soil properties, slope, and flow distance. These studies were analyzed and compiled into a database by Levine et al. (1993: Appendix B). Using this database, multivariate regression analysis was carried out for each nutrient and sediment. Then, best-fit equations were chosen from the regression analysis and applied to the data for the Timber Creek watershed. Due to data limitations, the linear multivariate regression analysis did not provide suitable results. Additional statistical modeling using nonlinear techniques was then performed to generate three models of trapping efficiency in a non-linear form. The three models are:

$$TP_{\text{trapped}} = 1 / (1 + e^{(1.47 - 0.416d + 0.012 \text{sqrd} + 0.296p - 5.74n)}),$$

$$TN_{\text{trapped}} = 1 / (1 + e^{(-10.14 + 0.016d + 26.83\theta - 4.58\ln(n) + 2.87\ln(mpd) + 1.47dn - 1.63d\theta)}),$$

$$TSS_{\text{trapped}} = 1 / (1 + e^{(-3.57 - 0.33d + 0.011\text{sqrd} + 22.82\theta + 0.73p)}),$$

where:

$TP$  = trapping efficiency for total phosphorus,

$TN$  = trapping efficiency for total nitrogen,

$TSS$  = trapping efficiency for total suspended sediments,

$d$  = distance of flow (meters),

$\text{sqrd}$  = distance of flow squared (meters<sup>2</sup>),

$p$  = soil permeability (inches/hour),

$\text{mpd}$  = soil mean particle diameter (mm),

$n$  = Manning's roughness coefficient (unitless),

$\theta$  = theta, slope angle (radians),

$\ln$  = natural log.

We already created an image of distance of flow,  $d$ , when we created LENGTH. Data on soil permeability and mean particle diameter were obtained from county soil surveys. Two attribute values files, SOILPERM and SOILMPD, list the data on soil permeability and mean particle diameter respectively for soils in the Timber Creek Watershed. Manning's roughness coefficient characterizes the roughness of a vegetated surface and depends on landuse type. The Exercise Details section lists the coefficients as assigned to landuse type. These values were used to create an attribute values file called TCROUGH. The image SLOPES, which we created earlier, will be used to create  $\theta$ . These files will be used in the calculation of trapping efficiencies.

Each of the three models produces numbers in the range between 0 and 1 representing the portion of nutrient or sediment that could be trapped (retained) in a cell. By subtracting the trapping efficiency from 1, delivery ratios can be calculated. To calculate delivery ratios using the above formulae, we will use macros. First we will use a macro for calculating the surface parameters and then we will use three macros for calculating the delivery ratios. These four macros are

included in the data set as:

PARAM.IML	file that creates images of the surface parameters (mpd, p, n, $\theta$ , sqrd) to be used in the equations;
TCTP.IML	file that creates an image of delivery ratio for total phosphorus,
TCTN.IML	file that creates an image of delivery ratio for total nitrogen,
TCTS.IML	file that creates an image of delivery ratio for total sediments.

You can see these files by running Edit, opening a macro, and then specifying the name of the macro. Each command executed in a particular macro creates an image. Since there are several steps involved in the calculation of delivery ratios, many intermediate images (called TEMP\*.RST) will be created in the process. A line-by-line description of these macros is provided in the Exercise Details section.

The operation that converts trapping efficiency into delivery ratio is included in the macros so that the resulting images represent the delivery ratios. Since these images will be used later by programs requiring data in an integer format, the range of values in the images is set to be from 0 to 100 instead of from 0 to 1. This operation is also included in each of the delivery ratio macros. Thus, the values in resulting images represent the percent of total available nutrient or sediment that can be delivered from a cell.

- q) Select Run Macro from the File menu and specify the file PARAM. When the macro is completed, open IDRISI Explorer to see the new files which were created. Their names correspond to parameters in the formulas, but their titles reflect the operation through which they were produced. Use Metadata to change the titles and units (where necessary) of these images as follows:

Image	New title	New value units
MPD	Soil mean particle diameter	mm
P	Soil permeability	inches/hour
N	Manning's roughness coefficient	none
Theta	Slope angle	radians
Sqrd	Distance of flow squared	sq. m

Note that calculation of d (distance of flow) is not included in this macro. This image (LENGTH) was created earlier in the Data Development section. Since the trapping efficiency formulae require the slope image to be in radians, but the SLOPES image created earlier is in percent, conversion of the slope image into radians (THETA) is included in this macro.

- r) Select Run Macro again and specify the file TCTP. After the macro has finished, change the title of the resulting image TPRAW to "Delivery ratio for total phosphorus" in IDRISI Explorer's Metadata. Display TPRAW with the Quantitative palette. Use Cursor Inquiry Mode to explore the range of values in TPRAW.
- s) Run the macro TCTN. After the job is completed, use Metadata to change the title of the TNRAW to "Delivery ratio for total nitrogen." Display TNRAW with the Quantitative palette. Use Cursor Inquiry Mode to explore the range of values in the image.
- t) Run the macro TCTS. Change the title of the resulting image TSSRAW to "Delivery ratio for total suspended

sediments." Display TSSRAW with the Quantitative palette. Use Cursor Inquiry Mode to explore the range of values in TSSRAW.

This completes the second step of the nonpoint pollution model. We have calculated delivery ratios, or the proportion of the available material transported from each cell, for total phosphorus, total nitrogen, and total sediments for each cell in the watershed.

### **Step 3: Stream Network Delineation**

The delivery ratio models described in the previous section do not make a distinction between cells that are outside the stream and cells that fall into the stream. In reality, when a storm occurs, overland water flows down the slope forming storm sewers or drainage streams. It is assumed that all of the nutrients and sediments entering a stream cell are carried by water energy down stream to the next cell and that the delivery ratio in cells falling within a drainage stream is 100. In order to introduce this assumption into our model, we have to first delineate streams in the watershed and then assign a delivery ratio of 100 to the cells falling within the streams.

Stream network delineation is an important issue in nonpoint source pollution modeling. Different densities of the network yield different model results since they change the individual cell delivery ratios and total flow path delivery ratios. By interactively changing the density of the stream network, one can run the model several times, compare the results with observed sediment and nutrient loads, and select a drainage density network that is most appropriate for the model. This approach was used by Levine et al. (1993) for calibrating their model.

- u) Display the image COUNT with the Quantitative palette. This image shows the result of a program that counts the number of cells that flow into any one cell based on the direction of flow in each cell.<sup>3</sup> Thus, the values increase from higher elevations in the watershed towards the streams. The watershed outlet, or "seed" cell, has the highest value. Once the image showing the number of cells flowing into each cell is created, a threshold can be applied to it to delineate the stream network. This network consists of both permanent streams and temporary drainage channels, the latter being a result of storm activity. The lower the threshold, the higher the network density.

4. *What do the colored lines represent?*

- v) Use the Zoom Window tool to zoom into the area of the image with the highest values. Find the watershed outlet cell (or "seed cell") and write down its column and row number.

5. *What is the column/row position of the outlet cell? What is the value in this cell? What does this number mean?*

Next, we have to apply a threshold to delineate the stream network. Levine et al. (1993) found that the threshold of 15 cells resulted in the best agreement between observed and estimated sediment and nutrient loads in their study area. In other words, a cell that has 15 or more cells flowing into it is considered as part of the drainage stream whereas a cell with 14 or fewer cells flowing into it is considered as outside the drainage stream. To apply this threshold to COUNT, cells with values greater than 14 will be assigned a value of 100 and the rest will be assigned a value of 0. Every cell outside the stream network will retain the original delivery ratio value. Stream cells will be assigned a value of 100 because the delivery ratio in the streams is assumed to be 100. This image will be used to update the three delivery ratio images (TPRAW, TNRAW and TSSRAW) to account for stream flow.

- w) Run RECLASS and specify COUNT as the input image and COUNT15 as the output image. Assign the new values as follows: 0 for all values ranging from 0 to those less than 15; and 100 for all values ranging from 15 to those less than 300,000.

---

3. This program was originally an IDRISI interface to COUNT.EXE - a flow direction program recompiled for DOS-Fortran in the Clark Labs (using Fortran Visual Workbench software) from the original COUNT.FOR program written by Sue Jensen, EROS Data Center.

- x) Display COUNT15 with the Qualitative palette.

As you can see in the image, the threshold delineates a network of linear streams and several non-linear features. These features correspond to flat areas in the digital elevation model, TCDEM. Each cell in these flat areas accumulates flow from 15 or more surrounding cells since the elevation of the surrounding area is higher.

Now that the stream network has been delineated, we have to update the images of cell delivery ratios by changing the values of cells falling within the streams to 100. To do this, we will need to overlay the stream network image COUNT15 with each of the cell delivery ratio images. The procedure that allows us to cover pixels of one image with those of another, except where the covering image has values of zero, is the "cover" operation in the OVERLAY module. Where the values in COUNT15 are 0, the original values of the cell delivery ratio images will remain. Where the values in COUNT15 are 100, the cell delivery ratio images will be changed to 100.

- y) Run OVERLAY and specify COUNT15 as the first image, TPRAW as the second, and the output as TP. Select the option called "First covers Second except where zero." Explore the range of values in the output image. This is the final image representing the delivery ratio of phosphorus for each cell.

- z) Run OVERLAY. Specify COUNT15 as the first image, TNRAW as the second, and the output as TN. Select the cover option. Explore the range of values in the image. This is the final image representing the delivery ratio of nitrogen for each cell.

6. *What is the major difference between these images in terms of the distribution of values? Which nutrient, phosphorus or nitrogen, has the most favorable conditions for transport? (To answer this question, use HISTO for each image with a display minimum of 1, display maximum of 99, a class width of 1 and graphic output).*

- aa) Run OVERLAY. Specify COUNT15 as the first image, TSSRAW as the second, and the output as TS. Select the cover option. This is the final image representing the delivery ratio of sediments for each cell.

We now have all of the images necessary for calculating total flow path delivery ratios. Other images will be provided for you.

### Step 4: Total Flow Path Delivery Ratios

We can now link the images of delivery ratios with flow path information to calculate total flow path delivery ratios. The difference between the *cell delivery ratio* and the *total flow path delivery ratio* is that the former refers to the percent of pollutant load in a cell that *can be transported* to the next cell in the flow path, whereas the latter refers to the part of that load in a cell which *actually reaches* the watershed outlet.

The example below explains how total flow path delivery ratios are calculated. For simplicity, in the example it is assumed that flow is downward and that there is no flow into the four cells from the cells on the left, right, and diagonal sides.

Direction of Flow	Cell Delivery Ratio	Total Flowpath Delivery Ratio
A ↓	80	24
B ↓	60	30
C ↓	50	50
D ↓	100	100

In this example, cell D with a cell delivery ratio of 100 belongs to a drainage stream, and the flow enters it from the cells above it. Cell C has a delivery ratio of 50. This means that 50% of the flow into it can be transported to the next cell down the slope (which is cell D). In this example, the flow into cell C comes only from cell B, which has a delivery ratio of 60. If

described in terms of the load coming from cell B, cell D receives 50% of the cell C load and 30% of the cell B load ( $0.5 * 0.6$ ). Therefore, the total flow path delivery ratio for cell B is 30. That is, half of the 60% available for transport from this cell is trapped in cell C down the slope and only 30% of the originally available load reaches the outlet. The flow into cell B comes only from cell A, which has a delivery ratio of 80. If described in terms of the load coming from cell A, cell D receives 24% of the cell A load ( $0.3 * 0.8$ ). Therefore, the total flow path delivery ratio for cell A is 24. That is, 60% of the 80% available for transport from this cell is trapped in cell B down the slope then 50% of what makes it to cell C is trapped there, and only 24% from cell A of the originally available load ( $0.8*0.6*0.5$ ) reaches the outlet.

In general, the calculation of total flow path delivery ratios starts at the watershed outlet and works up slope following the direction of flow. Each time, the cell delivery ratios of any two adjacent cells (horizontal, vertical or diagonal) along the path (the "receiving" cell and the "feeding" cell) are multiplied and the new value is assigned to the "feeding" cell. After this value is assigned, this cell becomes a "receiving" cell for the next cells upslope that flow into it, and the process continues until the watershed boundary is reached. Intuitively, we can expect that the farther a cell is from the watershed outlet or a receiving stream where the delivery ratio is 100, the smaller will be its contribution to the load at the watershed outlet and hence the smaller is its total flow path delivery ratio.

Images have been provided for you that show the total flow path delivery ratios for nitrogen, phosphorus, and sediments.<sup>4</sup> These images are called FLOWN, FLOWP, and FLOWS for nitrogen, phosphorus, and sediments respectively. They show the portion of potential load of the pollutant in a cell that can actually reach the watershed outlet under the given topographical and surface conditions. As you can see, the farther the cell is from the network, the smaller its value. The cells with flowpath delivery ratios over zero are called load-contributing areas. These areas are different for each pollutant.

7. *Which of the two, FLOWN or FLOWS, has the larger load-contributing area? (To answer this question, use HISTO (numeric output) and compare the proportion of cells with non-zero values in these two images.)*

The total contributing areas are smallest for sediments and the largest for nitrogen. As Levine et al. (1993: 83) explain, "sediment delivery is dependent on the load-carrying capacity during overland flow. Any vegetation along a flow path quickly reduces load carrying capacity and reduces the delivery. Because large solid particles are removed from the solution first and phosphorus is preferentially adsorbed<sup>5</sup> to the smaller clay particles in sediment, contributing areas for total phosphorus are slightly larger than for total suspended sediments." Total nitrogen transport is linked to both dissolved and particle phases and therefore has a larger contributing area.

The images FLOWP, FLOWN, and FLOWS, will be used to calculate total annual nutrient and sediment loadings.

## **Step 5: Total Annual Nutrient and Sediment Loadings**

In this section, we will calculate the actual mass of pollutants delivered to the watershed outlet from each cell. To do this, the potential loadings for each cell in the watershed have to be multiplied with the total flow path delivery ratios for the nutrients and sediments. Potential loadings are the amounts of sediments and nutrients available for transport from each cell. These were calculated in step 1. The total flow path delivery ratio refers to the part of the potential loadings which reaches the watershed outlet. These were calculated in step 3. For example, if the potential loading of phosphorus in a cell was 50 grams per cell per year (g/cell/year) and the flowpath delivery ratio was 60%, then the total annual phosphorus load from this cell will be 30 grams ( $50*0.6$ ).

First, we will convert the values in the total flow path delivery ratio images from percents to proportions to be used in multiplication by dividing the images by 100.

---

4. These images were produced by a program that was donated by Daniel Levine from the Environmental Sciences Division of the Oak Ridge National Laboratory. It was written originally in FORTRAN 77 for workstations and was compiled for DOS-Fortran in the Clark Labs (using FORTRAN Visual Workbench software).

5. Adsorption is the condensation of gases on the surfaces of solids.

- ab) Run the module SCALAR from the GIS Analysis/Mathematical Operators menu and specify FLOWP as the input image and FLOWPO as the output image. Select the option for division and specify the scalar value of 100. Repeat this operation for FLOWN and FLOWS, and call the resulting images FLOWNO and FLOWSO respectively.
- ac) Run OVERLAY. Specify the first image as POTP, the second as FLOWPO, and the resulting image as LOADP. Select the option for multiplying two images. In the Output Documentation box, specify the value units as "g/cell/year." Repeat this procedure for nitrogen by multiplying the images POTN and FLOWNO, and call the resulting image LOADN. Do the same for sediments by multiplying FLOWSO and POTS and call the resulting image LOADS. This time, for value units specify "tons/cell/year" (since POTS was calculated in tons/cell/year).

The values in these images represent the annual amount of phosphorus, nitrogen, and sediments that reaches the watershed outlet from each cell respectively.

To estimate the total annual mass of phosphorus that passes through the watershed outlet, we need to add together the values for all cells in the image LOADP.

- ad) Run EXTRACT. Specify TCMASK as the feature definition file and LOADP as the image file to be processed. Select the option for the summary to be a total (sum) and then select the option to display the results in tabular form. The value in category 1 will show the total annual mass of phosphorus (in grams) that passes through the watershed outlet.

8. *What is the total annual load of phosphorus in tons? Write down the number in the table below. (To convert from grams to tons, divide by 1,000,000.)*

Total mass of P delivered to the watershed outlet per year, tons/year	
Total mass of N delivered to the watershed outlet per year, tons/year	
Total mass of sediments delivered to the watershed outlet per year, tons/year	

- ae) Repeat the same procedure for LOADN and LOADS and write the results in the table above. Remember that while LOADN values are in g/cell/year and need to be converted into tons/year, the values in LOADS are already values in tons/year.

## Conclusions

In this exercise, we modeled the nonpoint pollution delivery process from the source to the receiving waters. First, we calculated the amount of nutrients and sediments available for transport from each cell. Then we estimated the proportion of this amount that could be carried away with surface water flow from each cell, depending on the surface conditions (soil permeability, slope, and vegetation density). In the next step, we delineated a network of permanent and temporary streams present in the watershed after an intense storm. Using this data, the individual path of water flow from each cell toward the stream network was identified. This flow path information was used to calculate the total flow path delivery ratios which express the part of the available load that actually reaches the stream. The final step in the model involved the calculation of the total mass of sediments and nutrients delivered from each cell in the watershed to the stream.

Levine and colleagues calibrated the model by interactively changing the density of the stream network and comparing estimated loads of pollutants with observed values for 1985-86, which was a medium rainfall year. "The model could be calibrated to represent low and high rainfall years, provided the water quality data were available. [This mechanism allows one to] incorporate hydrologic responses to climate change into the model. With this capability, one could also test the relative importance of climate change vs. land-use change on water quality" (Levine et al. 1993: 76). Different climate change sce-

narios could be simulated by changing the drainage network threshold, while new landuse maps could be created to simulate possible changes in land-use patterns. Each of these changes could be separately incorporated into the model, and the resulting loads could be compared to each other.

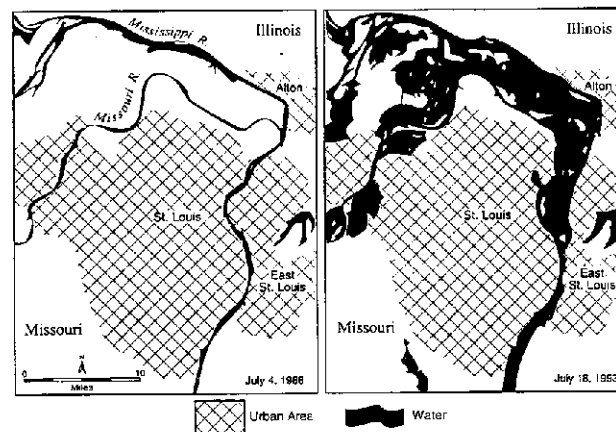
Results of the model also have important implications for management of water resources. The spatial character of the model allows one to identify pollutant-contributing areas (that is areas with high flow path delivery ratios). "The results from this model suggest that the pollutant-contributing area is irregularly shaped...and is different for each pollutant" (Levine et al. 1993: 76). These areas could be targeted for management action, such as creating buffer zones around streams to protect water resources.

## References

- Atkinson, S.F. 1988. Nonpoint pollution control site selection planning. *Proceedings, GIS/LIS '88*, Vol. 2: 685-694. Washington, D.C.: American Congress on Surveying and Mapping.
- Dunne, T., and L. B. Leopold. 1978. *Water in environmental planning*. New York, NY: W.H. Freeman.
- Engman, E.T. 1986. Roughness coefficients for routing surface runoff. *Journal of Irrigation and Drainage Engineering* 112(1): 39-53.
- James, D.E., and M.J. Hewitt, III. 1992 (November/December). To save a river: Building a resource decision support system for the Blackfoot River drainage. *Geo Info Systems* 2(10): 37-49.
- Jenson, S. K., and J.O. Dominique. 1988. Extracting topographic structure from digital elevation data for geographic information system analysis. *Photogrammetric Engineering and Remote Sensing* 54 (11): 1593-1600.
- Kim, K., and S. Ventura. 1993. Large-scale modeling of urban nonpoint source pollution using a Geographic Information System. *Photogrammetry Engineering and Remote Sensing* 59(10): 1539-1544.
- Levine, D. A., C.T. Hunsaker, S.P. Timmins, and J.J. Beauchamp. 1993. *A Geographic Information System approach to modeling nutrient and sediment transport*. Oak Ridge National Laboratory, Environmental Science Division, Publication No. 3993. Oak Ridge, TN: Oak Ridge National Laboratory.
- Levine, D.A. 1995. Personal communication.
- Mertz, T. 1993 (April). GIS targets agricultural nonpoint pollution. *GIS World* 6(4): 41-46.
- Novotny, V., and G. Chesters. 1989. Delivery of sediment and pollutants from nonpoint sources: A water quality perspective. *Journal of Soil and Water Conservation* 44(6): 568-576.
- Reckhow, K.H., M.N. Beaulac, and J.T. Simpson. 1980. *Modeling phosphorus loading and lake response under uncertainty: a manual and compilation of export coefficients*. EPA 440/5-80-011. Washington, D.C.: U.S. Environmental Protection Agency.
- Schwab, G.O., R.K. Frevert, T.W. Edminster, and K.K. Barnes. 1981. *Soil and water conservation engineering*. 3rd edition. New York, NY: John Wiley.
- Wischmeier, W.H., and D.D. Smith. 1978. *Prediction rainfall erosion loss - a guide to conservation planning*. Agriculture Handbook 537. Washington, D.C.: U.S. Department of Agriculture.



## ***Exercise 6: Using Remote Sensing to Assess the Great Midwest Flood of 1993***



Source: EOSAT

## Introduction

In the last few years, floods have caused havoc in many parts of the world. In the United States, the great flood of 1993 in the Midwest, associated with rivers such as the Mississippi and the Missouri, resulted in 48 deaths, property damages of \$10 to \$12 billion, and millions of dollars in indirect losses (Tobin and Montz 1994). Floods associated with the Rhine River in Germany in 1993 were the largest in over 50 years and caused widespread damage. Unlike the coastal flooding associated with extreme storms (Exercise 2), riverine floods often develop slowly, extend over large areas and for long time periods, and inundate land and property to considerable depths.

An important source of data about such floods are remote sensing satellites (Kruus et al. 1981, Walter 1994, Speed 1994). One application of remotely sensed data is during the flood itself, to monitor the progress of a flood and show the extent of flooding. In the case of the 1993 midwest floods in the United States, for example, data from LANDSAT 4 and 5 satellites were processed daily to map the progression of the flood. In combination with other data such as Digital Elevation Models (DEMs), it identified the areas that were likely to be flooded in the near future (Speed 1994). The turn-around time for such analysis was usually 24 to 48 hours after the data was obtained from the satellite (Gardner 1994). Remotely sensed data can also be used for disaster planning and mitigation. For example, the data can be used to create landuse maps or delineate the area inundated by past floods of various magnitudes.

In this exercise, we will illustrate the use of remotely sensed data to assess the 1993 midwest floods for a small area near the city of St. Louis, Missouri, USA, which was inundated by the Missouri River. The data was donated by EOSAT Corporation which operates and maintains the LANDSAT series of satellites.<sup>1</sup> The first section of the exercise describes the data and its characteristics. The second section examines the use of the data in identifying the flooded areas. The third and final section demonstrates a technique for determining the area covered by the flood.

## Image Exploration

The imagery we will work with is from the Thematic Mapper (TM) sensor, which is carried aboard the LANDSAT 4 and 5 satellites. The TM sensor collects imagery in seven regions, or bands, of the electromagnetic spectrum ranging from visible blue to thermal infrared wavelengths. We will use the following three of these bands in this exercise: band 3, visible red (0.63- 0.69  $\mu\text{m}$ ); band 4, near infrared (0.76 - 0.90  $\mu\text{m}$ ); and band 7, mid infrared (2.08 - 2.35  $\mu\text{m}$ ). The resolution of TM data is 30 meters, meaning that each pixel in the imagery corresponds to a 30m by 30m area on the ground. Since only one value can be recorded per pixel, the values represent the average reflectance of all the surface types within each 30m by 30m area.

We have imagery for two dates, July 4, 1988 and July 18, 1993, representing states of the Missouri River near the city of St. Louis before the flood and during the flood respectively. The period around July 4, 1988, was considered a drought period by the U.S. Army Corps of Engineers. The period around July 18, 1993 was at the height of the flooding in this part of the Midwest in 1993. The names of the images for these two dates and the bands to which they correspond are as follows:

88BAND3	Band 3 (red) for July 4, 1988
88BAND4	Band 4 (near infrared) for July 4, 1988
88BAND7	Band 7 (mid infrared) for July 4, 1988
93BAND3	Band 3 (red) for July 18, 1993
93BAND4	Band 4 (near infrared) for July 18, 1993
93BAND7	Band 7 (mid infrared) for July 18, 1993

- a) Display the image 88BAND4 with the GreyScale palette. Use Cursor Inquiry Mode and the Zoom Window tool

---

1. Dr. Joseph Gardner and Dr. Tina Cary of EOSAT assisted in obtaining the data. The data provided with this exercise should only be used for educational purposes. Any other purpose for which the data might be used requires prior permission from EOSAT Corporation.

to explore features in the image such as the river, roads and fields.

Water absorbs very strongly in the near infrared band, and thus the Missouri river appears very dark in this image. The city of St. Louis lies to the lower right of the image. In the far lower right corner of the image, some runways of the Lambert Louis International Airport in St. Louis can be seen. We will compare this image with 93BAND4 which shows the same area during the flood.

- b) Display the image 93BAND4 with the GreyScale palette and drag it to the side so that both images are visible on the screen.

Visual comparison of the two images reveals the extent of flooding in 1993. We get a sense of the magnitude of the flood just by looking at the two images. However, we would like to perform more quantitative analyses, such as delineating the flooded areas (mapping the flood extent), and calculating the number of acres that were flooded. We will do this later in the exercise.

Note that the images from the two dates describe exactly the same place on the earth. If you check the location (column and row number) of easily-identified features in one image, then check the same feature positions in the other image, the locations are exactly the same. This spatial correspondence is known as *registration* and is very important to change analysis. The imagery of the two dates to be compared must be registered to each other so that we can be sure that what we identify as change between the two dates is truly change, and is not simply due to the fact that the pixels being compared describe different areas on the earth. Registration is accomplished by transforming the imagery from one date to match the other (or transforming the imagery from both dates to match a base map). This has already been done for us by EOSAT.

- c) Now, close the 1993 image and display the other two 1988 images, 88BAND3 and 88BAND7, with the GreyScale palette.

There are two important aspects to notice as you compare these three images. First, all of the images are registered to each other. This inter-band registration occurs automatically at the time of data collection by the sensor. The second aspect is that the scene appears slightly different in each band. While we can clearly recognize that all three images describe the same study area, the relationships between high and low reflectances from the various cover types present are not the same in all three bands. For example, there is more contrast between the river and the land in band 4 while there is more contrast between different agricultural fields in band 7. This is a characteristic of multi-spectral imagery which we will explore in greater detail in the next section on identifying the flooded areas.

## Identifying Flooded Areas

We are now ready to begin identifying the flooded areas. We could use our original imagery (which represents quantitative measurements of reflectance) to delineate the flood areas. Alternatively, we may create new images representing the qualitative categories of "water" and "non-water", and then perform the change detection between these qualitative categories. We will use the latter technique for this exercise.

We will rely on two fundamental principles of remote sensing to identify the water areas.<sup>2</sup> First, earth materials reflect different amounts of energy in each region of the electromagnetic spectrum. The pattern produced in reflectances by a land cover type is termed its *spectral reflectance pattern* or *spectral response pattern*. Given this, we can expect the reflectance value for water in each of the three bands for a single date to be different. Second, different land covers have different reflectance patterns. Hence, we can expect water to have a different characteristic reflectance pattern than urban areas, which will be different from agricultural fields. This is the reason the scene appeared slightly different when each band from 1988 was examined in the last section. To get a sense of these two principles in practice, we will query some different land covers and note their reflectance values in each band.

---

2. For a thorough discussion of the remote sensing and image processing topics mentioned in this exercise, see Campbell (1987) or Lillesand and Kiefer (1994).

1. Use the 1988 images and the Zoom Window and Cursor Inquiry Mode tools to fill in the reflectance values in the following table:

Landcover	Position		Reflectance Values		
	Column	Row	Red	Near Infrared	Mid Infrared
Field	96	191			
Road	305	411			
Water	345	179			

It is often useful to graph the reflectance values in order to gain a better understanding of the shape of the patterns represented. Plot the three reflectance values for each of the land cover types from the table above onto the graph in Figure 6.1 below, joining the three points for each land cover and labeling each line with its land cover type.

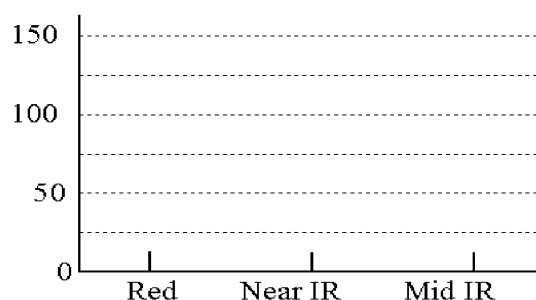


Figure 6.1

The figure above illustrates one of the advantages of using multiple-band imagery in identifying land cover types. While the reflectance values for water and the agricultural field in these examples are quite similar in the red band, they are quite different in the two infrared bands. If we were to try to differentiate water from other cover types using only the red band, we could expect to have some difficulty. By using all three bands, however, we increase the likelihood of being able to distinguish water from other covers. Classification techniques in image processing often allow up to seven or more bands to be analyzed simultaneously to enhance the analyst's ability to differentiate cover types.

In image classification, there are two basic approaches that may be taken: *supervised* and *unsupervised*. Supervised classification requires that the operator identify areas that exemplify each cover of interest in the image. Statistics are developed for each identified cover type, and a set of rules are applied by the computer program to decide to which identified cover type each pixel should be assigned. Different classification algorithms, termed *classifiers*, use different sets of rules to determine the assignments.

Unsupervised classification differs in that no advance knowledge of the study area is required of the operator. In this approach, the computer program uses a set of rules to assign all the pixels of the study area to a number of different groups, depending on the reflectance values of each pixel across multiple bands. The program produces a resultant image representing groups of pixels that are spectrally distinct. It is then the task of the analyst to determine what these groups represent in terms of land cover types. Again, various rule sets may be used in the analysis.<sup>3</sup>

---

3. A more detailed discussion of supervised and unsupervised classification with examples is provided in the introductory exercises on image processing in the IDRISI Tutorial.

We will use the unsupervised approach to distinguish water from non-water areas for each of our two dates. In doing so, we will not be concerned with differentiating different types of non-water covers. In IDRISI, unsupervised classification is provided through clustering algorithms in the modules CLUSTER and ISOCLUST. In this exercise, we will use the module CLUSTER which requires input image bands.

- d) Open the module CLUSTER from the Image Processing/Hard Classifiers menu. Specify the three 1988 image bands 88BAND3, 88BAND4, and 88BAND7 as inputs and 88BROAD as the output filename. Select a broad generalization level and the clustering rule to retain all clusters. Leave the other defaults. When CLUSTER has finished, examine 88BROAD.

2. *How many clusters, or distinct groups, were identified? Which cluster appears to represent water? (Hint: The clusters are numbered from lowest to highest according to the amount of area they occupy).*

- e) Use the module HISTO with 88BROAD to examine the frequency distribution of the clusters.

As you can see from the histogram, the clusters are ordered according to the area they cover in the image. There are two very prominent land cover clusters that occupy most of the image, followed by cluster 3 and then cluster 4 (which represents water). We will now create a Boolean image of the water areas in 1988.

- f) Open Edit and enter the following numbers in the file separated by a space.

4 1

After you have finished, save the data as an attribute values file named WATER, specify integer as the data type and exit Edit.

- g) Now use ASSIGN and specify 88BROAD as the feature definition image, WATER as the attribute values file, and 88WATER as the output image.

88WATER is an image in which all the values originally in cluster 4 (representing water) have been assigned the new value 1, and every other value in the image has been assigned the new value 0. We will follow the same methodology to create a Boolean image of the water areas in 1993.

- h) Open COMPOSITE from the Image Processing/Enhancement menu. This time, specify 93BAND3 as the blue band, 93BAND4 as the green band and 93BAND7 as the red band. Call the resulting image 93FCC (for 1993 false color composite). Create a 24-bit composite. Choose a linear with saturation points stretch and specify 1% saturation. Do not omit zeros. When COMPOSITE has finished, 93FCC will be displayed with the Color Composite palette.

- i) Run CLUSTER with the input bands 93BAND3, 93BAND4, and 93BAND7. Select the broad clustering technique and retain all clusters. Call the resulting image 93BROAD.

3. *Which cluster represents water in 93BROAD? Why is water represented by a different cluster in 1993 than in 1988?*

- j) Use Edit and ASSIGN as before to create a Boolean image of water in 1993 and call the result 93WATER. Display the result with the Qualitative palette.

## Change Detection

Now that we have created Boolean images representing water and non-water for both dates, we are ready to compare the two. This type of analysis falls under the application area of *change analysis* since: (1) we are comparing data for the same study area, but from different dates; and (2) we are looking for the changes that have occurred from one date to the next. For good reviews of techniques of change analysis using remotely sensed data, see Eastman, McKendry, and Fulk (1995), and Singh (1989).

Since our data are qualitative in nature ("water" and "non-water" classes), we will use a cross-classification technique that will assign a new value to each unique combination of original values. Since our two input images each contain two classes, zero and one, we can expect the resulting cross-classification image to have at most four classes, as illustrated in Figure 6.2 below.

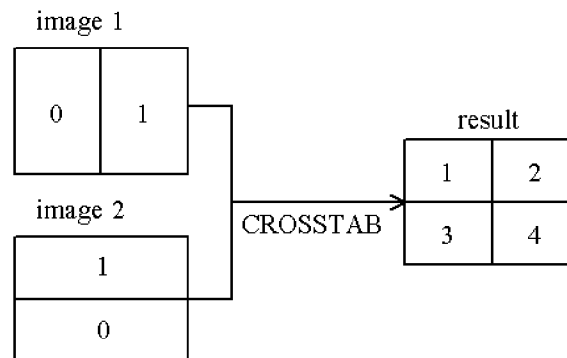


Figure 6.2

Cross-classification is available through the IDRISI module CROSSTAB.

- k) Run the module CROSSTAB from the GIS Analysis/Database Query menu and specify 88WATER as the first image and 93WATER as the second image. Choose to create a cross-classification image and call the output image CROSS.

The output image of CROSSTAB is interpreted by examining the title and legend captions. The legend captions show the combination of original values that are represented by the new value (in the same order as the original image names are given in the title). In CROSS, for example, the first category has the legend caption 0|0, indicating that it represents those areas that had a zero value in the first image, 88WATER, and a zero value in the second image, 93WATER.

4. Which category in CROSS represents areas affected by the 1993 flood? How can you explain the second category in CROSS?

## Conclusions

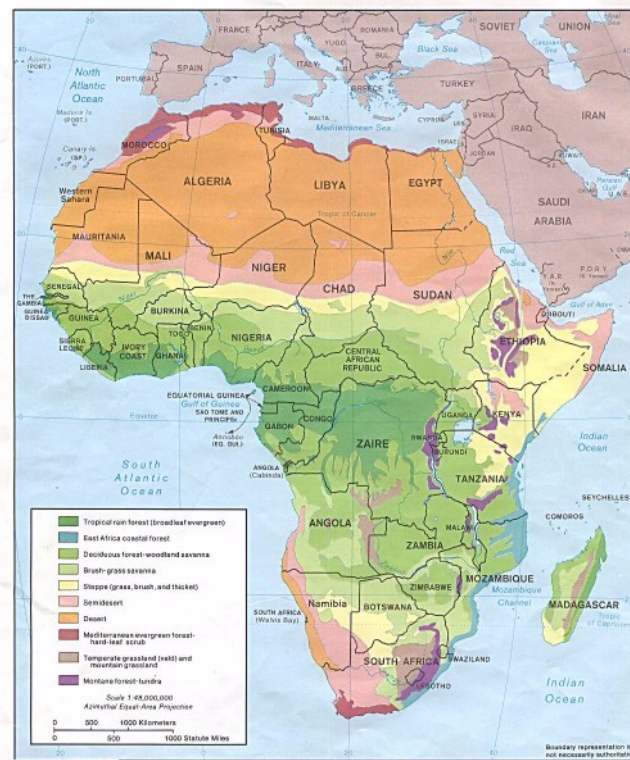
In this exercise, we used remotely sensed data provided by the LANDSAT satellite to identify an area near the city of St. Louis flooded by the Missouri River during the 1993 midwest floods. Using cross-classification, we also calculated the extent of flooding. If landuse information for the study area just prior to the flooding was available, we could have identified the type and acreage of agricultural crops, the amount of residential and commercial landuse, and so forth that were affected by the floods. Users of the workbook interested in demonstrating these types of socioeconomic impacts for educational purposes may wish to acquire such data and combine them with the imagery provided with this exercise.

## References

- Campbell, J. B. 1987. *Introduction to remote sensing*. New York: The Guilford Press.
- Eastman, J.R., J.M. McKendry, and M.A. Fulk. 1995. *Explorations in Geographic Information Systems technology. Volume I: Change and Time Series Analysis, Second Edition*. Geneva, Switzerland and Worcester, MA: United Nations Institute for Training and Research (UNITAR) and the Clark Labs, Clark University.
- Gardner, J.V. 1994. Landsat and the Midwest flood of 1993. Presented to the Second Thematic Conference on Remote Sensing for Marine and Coastal Environments. New Orleans, LA: January 31 to February 2.

- Kruus, J., et al. 1981. Flood applications of satellite imagery. In *Satellite Hydrology*, ed. M. Deutsch, pp. 292-301. Minneapolis, MN: American Water Resources Association.
- Lillesand, T.M., and R.W. Keifer. 1994. *Remote sensing and image interpretation*. New York: John Wiley & Sons.
- Singh, A. 1989. Digital change detection techniques using remotely sensed data. *International Journal of Remote Sensing* 10, 989-1003.
- Speed, V. 1994. GIS and satellite imagery take center stage in Mississippi flood relief. *Geo Info Systems* 4, 40-43.
- Tobin, G.A., and B.E. Montz. 1994. *The great midwestern floods of 1993*. Fort Worth, TX: Harcourt Brace College Publishers.
- Walter, L.S. 1994. Natural hazard assessment and mitigation from space: the potential of remote sensing to meet operational requirements. In *Natural hazards and remote sensing*, ed. G. Wadge, pp. 7-12. London, UK: The Royal Society.

## ***Exercise 7: Time Series Analysis as an Early Warning Tool for Disaster Mitigation: An Exploratory Analysis of Drought in Africa***





## **Introduction**

Unlike rapid onset natural hazards such as hurricanes, drought is a slow onset natural hazard which develops over a period of weeks and months. However, the adverse effects of drought can be as devastating as those of the rapid onset hazards. In Africa, a combination of drought and civil war contributed to the 1984-85 famine in Ethiopia in which thousands perished and millions were affected (Timberlake 1986). In the United States, the annual average loss from drought is estimated to be \$6 to \$8 billion dollars (NRC 1994).

Early warning about the onset of drought and the occurrence of famine linked to drought is playing a crucial role in drought disaster mitigation. A number of early warning systems have been established, including several based upon satellite data (Hutchinson 1991). One application of satellite data for early warning is to estimate rainfall over large areas and monitor the progression of rainfall. This is achieved by using the thermal infrared band to identify cloud cover over a region as well as the clouds that are likely to be precipitating based upon the temperature at the top of the cloud (Grimes, Dugdale, and Milford 1994). A second application of satellite data for early warning is the mapping of vegetation patterns and estimation of the length of the growing period. An index of vegetation greenness derived from satellite data, the Normalized Difference Vegetation Index (NDVI), has been used to map vegetation patterns and relate them to areas of severe drought and famine in Africa (Hellden and Eklundh 1988).

Early warning systems for drought have also incorporated data on a meteorological event, the El Nino/Southern Oscillation (ENSO), since this event affects rainfall patterns on a global scale. During an ENSO event, surface temperatures of the ocean in the equatorial Pacific increase from 1°C to 4°C. This increase results in a dislocation of normal rainfall patterns around the world, with below-normal rainfall occurring in some parts and above-normal in others (Rasmusson 1987). The areas with below-normal rainfall during an ENSO event, such as southern Africa and India, face an increased likelihood of drought, whereas those with above-normal rainfall, such as North America and Peru, face an increased likelihood of flooding. For example, in southern Africa, drought during the years of 1982-83 and 1992-93 has been linked to the below-normal precipitation in the region during the ENSO events in 1982-83 and 1991-92, respectively. An ENSO event occurs about every three to seven years, and progress has been made in identifying the onset of an ENSO event up to a year in advance (Golnaraghi and Kaul 1995). Because of this forecasting capability, nations most affected by ENSO-related impacts have established or are in the process of establishing early warning systems. For example, Brazil and Peru used forecasting information about ENSO to mitigate the impacts of the 1986-87 and 1991-1992 events (Golnaraghi and Kaul 1995).

This exercise explores the potential of GIS as an early warning system for mitigating the impacts of drought. The focus is on the use of GIS in conjunction with remote sensing to map and analyze patterns of vegetation over time and space. These patterns, in turn, can be related to meteorological events such as ENSO, and to the occurrence of severe drought and famine. The analysis in the exercise uses an exploratory time series analysis technique based upon principal components analysis. The study area is the continent of Africa which has been devastated by droughts.

The exercise is divided into three sections. The first section describes the Normalized Difference Vegetation Index (NDVI) data used in this exercise. The second section describes the time series analysis technique that we will use for analyzing the NDVI data. The third section discusses time series analysis of NDVI images of Africa for the seven-year period 1987 to 1994 and explores the use of the results of the analysis in early warning for drought.

### ***The Normalized Difference Vegetation Index (NDVI)***

To map vegetation patterns in Africa, we will use an index created from satellite imagery, called the Normalized Difference Vegetation Index (NDVI). NDVI is calculated from the red and infrared bands of satellite imagery as:

$$\text{NDVI} = (\text{Infrared} - \text{Red}) / (\text{Infrared} + \text{Red})$$

Vegetated areas will generally yield higher values for this index because of the relatively high near-infrared reflectance and low visible red reflectance. Because of this contrast, the NDVI will enhance the differences in the reflectance patterns of vegetation in these two bands (Lillesand and Keifer 1987, Tucker and Sellers 1986). NDVI varies in values from -1 to +1. High values of NDVI (near +1) indicate the presence of healthy green vegetation whereas low values of NDVI (near -1)

indicate the absence of such vegetation.

The original source of the red and infrared bands of imagery used in this exercise is the Advanced Very High Resolution Radiometer (AVHRR) instrument aboard the National Oceanic and Atmospheric Administration (NOAA) satellite series. The resolution of this data is appropriate for continental-scale analysis, which is the focus of this exercise.<sup>1</sup> While it is simple to produce NDVI from original red and infrared images (using the VEGINDEX module in IDRISI, for example), for this exercise we will work with data that has already been processed into NDVI by the United States Agency for International Development (USAID) for the Famine Early Warning System (FEWS) database for Africa. The processed NDVI images are available on a monthly basis. These monthly images are produced by selecting the maximum value among three images for a month. The maximum value was selected (as opposed to the mean or the median) since it has been found to reduce the effects of cloud cover in the data (Holben 1986).

The original images obtained from USAID had a resolution of 7.5 kilometers. The data was subsequently aggregated to a resolution of 30 kilometers (using the IDRISI module CONTRACT) as this scale was found to be appropriate for the identification of interannual patterns associated with ENSO (Anyamba, Eastman, and Fulk 1994). Included for use with this exercise are monthly images for 1993 and the results images of an analysis performed on an 84 image series from March 1987 to April 1994.<sup>2</sup>

- a) Display JAN93, the NDVI image for January of 1993, with the NDVI palette and the autoscale option turned on. Use the Add Layer option in Composer to overlay the vector file COUNTRY with the Uniform Black symbol file.

1. *From the definition of NDVI, describe what you see in this image.*

We can view the remaining NDVI images for 1993 one by one in the same way. We can also see the sequence as a video loop using IDRISI's Media Viewer.

- b) To create a video from the twelve NDVI images, go to the Display menu and click on Media Viewer. The Media Viewer dialogue box will appear on the screen. Click on its File menu and then click on New Video. Specify TWELVE as the AVI file to create. For the playback rate (seconds per frame), specify 1. Click on Time Series File and specify TWELVE as the file to use. The images listed in the time series file TWELVE will be converted to an AVI file also called TWELVE. (We will see the structure and contents of time series files later in the exercise). Specify IDRIS256 as the palette file to be used. Click OK to create the AVI video.
- c) Click on the File menu in the Media Viewer dialogue box. Click Open AVI Video and choose the file TWELVE. The video will begin playing automatically.

As the video plays, note the geographic progression of high NDVI values (and therefore amount of green vegetation) through the months. To exit Media Viewer, click on its File menu and choose Exit.

2. *In which months is NDVI highest in the North? in the South?*

Although a qualitative interpretation of NDVI images using a time series display is interesting, it could become difficult if the time period involved is more than one year. For example, a three-year time period would involve an interpretation of 36 images! Moreover, time series images tend to be highly correlated. For example, all of the images displaying vegetation patterns during the summer season are likely to be highly correlated over multiple years. Therefore, it may be desirable to reduce the larger set of images to a smaller set which contains the same information but in which the images are not correlated. To accomplish this, we will rely upon a technique that is based upon standardized principal components analysis.

---

1. NDVI can also be calculated from red and infrared bands captured by other types of satellites such as LANDSAT or SPOT.

2. The entire data set is not provided because of limited storage space.

## Time Series Analysis

Principal Components Analysis (PCA) allows a set of original images to be transformed to a set of new images (called *components*) such that the new images contain all of the information in the original images and are uncorrelated with one another (Richards 1984). With this technique, the components extracted are ordered in terms of the amount of variation they explain in the original set of images. The first few components tend to explain most of the variation in the original set and hence carry most of the information from the entire time series. Thus, one need only retain the first few components to keep most of the information. PCA therefore compresses the original time series images into a smaller number of component images which retain all of the *information* in the original set. The interpretation of the extracted components relies on a combination of spatial and temporal analysis.

In IDRISI, PCA for time series analysis is performed using the Earth Trends Modeler (ETM) facility. If you have not done so already you should review the ETM tutorials to prepare for this exercise. Running PCA the maximum number of components that can be extracted equals the number of input images, although the number of components yielding useful information is typically much smaller. The output from ETM includes component images that show the spatial patterns extracted as well as graphs (called loadings) for each component showing its correlation with each input image. The latter is used for temporal analysis. We will run PCA in Earth Trends Modeler on the set of 12 NDVI images for 1993 viewed earlier and interpret the results.

The input to ETM is a time series file indicating the images to be analyzed. For the twelve images for 1993, we already have this time series file, named TWELVE.

- d) Open ETM. When launched, the Project panel is open under the Explore tab. From the Project panel select the Create new project option and specify TWELVE as the project name. This will save the ETM project and settings. Click the Add button and insert TWELVE as the time series file. Change the ETM tab from the Explore tab to the Analysis tab and click on the PCA (Principle Component Analysis) panel. Keep the default processing option of using standardized variables. Make sure TWELVE is the input series and specify TWELVE as the output prefix. Set the number of components to be extracted to 3. Click Run.

A new folder called \twelve\components will be created within your working folder and is added automatically to the IDRISI project. A raster group file and the 3 individual component images (twelve\_PCA\_std\_comp1, twelve\_PCA\_std\_comp2, twelve\_PCA\_std\_comp3) are written to this folder.

### Interpreting the Components and Loadings<sup>3</sup>

The PCA loadings graph is automatically created for the 12 components even though we chose to create only 3 component images. This loadings graph is displayed automatically in the ETM panel Explore PCA under the Project tab when the PCA is finished running. This graph shows you the percent variance in the original image set that is explained by each component image. The x-axis of the graph has twelve tick marks for the twelve original images for 1993 (JAN93 through DEC93). The y-axis shows the correlations of the first component with the 12 original images. The title on the top of the graph shows which component is being displayed and the total percent variance explained for all 12 images. By default component 1 is displayed and explains 95.51 percent of the overall variance for the 12 original images.

- e) To view the other components and their respective loadings graphs click the component drop down box and select a new component for display (the first component image was automatically displayed when running PCA). Each component can also be displayed as an image by clicking the Display icon next to the component drop down menu.

---

3. The interpretations of component images and loadings graphs in this section and the next draw extensively upon the work reported in Eastman and Fulk (1993), and Eastman, McKendry, and Fulk (1994).

3. *What percent of variance in the original images is explained by the second component? by the third component? by the first three components taken together?*

- f) Display the first component image using the Display icon on the Explore PCA panel, next to the Component number. Use the Add Layer option to overlay the vector file COUNTRY with the Uniform Black symbol file. Use the cursor inquiry option to explore the values in the image.

The values in the component image range from large negative values to large positive values. Both the positive and negative values are referred to as "anomalies" since they reflect deviations from the typical value for each pixel across the entire time series. We will use the anomalies in interpreting the spatial and temporal patterns of vegetation in Africa.

The first component image shows that the anomalies are low in the Sahara desert in northern Africa and in the Namib desert in southwest Africa, indicating the presence of little vegetation in these desert areas (low NDVI values). The anomalies are high in the central and the east African highland rainforests (high NDVI values).

- g) Look again at the graph for Component 1.

All of the correlations are extremely high and fall within the very narrow range of 0.96 to 0.99. This indicates that all of the twelve monthly input images contain vegetation patterns that are quite similar to that shown in Component 1. Therefore, we can say that the pattern seen in Component 1 is the typical vegetation pattern regardless of season. This confirms what is obvious -- in general, vegetation is abundant in the rain forests and scarce in the deserts of Africa.

However, remember that the components are numbered according to how much of the information of the original data set they contain. The first component, as you may recall, explains 95.51% of the variation in the original image set. As we look at Components 2 and 3, we will begin to uncover more subtle vegetation patterns and changes that are not so obvious, and in fact these changes may have been masked by the typical vegetation in the original images.

- h) Display the second component image, with the default palette. Use the Add Layer option to overlay the vector file COUNTRY with the Uniform Black symbol file.

Note the high anomalies in the Sahelian region and the low anomalies in the southern half of Africa. It is the areas of highest and lowest values that we will focus on in our interpretation. Similarly, when we look at the loadings graph to aid our interpretation of the second component image, we will focus on the peaks and valleys of the graph.

- i) Select component 2 from the drop down component box in ETM to view the loading graph.

Unlike the first loadings graph, this loadings graph shows low correlation values (ranging from -0.18 to 0.25) for the original images. The loadings are low because the second component explains the variation in the original images after the main source of variation that is explained by the first component has been removed. The variation explained by the second component is 2.865% of that contained in the entire original time series as compared to 95.51% explained by the first component. Another striking difference between the loadings graphs for Components 1 and 2 is that for the former all of the input images had similar correlations with Component 1, but for Component 2 some input images are much more highly correlated (either positive or negative) than others. In fact, there appears to be a coherent pattern to the correlations across the months of the year.

The peak in the loadings graph occurs in August and September. This indicates that if one were able to remove the typical pattern described by Component 1, what would be left of the August and September images are most similar to the pattern shown in Component 2. Positive anomalies in the Component 2 image correspond to higher-than-typical NDVI regions of the August and September images. During the summer months, the Sahelian region experiences a seasonal increase in NDVI.<sup>4</sup> Southern Africa, on the other hand, experiences a decrease in NDVI values during these months, which is shown by the negative anomalies in that region in the Component 2 image.

---

4. The seasonal terms used throughout this exercise are specific to the northern hemisphere of Africa.

Images of the winter months, December, January, and February, show a negative correlation with the Component 2 image. This indicates that these months have a pattern that is the inverse of that shown in the Component 2 image (that is where the component image shows positive anomalies, the winter monthly images have lower-than-typical NDVI values and where the component image shows negative anomalies, the winter monthly images have higher-than-typical NDVI values).

- j) To help visualize the inverse pattern, we could inverse the component image by multiplying it by -1 (using SCALAR or Image Calculator). However, an easier approach is to apply a palette that is the inverse of the one we are using. To prepare such a palette, open Symbol Workshop from the Display menu. Choose File/Open from the Symbol Workshop menu and choose to open a palette file. Double click in the file input box and choose IDRIS256 from the IDRISI/Symbols directory. Click on OK. Now, click the button in the bottom left corner of Symbol Workshop that reads Reverse Sequence in Autoscale Range. Save the reversed palette (File/Save As -do not click on just "Save") as INVERSE. Close Symbol Workshop. Now, display another copy of component 2 with DISPLAY Launcher. In the Composer box, click on the Layer Properties button. In that menu, click on the pick button for the palette file and choose INVERSE from your working directory. Drag it so that you can see the original and the inverse display simultaneously. Applying the inverse pattern helps visualize the pattern that is being described by the months that have negative correlations.

Note that the winter pattern for Component 2 (January through March and November through December) shows higher NDVI in much of the southern hemisphere and lower NDVI along a band following the equator.

When you used Media Viewer in the first part of this exercise to watch a video of the twelve monthly images, you observed the pattern of high vegetation (shown in green in the NDVI palette) shift from south to north to south again during the course of the year. After the typical vegetation pattern for Africa is accounted for by the first component (i.e. vegetation is high in the forests, low in the deserts), then the most important vegetation pattern in Africa is this seasonal summer/winter pattern that is explained by the second component. It is the seasonal movement of the Inter-Tropical Convergence Zone (ITCZ), and with it the rainy season, that produces this pattern of seasonal change.

- k) Display the third component image, with the default palette. Use the Add Layer option to overlay the vector file COUNTRY with the Uniform Black symbol file.

The anomalies are high in the Sahel region, in south central Africa, and in parts of southern Africa. They are low in the central and southeastern lowland rain forests.

- l) Now select component 3 from the drop down component box in ETM as you did before to view the component 2 loadings graph.

The peaks in the loadings occur in December and January, indicating that the vegetation pattern shown in Component 3 occurs during that time. High negative loadings for the summer months suggest that in the summer an inverse vegetation pattern of the one shown in Component 3 is evident.

The distribution of anomalies across Africa in this image and the values of the loadings graph suggest that this component is related to change associated with the late spring and late autumn periods, particularly in the areas north and south of the central equatorial forest regions.

The high anomalies in the Sahel are surprising because in late autumn there is a significant decrease in vegetation in this region. Eastman and Fulk (1993) suggest that a possible cause of these abnormally high values is an increase in airborne dust due to the Harmattan winds, a seasonal wind pattern from the Sahara. The dust would cause a greater scattering (and therefore a smaller recorded reflectance) of the shorter red wavelengths compared to the longer near-infrared wavelengths, thus producing a larger NDVI value than expected.

We chose to write only three components for this analysis. The later component images mostly contain information describing the noise in the data set. As you might imagine, the component images that describe noise do not show meaningful geographic patterns of anomalies. The loadings graphs of these components do not show regular month-to-month

transitions, but rather have values that vary widely and show no discernible pattern in time.<sup>5</sup>

Now that we have illustrated the use of principal components analysis using the ETM module for one year, we will explore its application for a time period of seven years. Using seven years of data, it is possible to illustrate changes in NDVI intra-annually (within the year) as well as inter-annually (across years). The intra-annual changes will be similar to those examined in this section, as for example, seasonal changes. The inter-annual changes, or inter-annual variability, will require additional explanation and clarification. We will show that two components of the inter-annual variability are related to the ENSO phenomenon and hence are of particular significance to the use of PCA as an early warning tool for drought. Much of the analysis presented here is exploratory in nature. More research using this technique is needed.

## **Long Time Series Analysis of NDVI Data**

In this section we will discuss the results obtained from using PCA from Earth Trends Modeler on a data set of 84 monthly NDVI images from March 1987 to April 1994.<sup>6</sup> The entire data set is not included with this exercise because of the significant amount of disk space it would require. Only the results of the PCA analysis are provided. The approach adopted for using PCA is similar to that in the previous section. From a run of PCA on this data set eight components were extracted, and are presented here as CMP1 through CMP8. The loadings graphs for the component images are shown in Figures 7.1 through 7.8 at the end of this exercise. As in the previous section, we will interpret each component image and its loadings graph together.

- m) Run Edit from the Data Entry menu and open the file CMPEIGEN.AVL. This is the eigenvector statistics derived from the principal components analysis for the 84 images.

4. *What percent of variance is explained by the first component? by the seventh component? by the eighth component?*

Although the amount of variation explained by the seventh and eighth components is small, these components play an important role in the use of time series analysis as an early warning tool for drought in this region. We will discuss each of the eight components extracted in the analysis.

- n) Display CMP1, the first component image. Use the Add Layer option to overlay the vector file COUNTRY with the Uniform Black symbol file. With the image onscreen, look at the loadings graph for this component shown in Figure 7.1 (at the end of this chapter). The y-axis in the loadings graph shows the loadings (correlations) of the first component with the 84 images used in the analysis. The x-axis shows the tick marks for the 84 months. Every sixth month is labeled, beginning with April 1987 (a87 refers to April 1987, o87 refers to October 1987, and so on).

5. *Compare CMP1 with the first component image extracted for the twelve images from 1993. Do you see any significant differences? Interpret this component and its loadings graph.*

- o) Display CMP2, the second component image. Use the Add Layer option to overlay the vector file COUNTRY with the Uniform Black symbol file.

The image shows low anomalies in the Sahara and Namib desert regions and high anomalies in the equatorial rainforests and the rainforests in southeastern Africa. With the image onscreen, look at Figure 7.2, the loadings graph for this component. The peaks in the loadings graph occur in the summer months, and the minimum (negative) loadings in the winter months. This component represents the summer/winter influence on vegetation patterns in Africa.

- p) Display CMP3, the third component image.

---

5. Since the loadings graphs are automatically written for all possible components (12 in this case) no matter how many component images you choose to write, you may verify this by looking at the graph for Component 12 as before.

6. This section is based on research conducted at the Clark Labs by Assaf Anyamba, Ron Eastman, and Mahadevan Ramachandran.

The image shows high anomalies in the Sahel region of Africa. In contrast with these high anomalies are the low anomalies in central Africa, especially on the west coast and in the equatorial rain forests. With the image onscreen, look at Figure 7.3, the loadings graph for this image. The graph shows a change in the loadings, first in late spring and then in late autumn. This component then represents the seasonal change corresponding to spring and autumn.

q) Look at Figure 7.4, the loadings graph for the fourth component.

There is a double peak in the loadings for each year. This double peak coincides with the two rainy seasons experienced each year by certain regions in Africa, such as the equatorial rain forests.

r) Display CMP4, the fourth component image.

The regions with the double peak appear in the component image as green and have high positive anomalies.

Thus far, the components and loadings we have discussed explain changes and patterns in vegetation related to *intra-annual* phenomena such as seasonality in the rainfall regime. The discussion has been similar to the analysis for twelve months carried out in the previous section. In the remaining four components, we will discuss *inter-annual* variability, which can be attributed to the satellite system, and to meteorological phenomena such as ENSO.

s) Display CMP5, the fifth component image.

The image shows peculiar positive anomalies over the Sahara and Namibian deserts and even in water bodies such as Lake Victoria.

t) Look at Figure 7.5, the loadings graph for this component.

The loadings exhibit a gradual decrease until the middle of 1989, after which they exhibit a sharp increasing trend until the end of the study period (March 1994).

This pattern implies that NDVI was increasing in the desert regions from 1990 to 1994 which is clearly not possible. A false trend has therefore been picked up in the analysis of the long time series of NDVI data. This false trend can be attributed to the gradual decay in the satellite orbit at the time it crosses the equator. Because of this decay, the satellite crosses the equator at a later time with each cycle. One effect of this decay is that the reflectances in the red wavelength decrease relative to the infrared wavelength (Tateishi and Kajiura 1992). This tends to increase the computed NDVI values, and hence the positive anomalies over the desert and lakes regions.

u) Look at Figure 7.6, the loadings graph for Component 6.

The loadings show a gradual increasing trend over the seven year period. There are also two peaks in the loadings for each year, but the amplitude in the peaks decreases after 1989.

v) Display CMP6, the sixth component image. Notice the high negative anomalies in the rainforest regions in Africa.

The double peaks for each year in the loadings graph relate to the double precipitation regime found in certain regions of Africa, as illustrated in Component 4. The decrease of the amplitude in the peaks is likely to contribute to a decreasing range of NDVI values and correspondingly high negative anomalies in the forest regions. The decrease of the amplitude can be attributed to a change in the sensor as a result of the change over in satellite in late 1988 (from NOAA-9 to NOAA-11).

Thus, the inter-annual variability extracted in the fifth and sixth components through the PCA analysis is related to orbital characteristics of the sensor and the satellite system. Remember that all of the components are uncorrelated with one another. Therefore, in the remaining two components, Components 7 and 8, the effects of all of the previous components have been removed.

w) Display CMP7, the seventh component image. The image shows positive anomalies in much of eastern and

southern Africa. Look at the graph of the loadings for this component in Figure 7.7. The loadings are negative for much of 1987, and then again for most of 1991 and 1992.

Component 7 describes the ENSO warm phase events of 1986-87 and of 1991-92 in southern Africa. The effect of the 1991-92 ENSO is more pronounced than that of the 1986-87 event, perhaps because the study period started in April 1987. During an ENSO warm phase, there is a significant decrease in rainfall in southern Africa leading to drought conditions.

- x) Display CMP8, the eighth component image. The image shows a band of negative anomaly that stretches across the Sahel and into east Africa, especially in the countries of Ethiopia, Kenya, and Somalia. The graph in Figure 7.8 shows negative loadings for most of 1987 and 1988 as well as for 1992 and 1993.

It appears that Component 8 is capturing the ENSO warm phase events of 1986-87 and 1991-92 in the Sahel and in eastern Africa. As a result of the 1991-92 ENSO, some of the countries in eastern Africa such as Ethiopia and Kenya experienced severe drought. Thus, the inter-annual variability captured by Components 7 and 8 can be linked to ENSO phenomena. A study conducted on a three-year period from 1986 to 1988 yielded similar evidence of the linkages between the two components and ENSO (Eastman, McKendry, and Fulk 1994).

Also note the relationship of Components 7 and 8 with that of the Southern Oscillation Index (SOI) shown in Figures 7.7 and 7.8 respectively<sup>7</sup>. The SOI is an index of the relationship of air pressure as measured at two points, one in Australia and the other in Tahiti. The SOI is often used as an indicator of ENSO. The smoothed curved lines are polynomial transformations of the index and components showing a positive relationship with that of Component 7 and negative relationship with that of Component 8. This provides additional evidence that the inter-annual variability captured by Components 7 and 8 are related to ENSO phenomena.

## Conclusions

In this exercise, we used a technique based upon principal components analysis to analyze NDVI data to extract patterns of vegetation in Africa over time and space. An exploratory analysis of NDVI data for the seven-year period from 1987 to 1994 yielded eight components. The spatial patterns of the values in these components correspond with intra-annual variability such as that produced by seasonal changes as well as inter-annual variability produced by the sensor and satellite system. Particularly interesting are two components, Components 7 and 8, which appear to be related to ENSO.

As the ENSO warm phase is usually accompanied by reduced rainfall and the onset of drought in certain parts of Africa, these components may provide a basis for drought early warning. More research is required to realize the full potential of this technique. For example, research has shown that some areas in eastern Africa are better related to the inter-annual events monitored by SOI (Farmer 1988). Thus, a regional analysis across eastern Africa might give us a better understanding of the relationships between NDVI anomalies, rainfall, and ENSO. Additionally, the integration of socioeconomic data into analyses of this kind remains a challenge for future research. Nonetheless, the technique is an exciting approach for analyzing short-term climatic variation and its impacts over Africa as well as other parts of the world.

## References

- Anyamba, A., J. R. Eastman, and M. Fulk. 1995. NDVI as an indicator of climatic variability. *Proceedings of the ACSM/ASPRS conference*, Volume 3 (ASPRS): 714-723. Bethesda, MD: American Congress on Surveying and Mapping, and American Society for Photogrammetry and Remote Sensing.
- DMC (Drought Monitoring Center). 1994. *Drought Monitoring Bulletin: Eastern and southern Africa*. Nairobi, Kenya and Harare, Zimbabwe: Drought Monitoring Centers and Centres de Suive de la Secheresse.

---

7. It may be noted that negative SOI deviations indicate a drier than normal period in southern Africa and wetter than normal period in eastern Africa and vice versa for positive SOI deviations.



- Eastman, J.R., and M. Fulk. 1993. Long sequence time series evaluation using standardized principal components analysis. *Photogrammetric Engineering and Remote Sensing* 59 (8): 1307-1312.
- Eastman, J.R., J. McKendry, and M. Fulk. (eds.). 1994. *Change and time series analysis, 2nd edition*. Explorations in Geographic Information Systems Technology, Volume 1. Geneva, Switzerland: United Nations Institute for Training and Research (UNITAR).
- Farmer, G. 1988. Rainfall data bases and seasonal forecasting in eastern Africa. In *Recent Climatic Change*, ed. S. Gregory (ed.), 193-202. New York: Bellhaven.
- Golnaraghi, M., and R. Kaul. 1995. The science of policymaking: responding to ENSO. *Environment* 37(1): 16-20, 38-44.
- Grimes, D., G. Dugdale, and J.R. Milford. 1994. Contribution of meteorological satellites to agriculture and hydrological hazard warning in the semi-arid tropics. In *Natural Hazards and Remote Sensing*, ed. G. Wadge, 75-80. London, UK: The Royal Society.
- Hellden, U., and L. Eklundh. 1988. *National drought impact monitoring: A NOAA NDVI and precipitation data study of Ethiopia*. Lund Studies in Geography Series No. 15. Sweden: Lund University Press.
- Holben, B.N. 1986. Characteristics of maximum value composite images from AVHRR data. *International Journal of Remote Sensing* 7(11): 1417-1434.
- Hutchinson, C.F. 1991. Use of satellite data for famine early warning in sub-saharan Africa. *International Journal of Remote Sensing* 12(6): 1405-1421.
- Lillesand, T.M., and R.W. Kiefer. 1987. *Remote sensing and image interpretation*. New York: John Wiley & Sons.
- NRC (National Research Council). 1994. *Facing the challenge: The U.S. national report to the IDNDR world conference on natural disaster reduction, Yokohama, Japan, May 23-27, 1994*. Washington, D.C.: National Academy Press.
- Rasmusson, E.M. 1987. Global climate change and variability: effects on drought and desertification in Africa. In *Drought and hunger in Africa: Denying famine a future*, ed. M. Glantz, 3-22. Cambridge, UK: Cambridge University Press.
- Richards, J.A. 1984. Thematic mapping from multitemporal image data using Principal Components transformation. *Remote Sensing of Environment* 16: 35-46.
- Tateshi, R., and K. Kajiwara. 1992. Global land cover monitoring by AVHRR-NDVI data. *Earth Environment* 7: 4-14.
- Timberlake, L. 1986. *Africa in crisis: The causes, the curse of environmental bankruptcy*. Philadelphia, PA: New Society Publishers.
- Tucker, C.J. 1978. A comparison of satellite sensor bands for monitoring vegetation. *Photogrammetric Engineering and Remote Sensing* 44: 1369-1380.
- Tucker, C.J., and P.J. Sellers. 1991. Satellite remote sensing of primary production. *International Journal of Remote Sensing* 7(6): 1395-1416.

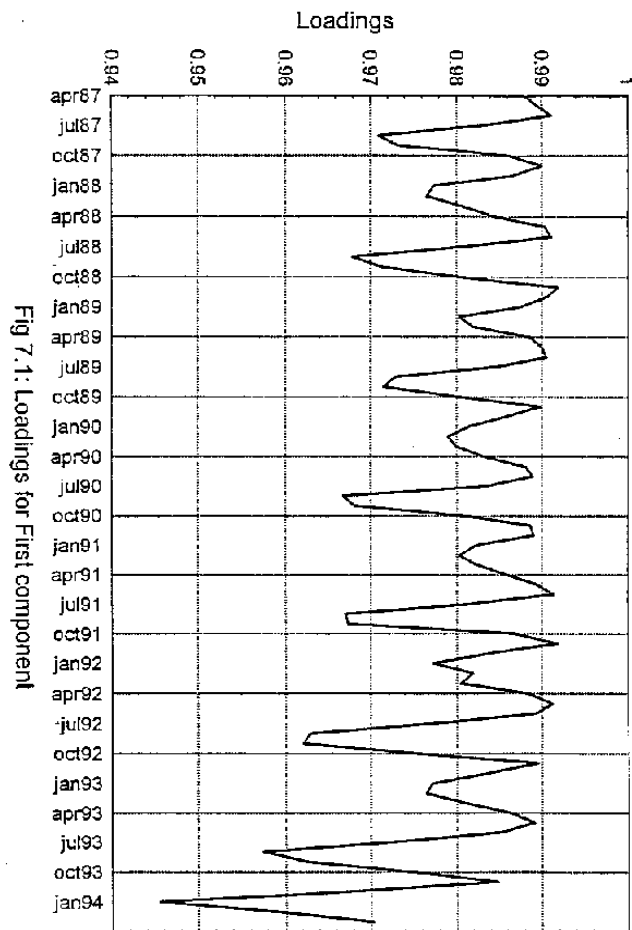


Fig 7.1: Loadings for First component

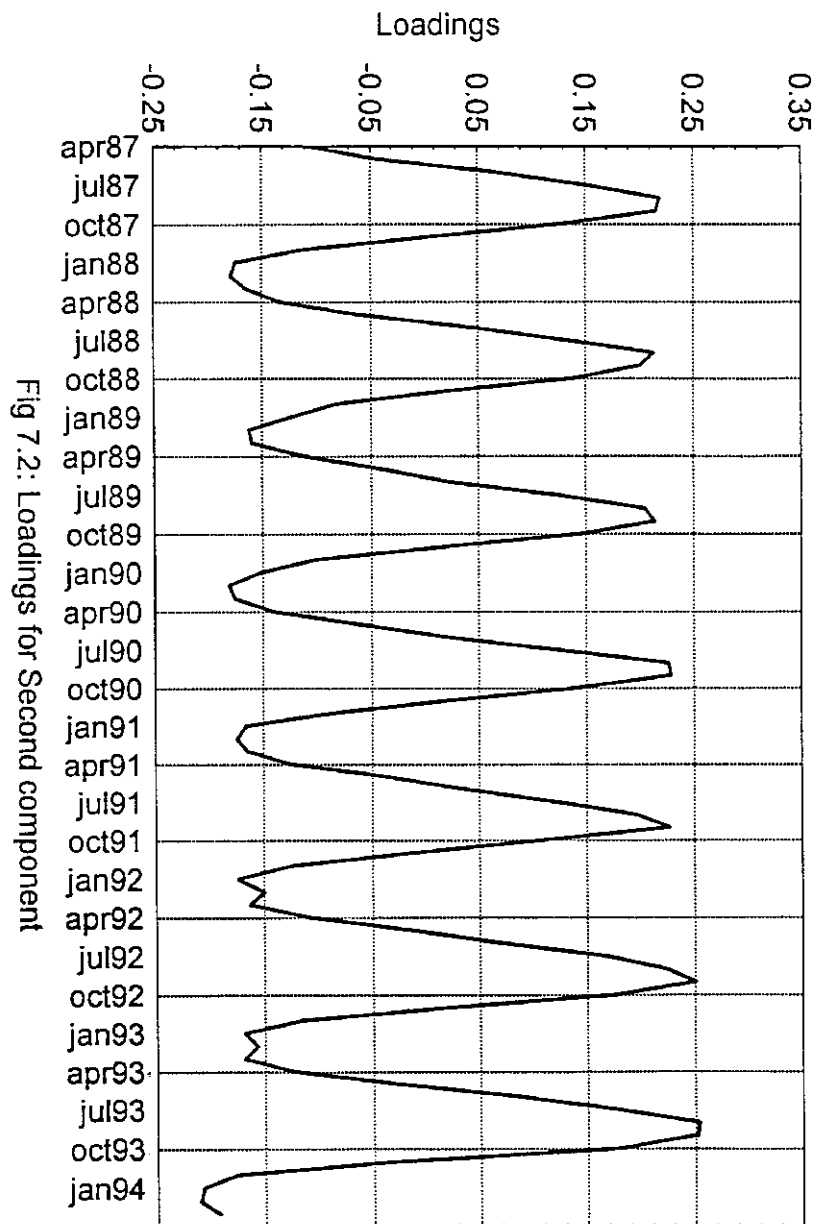
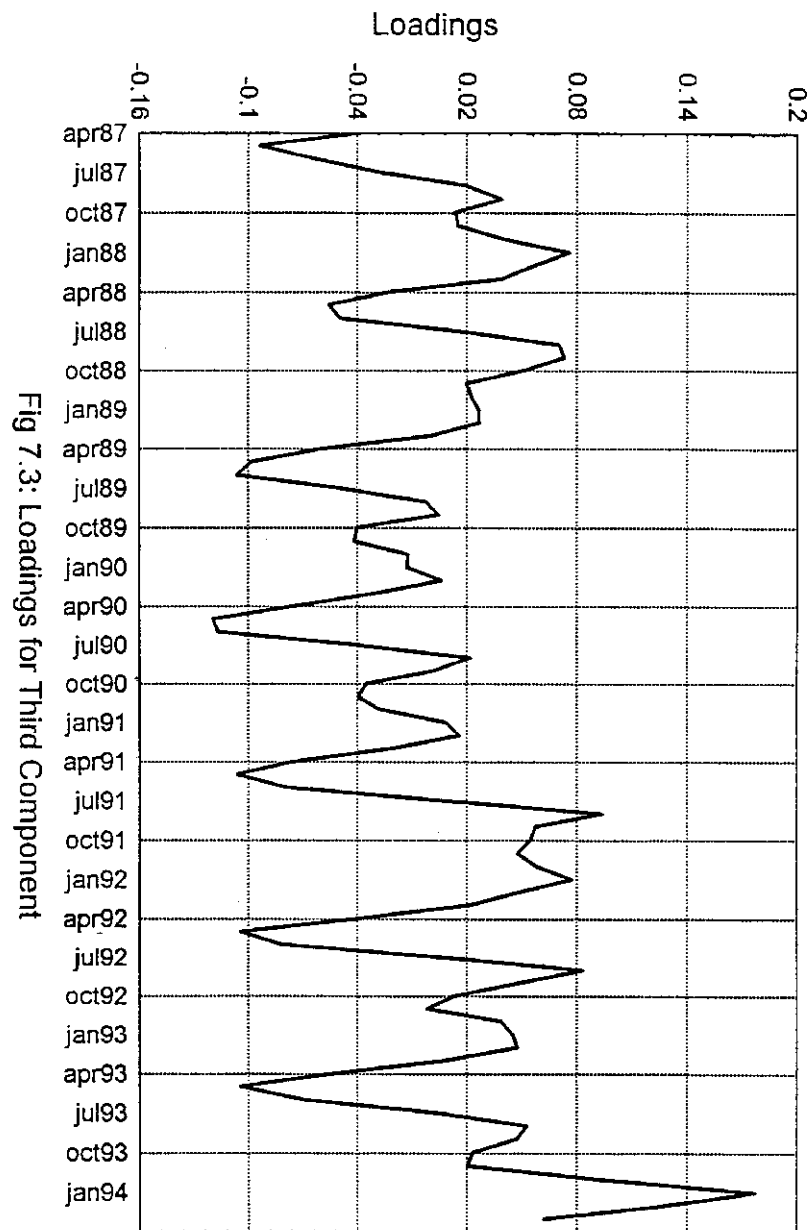
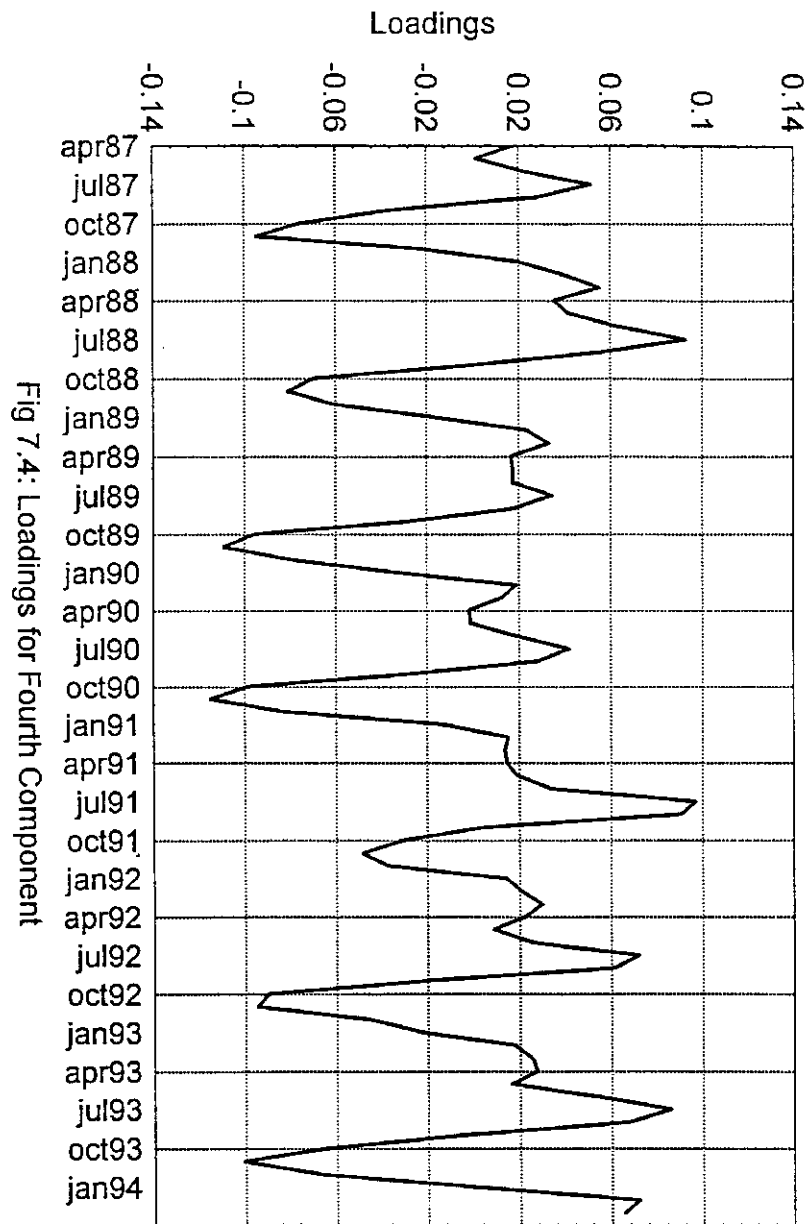


Fig 7.2: Loadings for Second component





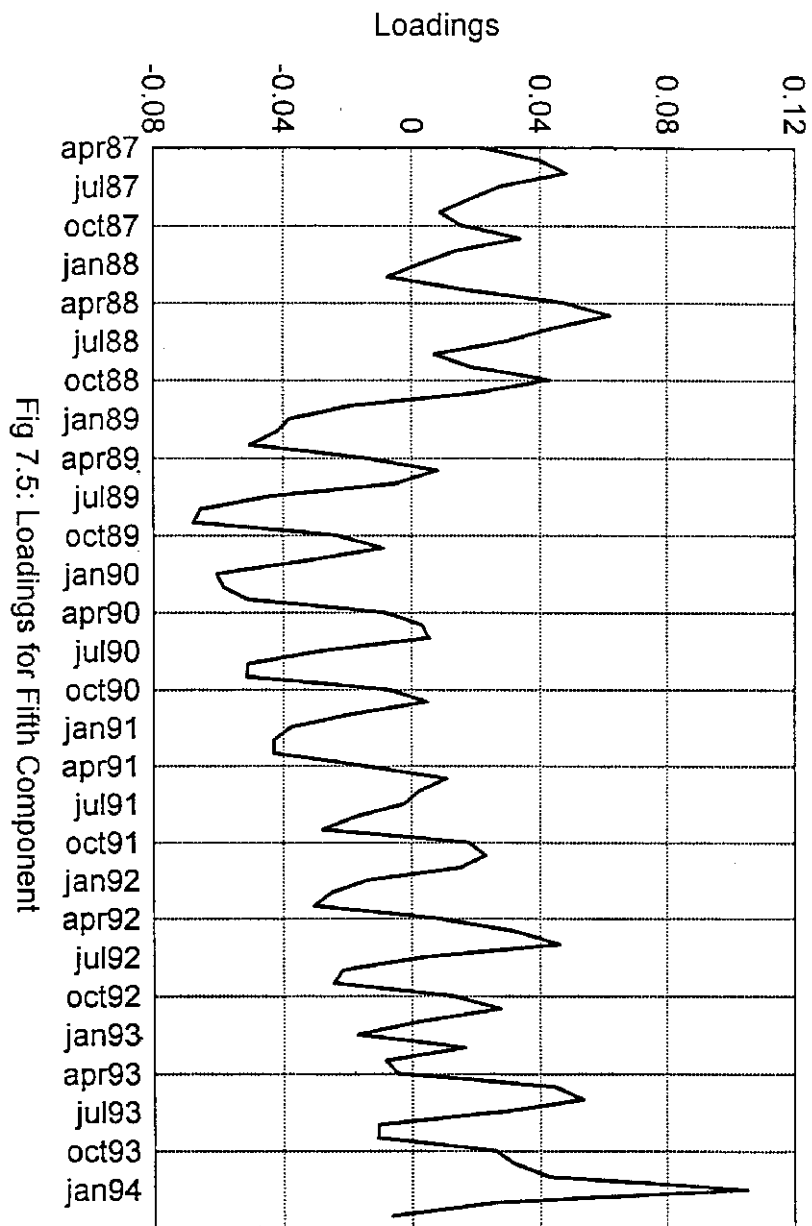


Fig 7.5: Loadings for Fifth Component

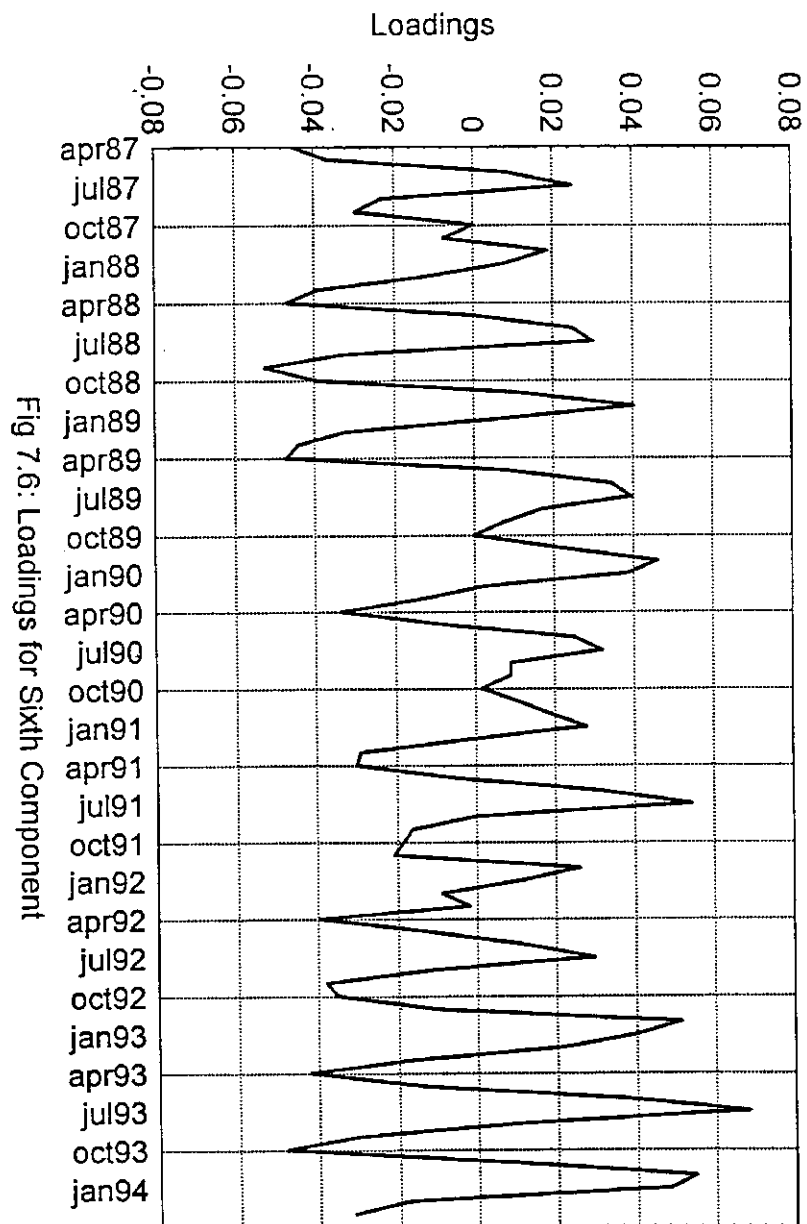


Fig 7.6: Loadings for Sixth Component

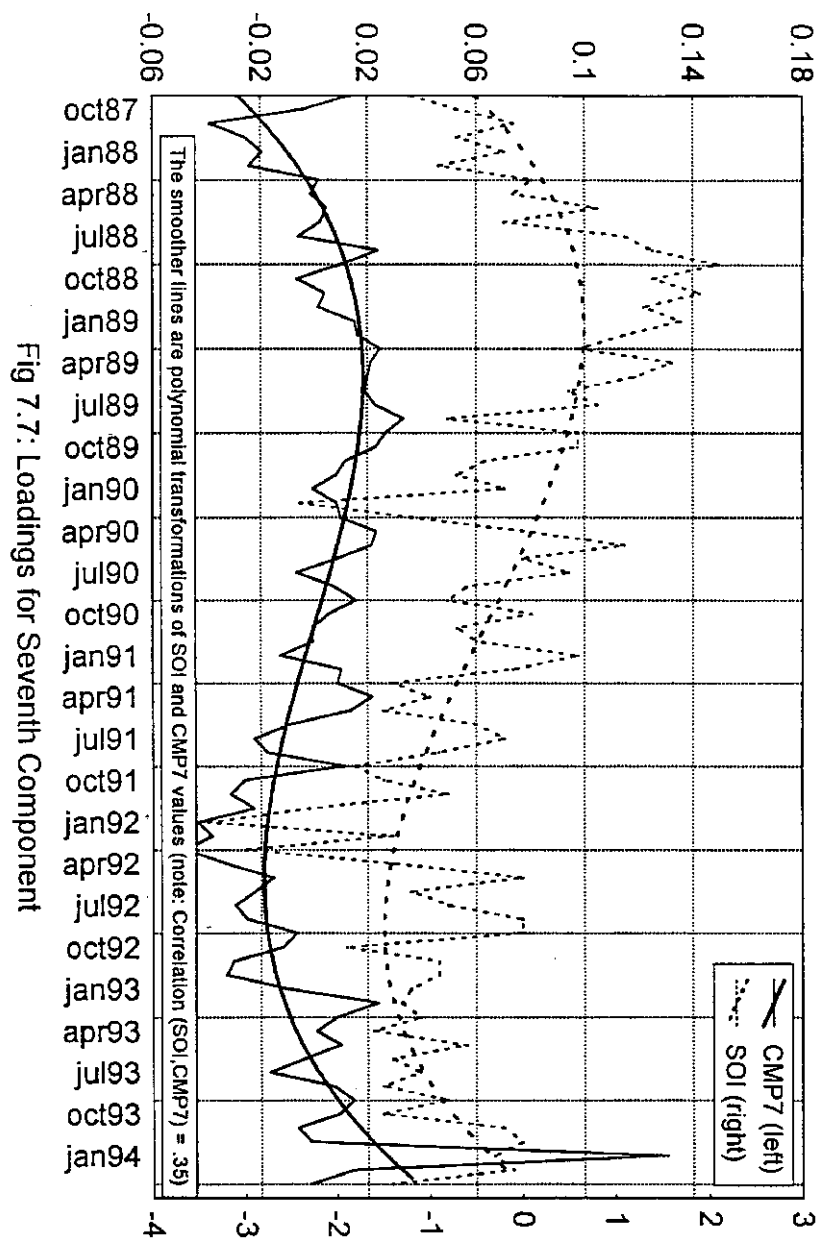


Fig 7.7: Loadings for Seventh Component



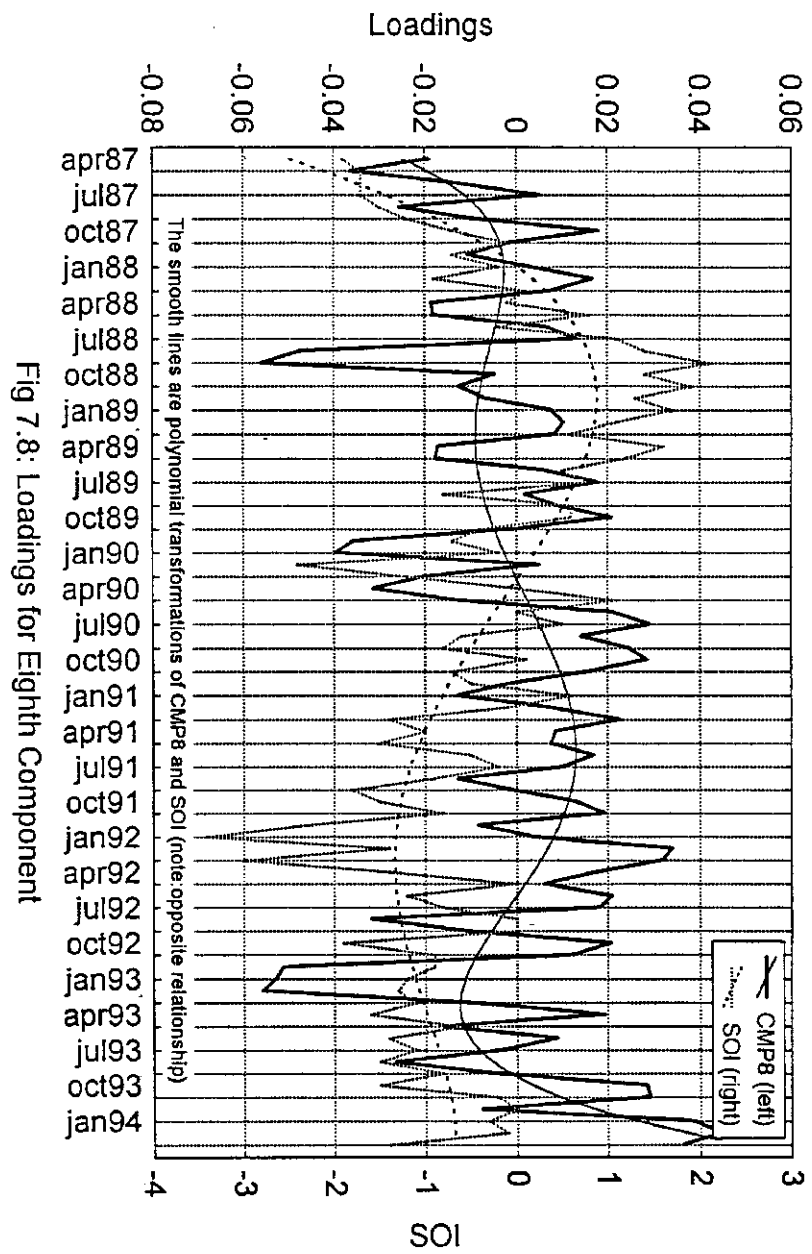


Fig 7.8: Loadings for Eighth Component

# Answers

## Exercise 1

1. All three types of crops, Strategic, Export, and Basic, are cultivated in the high drought hazard areas.
2. The total area (in acres) for the three types of crops is shown below. The crops with the highest proportion grown in the high drought hazard areas are export crops (59%).

Strategic	129,446
-----------	---------

Export	27,081
--------	--------

Basic	38,621
-------	--------

3. Another approach is to use the Edit/ASSIGN option. First use Edit to create an attribute values file with a single line containing the following numbers separated by a space:

6 1

Then, use ASSIGN to assign the values file to the image SEISMIC to produce an image of areas with high earthquake hazard.

4. The areas determined by the all-hazards assessment are shown in the answer image ANS4EX1 in the Answer Image folder.

5. All three types of crops (strategic, export, and basic) are cultivated in the areas determined by the all-hazard assessment (see the image ANS5EX1). The area (in acres) of crop cultivation in the all-hazard assessment areas are:

Strategic	1,097
-----------	-------

Export	1,389
--------	-------

Basic	49
-------	----

## Exercise 2

1. HIGHRISK is a Boolean image. The value 1 represents areas at high risk to flooding from nor'easters in Revere; the value 0 represents all other areas.

2. The dominant landuse in the community is residential. The landuses near the coast include residential, recreation, commercial, and transportation.

3. The categories in REVLUSE for the following landuses are:

Residential	6
-------------	---

Commercial	8
------------	---

Industrial	9
------------	---

4. Area (in acres) exposed to flooding and wave action are:

Residential	308
-------------	-----

Commercial	74
------------	----

Industrial	46
------------	----

5. There are 44 block groups in Revere.

6. There is only one such block group (with 43% of population over 65 years) located on the coast. Another block group (with 60% of population over 65 years) is in proximity to the coast and could be at risk from nor'easters. These areas of the community can be given special attention by emergency planners.

7. The high value in RESIST is 23.67; the low value is 2.

8. The analysis for both HISPANIC and POVERTY show that block groups with high percentages of these vulnerable populations do not fall in the areas at high risk to flooding and wave action. The resulting image when the field HISPANIC% is considered is ANS8AEX2 and the resulting image when the field POVERTY% is considered is ANS8BEX2. Both these answer images are provided in the Answer Image folder.

### Exercise 3

1. Number of columns= [Maximum X-Minimum X]/size of grid cell =  $[-80-(-100)]/0.25 = 80$

Number of rows= [Maximum Y-Minimum Y]/size of grid cell =  $[32-24]/0.25 = 32$

2. The command line parameters for the operation "add ELEVATION and EROSION" is:

```
overlay x 1*elevation*erosion*tmp
```

3. First cell of CVI1 in Figure 3.2 is:  $\sqrt{(1*4*3*2*5*3*1/7)} = 7.17$

Second cell of CVI1 in Figure 3.2 is:  $\sqrt{(0*1*5*5*3*5*2/6)} = 11.18$

Third cell of CVI1 in Figure 3.2 is:  $\sqrt{(0*0*0*3*2*4*2/4)} = 3.46$

Fourth cell of CVI1 in Figure 3.2 is:  $\sqrt{(1*4*5*0*0*5*1/5)} = 4.47$

4. Contents of STEP3.IML are as follows:

```
reclass x i*elevation*elevrec*2*1*1*6*-9999
```

```
reclass x i*subsid*subrec*2*1*1*6*-9999
```

```
reclass x i*geology*georec*2*1*1*6*-9999
```

```
reclass x i*geomorph*geomrec*2*1*1*6*-9999
```

```
reclass x i*erosion*erorec*2*1*1*6*-9999
```

```
reclass x i*wvehgt*wverec*2*1*1*6*-9999
```

```
reclass x i*tidal*tidrec*2*1*1*6*-9999
```

5. Contents of STEP4.IML are as follows:

```
overlay x 1*elevrec*subrec*tmp1
```

```
overlay x 1*tmp1*georec*tmp2
```

```
overlay x 1*tmp2*geomrec*tmp3
```

```
overlay x 1*tmp3*erorec*tmp4
```

```
overlay x 1*tmp4*wverec*tmp5
```

```
overlay x 1*tmp5*tidrec*divider
```

6. The higher the value in CVI1, the greater is the vulnerability of the Gulf Coast area covered by the grid cell to the risks of erosion and inundation.

7. First, use RECLASS on CVI1 to create a new image called LVI1REC:

assign a new value of:	1
to the old values ranging from:	1
to those just less than:	16
assign a new value of:	2
to the old values ranging from:	16
to those just less than:	22
assign a new value of:	3
to the old values ranging from:	22
to those just less than:	9999

Then, display TMP1 with the user-defined palette RISK. Use the Add Layer option to first overlay CELLS with the default symbol file and then overlay COAST with the default symbol file. Finally, use the window option to zoom into the area shown in Figure 3.3.

8. The highest value for CVI2 is 84; the lowest value is 0. The answer image for this question, ANS8EX3, is provided with the data set for this exercise.

### **Exercise 4**

1. Total population at risk = 40,486 (Note: This figure may differ slightly from user to user because of differences in rounding off decimal digits during the calculation).
2.  $\text{Risk} = (1.5 \times 10^{-4}) \times 40,486 = 6.07$  (See note above).
3. Population at risk = 1,986
4. Population at risk = 4,676

### **Exercise 5**

1. Northern direction is predominant in the image.
2. The distance is 20 m for cells with horizontal and vertical flow and 28.284 m for the cells with diagonal flow.
3. The minimum value is 0. It corresponds to the background cells. The maximum value is 5.822 tons/cell/year.
4. The colored lines represent the stream network. The watershed outlet is located in the southern part of the image.
5. The column/row position of the "seed cell" is 535/891. The value in the cell is 241761. It means that this cell receives pollutants from 241761 cells in the watershed.
6. TN has higher values than TP meaning that nitrogen has more favorable conditions for transport.
7. FLOWN has the larger load-contributing area (31% non-zero values) compared to FLOWS (21% non-zero values).
8. Total annual load of phosphorus, nitrogen, and sediments delivered to the watershed outlet are:  
Phosphorus      3.062 tons

Nitrogen            16.99 tons  
Sediments           1417.408 tons

## Exercise 6

1. Values in the table should be:

Landcover	Position		Reflectance Values		
	Column	Row	Red	Near Infrared	Mid Infrared
Field	96	191	32	110	44
Road	305	411	63	72	56
Water	345	179	26	17	2

2. 6 clusters were identified; Cluster 4 represents water.
3. Cluster 1 in 93BROAD represents water. This is because water occupies the largest area in the images for 1993.
4. Category 3 in CROSS represents areas affected by the 1993 flood. One explanation for category 2 is that there were fields which were irrigated in 1988 but dry in 1993.

## Exercise 7

1. We can identify areas of high vegetation (green colors) and areas of low vegetation (red colors).
2. On broad visual inspection, we can see that NDVI values are highest in the months of July to October in Northern Africa and in the months of January to April in Southern Africa.
3. Percent of variance explained by second component is 2.9%; by third component is 0.5%; by the first three components together is 98.9%.
4. Percent variance explained by the first component is 96.1%; by the seventh component is 0.054%; by eighth component is 0.051%.
5. Component 1 represents the average NDVI values for the whole area (note the high positive correlations of greater than 0.9 for all months). Areas of the rainforest in Central Africa have much higher average NDVI (dark green) and areas in Sahel and the Namibian desert have much lower average NDVI (dark red). The dips in temporal loadings likely represent the change in growing seasons across Northern and Southern Africa.

# ***Glossary of Terms***

## ***Block groups, census tracts, and census blocks***

In U.S. census geography, a block group (BG) is a combination of census blocks within a census tract which have the same first digit in their identifying numbers. For example, BG 3 within census tract 1703 is a collection of all the census blocks numbered 301 to 397. A block group consists of 500 to 1000. A census tract is a small, relatively permanent statistical subdivision of a county in a metropolitan area or a selected nonmetropolitan county, delineated for the purpose of presenting decennial census. The boundaries of census tracts are usually major streets, natural features such as rivers, and corporate limits of the local government. A census tract contains between 2,500 and 8,000 inhabitants. A census block, on the other hand, is an area normally bounded on all sides by well-defined features such as streets, roads, streams, and railroad tracks. A census block usually contains about 250 to 500 households.

## ***DIME***

DIME stands for Dual Independent Map Encoding. It is a digital database developed for conducting the 1970 Census in standard metropolitan statistical areas (SMSAs) in the United States and subsequently extended to other urban areas for the 1980 Census. The DIME for an SMSA or an urban area includes street segments, address ranges, identifiers for census units such as census blocks and census tracts, and non-street segments such as railways and rivers.

## ***ETAK***

The ETAK database is a detailed digital database of streets, roads, and highways produced by Etak Inc., California, USA. The database is available for most urban areas in the country.

## ***FIRM***

The FIRM shows areas of a community at different levels of risk from flooding such as that from a 100-Y or 500-Y flood. These areas are determined by the United States Federal Emergency Management Agency (FEMA) through statistical analysis of historical records, topographic surveys, and hydrologic and hydraulic analysis.

## ***NDVI (Normalized Difference Vegetation Index)***

NDVI is calculated from the red and infrared bands of satellite imagery as:

$$\text{NDVI} = (\text{Infrared} - \text{Red}) / (\text{Infrared} + \text{Red})$$

Vegetated areas will generally yield higher values for this index because of the relatively high near-infrared reflectance and low red reflectance. Because of this contrast, the NDVI will enhance the differences in the reflectance patterns of vegetation in these two bands. NDVI varies in values from -1 to +1. High values of NDVI (near +1) indicate the presence of healthy green vegetation whereas low values of NDVI (near -1) indicate the absence of such vegetation.

## ***Nor'easters***

These storms derive their name from the prevailing wind pattern in the winter months of November to April that places the track of the storms North to Northeast along the Atlantic seaboard of the United States. The damages to coastal communities from nor'easters occur as a result of high winds, wave action, and flooding associated with storm surge. The impacts include property damage, loss of business, costs of emergency response and cleanup, and even injuries and fatalities.

## ***TIGER***

TIGER stands for Topologically Integrated Geographic Encoding and Referencing. TIGER is a digital database devel-

oped for almost all areas in the United States by the U.S. Census Bureau for conducting the 1990 Census. TIGER contains data on roads, railroads, and streams. In addition, TIGER has feature names, Federal Information Processing Standard (FIPS) codes for census entities such as census blocks, census tracts, cities and townships, and address ranges and zip codes for streets in urban/metropolitan areas.

### ***Toxic Chemical Release (TRI) Inventory***

The Toxic Chemical Release Inventory (TRI) is a computerized database of releases of chemicals to all media reported by certain industries to the U.S. Environmental Protection Agency (EPA) under the Emergency Planning and Community Right-To-Know Act or SARA Title III.

# Details for Exercises 3 & 5

## Exercise 3

### Descriptions of Variables Used in Gulf Coast Vulnerability Analysis

The data on the seven variables used in the vulnerability analysis in this exercise were compiled in the manner described below. The section relies heavily upon information provided by Gornitz and White (1994).

**1. Mean Elevation:** The data on elevation was obtained from the National Geophysical Data Center (NGDC) located in Boulder, Colorado. The data are organized in 5 minute x 5 minute cells, with negative values for cells that do not contain land within their boundaries, 0 values for cells with land at sea level, and positive values for cells with land above sea level. Each 0.25° grid cell in the study area may contain as many as nine 5 minute x 5 minute cells with non-zero values. The mean elevation was calculated by averaging the elevations of all nonnegative 5 minute cells within each 0.25° grid cell. For the Gulf Coast, mean elevation ranges from 0 to 29 meters with more than 95% of the Coast at or below 10 meters, placing it at high risk to erosion and inundation.

**2. Local Subsidence Trend:** The local subsidence trend was calculated as the difference between the relative sea-level trend variable and a global eustatic rate of sea level rise of 1.55 mm per year reported by the Inter Governmental Panel on Climatic Change (IPCC). The global eustatic rate was used since holocene paleo-sea-level indicators were not available for the Gulf Coast. The relative sea-level trend variable was calculated by fitting a linear regression line to the time series of mean annual sea-level elevations for each of 12 long-term tidal gauge stations on the Gulf Coast. For segments of the Gulf Coast lying between tide gauge stations, the following procedure was adopted (Gornitz and White, 1994: 19):

- (1) The tide-gauge stations and the sea-level trends were plotted along a 1:2,000,000 digitized U.S. Gulf coastline.
- (2) A 0.25° by 0.25° grid was then overlaid onto the tide-gauge stations with an Arc/Info IDENTITY command, whereby the grid cells were assigned sea-level trends from the tide-gauge stations lying within the cells.
- (3) For each coastal grid cell without data, the difference in relative sea levels was calculated between the two nearest gauge stations (i.e., occurring east and west or north and south of the given grid cell).
- (4) The difference between the relative sea levels was then divided by the number of grid rows, plus one, occurring between the grid cells containing gauge stations. This value was called the slope factor.
- (5) The slope factor was then multiplied by the number of grid rows from the grid cell being calculated to the nearest station (i.e., western-most or southern-most station) and added to the station's relative sea-level trend.

**3. Geology:** The data on geology was obtained by combining the 1:2,000,000 map of the Gulf coastline with state geologic maps ranging from 1:250,000 to 1:1,000,000 in the following manner (Gornitz and White 1994: 14):

- (1) Enlarged maps of the 1:2,000,000 digitized U.S. Gulf Coastline were plotted in small sections (i.e., approximately 5° latitude by 5° longitude).
- (2) Polygons (boxes) were drawn around each coastal segment as identified by state geologic maps.
- (3) The hand-drawn polygons were digitized into Arc/Info using the 1:2,000,000 digitized U.S. Gulf Coastline coverage as a backdrop.
- (4) These polygons were then overlaid onto the backdrop coverage with the Arc/Info IDENTITY command whereby the coastal segments took the values of the digitized polygons.
- (5) For the gridded data groups, a 0.25° latitude by 0.25° longitude grid was overlain onto the 1:2,000,000 digitized line coverage using an additional Arc/Info IDENTITY command. The grid cells then took on the geology values of the line segments.



Furthermore, if more than one rock type occurred in a grid cell the rock type associated with the greatest coastal length for that cell was assigned to the entire grid cell. Five classes of rock types were distinguished: old erosion resistant rocks, sedimentary rocks, unconsolidated sediments, recent volcanic materials, and coral reef. Among these rock types the Gulf Coast was found to consist in general of sedimentary rocks (limestones and sandstones) overlain by unconsolidated sediments. The tables below show additional rock types under this classification and the codes assigned to the rock types.

**4. Geomorphology:** Data on geomorphology of the Gulf Coast was derived in a manner similar to that of the geology data described above. The maps used in this case were United States Geologic Survey (USGS) 1:250,000 topographic maps of the coastline and maps from other published sources in conjunction with the 1:2,000,000 map of the coastline. Two broad geomorphological classes were distinguished: Erosional coasts and Depositional coasts. Each class was further subdivided into categories such as marine, nonmarine, glacial, nonglacial, and volcanic. The tables below show these geomorphological categories and the codes assigned to them.

**5. Mean Shoreline Displacement:** The source of the data on mean shoreline displacement was the Coastal Erosion Information System developed by May and colleagues (1983) and Dolan and colleagues (1989). The data was available in 3 minute by 3 minute grid cells and in areas where data was sparse in 7.5 minute by 7.5 minute or 15 minute by 15 minute grid cells. Like the data on elevation, data from these smaller grid cells were combined into several variables such as minimum, mean, and maximum for each 0.25° by 0.25° grid cell in the study area. In the Gulf Coast, these data show that the barrier islands of Louisiana face the greatest shoreline displacement with rates exceeding 8 to 10 mm per year.

**6. Mean Tidal Range:** The data on tide ranges was obtained from tide tables published by the National Oceanic and Atmospheric Administration (NOAA)'s National Ocean Service. The data were available for 187 tide stations located in the Gulf Coast. The mean tidal range for each grid cell was calculated as the average of the diurnal tidal ranges of all the stations within a 0.25° by 0.25° grid cell.

**7. Maximum Wave Heights:** The sources of the data on maximum wave heights were the published documents of the Coastal Engineering Research Center (CERC), U.S. Army Corps of Engineers, and Wave Information Study (WIS). The data were originally available in 0.5° grid cells, which were then transferred to the 0.25° grid cells covering the study area. The Arc/Info UNION command was used to determine the geometric intersection of the 52 0.5° grid cells with the 0.25° grid covering the study area and resulted in the creation of 208 0.25° grid cells.

## Classifications and Codes Used for Geology and Geomorphology Variables

**Table 1.** Geologic classification codes assigned to the coastal geology variable

Material description		Code
1.	Old Erosion Resistant Rocks (crystallines)	100
	A. Igneous, volcanic (basalt, rhyolite, andesite, etc.)	110
	B. Igneous, plutonic (granite, granodiorite, etc.)	130
	C. Metamorphic (schists, gneisses, quartzite, serpentinite, etc.)	150
2.	Sedimentary Rocks	200
	A. Shale	210
	B. Siltstone	220

	C.	Sandstone	230
	D.	Conglomerate	240
	E.	Limestone	250
	F.	Eolianite (calcite-sand)	260
	G.	Mixed or varied lithology	270
3.		Unconsolidated Sediments	300
	A.	Mud, Clay	310
	B.	Silt	320
	C.	Sand	330
	D.	Gravel, conglomerates	340
	E.	Glacial till	345
	F.	Glacial drift (fluvial-glacial)	350
	G.	Calcareous sediment	360
	H.	Mixed or varied lithology	370
4.		Recent Volcanic Materials	400
	A.	Lava	410
	B.	Ash, Tempura	420
	C.	Composite	430
5.		Coral Reef	500

**Table 2.** Geomorphology classification codes assigned to the coastal geomorphology variable

	Landform description	Code	Beach	Man-Modified
1.	Erosional coasts (scoured, beaches poorly developed)	1000		
	A. Marine with wave erosion and cliffs	1100		
	1. Low (5-30 m)	1110	1111	1119
	2. Medium (30-100 m)	1120	1121	1129
	3. High ( >100 m)	1130	1131	1139
	B. Nonmarine (land erosion)	1200-1500		
	1. Glaciated coast	1210	1211	1219
	a. Fjord (drowned valley)	1220	1221	1229

	b.	Indented fiard (low-lying inlet)	1230	1231	1239
		mud flats	1234		
		salt marsh	1235		
	c.	Rocky glacial coast	1240	1241	1249
2.		Nonglacial irregular coast	1300		
	a.	Strongly embayed, nonrocky	1310	1311	1319
	b.	Strongly embayed, rocky	1320	1321	1329
	c.	Estuaries	1330	1331	1339
		mud flats	1334		
		salt marsh	1335		
		mixed types	1338		
	3.	Ice coasts	1400		
	4.	Drowned larst topography	1500		
2.		Depositional coasts (sediment accumulations and well-developed beaches)	2000		
	A.	Marine deposit	2100		
	1.	Coastal plain beach	2110	2111	2119
		salt marsh	2115		
	2.	Beach rock (beach sediment cemented by carbonates)	2112		
	3.	Barrier coast	2120	2121	2129
	a.	barrier island	2122		
	b.	bay barrier	2123		
	c.	mud flats	2124		
	d.	salt marsh	2125		
	e.	cusplate foreland	2126		
	f.	split	2127		
	g.	mixed	2128		
	B.	River deposits	2200		
	1.	Alluvial plain	2210	2211	2219
	2.	Delta environment	2220	2221	2229
	a.	mud flats	2224		

	b.	salt marsh	2225		
	c.	mixed	2226		
C.		Marine/fluviial deposits (Lagoonal coast)	2250	2251	2259
	1.	Mud flats	2254		
	2.	Marsh/mangrove	2255		
	3.	Mixed	2258		
D.		Glacial deposits	2300		
	1.	Outwash plain	2310	2311	2319
	2.	Moraine	2320	2321	2329
	3.	Drumlin	2330	2331	2339
		salt marsh	2315		
	4.	Drift	2340	2341	2349
		salt marsh	2345		
	5.	Composite	2350	2351	2359
E.		Biogenic	2400		
	1.	Reefs (corals, oysters, algal)			
	a.	fringing	2410		
	b.	barrier	2411	2419	
	2.	Barrier reef with an associated mangrove swamp	2425		
	3.	Swamp/mangrove	2450	2451	2459
F.		Volcanic coasts	2500		
	1.	Lava flows	2510	2511	2519
	2.	Tephra, ash	2520	2521	2529
	3.	Composite/caldera	2530	2531	2539

---

Source: Gornitz and White (1994)

## Scores for Relative Risk Variables

**Table 1.** Assignment of relative risk factors for elevation, shoreline displacement, local subsidence trend, tidal range, and wave height

Variable	Very Low	Low	Moderate	High	Very High
Mean elevation (m)	> 30	> 20 and =< 30	> 10 and =< 20	> 5 and =< 10	> 0 and =< 5
Mean shoreline displacement (m/year)	> 2.0 Accretion	> 1 and =< 2	> -1 and =< +1	> -2 and =< -1	=< -2 Erosion
Local subsidence trend (mm/year)	< -1 Land rising	>= -1 and =< 1	> 1 and =< 2	> 2 and =< 4	> 4.0 Land sinking
Mean tidal range (m)	< 1.0 Microtidal	>= 1 and < 2	>= 2 and =< 4	> 4 and =< 6	> 6.0 Macrotidal
Maximum significant wave height (m)	>= 0 and < 3	>= 3 and < 5	>= 5 and < 6	>= 6 and < 6.9	>= 6.9

**Table 2.** Assignment of relative risk factors for geology

Relative risk score	Geology values <sup>a</sup>
1	100, 110, 130, 410
2	150
3	200, 210, 220, 230, 240, 250, 260, 270, 400, 430, 500
4	300, 340, 345, 370

<sup>a</sup> See Table 1 in the Classifications and Codes Used for Geology and Geomorphology Variables section for description of geology values.

**Table 3.** Assignment of relative risk factors for geomorphology

Relative risk score	Geomorphology values <sup>a</sup>
1	1130, 1139, 1210, 1219, 1220, 1229, 1230, 1239, 1240, 1249, 1320, 1329, 2510, 2519
2	1120, 1129, 1131, 1211, 1221, 1231, 1234, 1235, 1241, 1245, 1310, 1319, 2511
3	1110, 1119, 1121, 1311, 1321, 1335, 1338, 2112, 2115, 2125, 2225, 2255, 2300, 2315, 2320, 2329, 2330, 2339, 2340, 2345, 2349, 2350, 2359, 2400, 2410, 2419, 2420, 2425, 2429, 2450, 2459, 2500, 2530, 2539
4	1111, 1330, 1339, 2200, 2210, 2219, 2228, 2250, 2258, 2259, 2310, 2319, 2321, 2331, 2341, 2351, 2411, 2421, 2451, 2520, 2529
5	1331, 1334, 2110, 2111, 2119, 2120, 2121, 2122, 2123, 2124, 2126, 2127, 2128, 2129, 2211, 2220, 2221, 2224, 2229, 2251, 2254, 2311, 2521, 2531

<sup>a</sup> See Table 2 in the Classifications and Codes Used for Geology and Geomorphology Variables section for a description of geomorphology values.

Source: Gornitz and White (1994)

## Exercise 5

### The Cover and Management Factor, C

Land use/land cover	Cover and management factor, C
Forest	0.003
Barren	0.36
Cropland	0.26
Pasture	0.013
Rangeland	0.012
Developed	0.003
Water	0

Source: Dunne and Leopold (1978)

### Macro for USLE (USLE.IML)

The following line assigns the soil erodibility factor to different soils:

assign x tcsoil*temp1*soilk*2	assigns soil erodibility factor K using SOILK.VAL (TEMP1).
-------------------------------	--

The following four lines calculate slope length L:

reclass x i*slopes*temp2 *2 *1*0*4*2*4*4*3*4*50*-9999	reclassifies SLOPES into three categories: less than 4%, equal to 4% and greater than 4% (TEMP2).
assign x temp2*temp3*slopefac*2	assigns slope factor X to three slope categories using SLOPEFAC.VAL (TEMP3).
scalar x length*temp4*4*22	Divides length of slope by 22 (TEMP4).
overlay x 6*temp4*temp3*temp5	Calculates slope length L by exponentiating previous result to the power of X (TEMP5).

The following 6 lines represent calculation of slope steepness factor S:

scalar x slopes*temp6*5*2	Exponentiates slope image to the power of 2 (TEMP6).
scalar x temp6*temp7*3*0.043	Multiplies previous image by 0.043 (TEMP7).
scalar x slopes*temp8*3*0.3	Multiplies slope image by 0.3 (TEMP8).
overlay x 1*temp7*temp8*temp9	Adds two last images together (TEMP9).
scalar x temp9*temp10*1*0.43	Adds 0.43 to previous image (TEMP10).
scalar x temp10*temp11*4*6.574	Divides previous image by 6.574 (TEMP11).

The following line represents calculation of cover and management factor C:

assign x tcluse*temp12*coverfac*2	Assigns cover and management factor C to landuse image using COVERFAC.VAL (TEMP12).
-----------------------------------	---

The following 6 lines represent multiplication of the six factors in the equation  $A = RKLSCP$ :

scalar x temp1*temp13*3*616	Multiplies soil erodibility image by rainfall and run-off factor R equal to 616 (TEMP13).
overlay x 3*temp13*temp5*temp14	Multiplies previous image by slope length L image (TEMP14).
overlay x 3*temp14*temp11*temp15	Multiplies previous image by slope steepness factor S image (TEMP15).
overlay x 3*temp15*temp12*temp16	Multiplies previous image by cover and management factor C image (TEMP16).

scalar x temp16*temp17*3*0.2	Multiplies previous image by uniform support practice factor P value 0.2 (TEMP17).
scalar x temp17*pots*4*25	Converts soil loss per ha to soil loss per cell by dividing previous image by 25, since there are twenty five 20m x 20m cells in one hectare (POTS).

### Export Coefficients used for Total Phosphorus and Total Nitrogen Potential Loads

Coefficients were converted from commonly used units (kg/ha/year) to units used to model loads from individual cells in the spatial data base (g/cell/year).

$$(g/cell/year = kg/ha/year : \text{area of 1 cell in ha} : 1000)$$

Land use	Total phosphorus, g/cell/year	Total nitrogen, g/cell/year
Water	0	0
Barren	52	176
Developed	17.2	59.2
Pasture	58.4	245
Cropland	88	372
Rangeland	10	59.2
Forest	8.48	98.4

Source: Levine, et al. 1993: p. 37.

### Manning's Roughness Coefficient N.

Land use	Manning's roughness coefficient N
Water	0.046
Barren	0.05
Developed	0.04
Pasture	0.1
Cropland	0.18
Rangeland	0.24
Forest	0.4

Source: Engman (1986).



## Descriptions of Macro Files

(Names of the resulting images are given in parentheses)

### PARAM.IML

assign x tcsoil*mpd*soilmpd*2	Assigns mean particle diameter values to TCSOIL using SOILMPD.VAL (MPD)
assign x tcsoil*p*soilperm*2	Assigns soil permeability values to TCSOIL using SOILPERM.VAL (P)
assign x tcluse*n*tcrough*2	Assigns Manning roughness coefficient values to TCLUSE using TCROUGH.VAL (N)
scalar x slopes*temp1*4*100	Divides SLOPES by 100 (TEMP1)
transform x temp1*theta*12	Takes arctan of TEMP1 (THETA)
transform x length*sqr*6	Squares LENGTH (SQRD)

### TCTN.IML

scalar x length*temp1*3*0.016	Multiplies LENGTH by 0.016 (TEMP1)
scalar x theta*temp2*3*26.83	Multiplies THETA by 26.83 (TEMP2)
transform x n*temp3*2	Takes ln of N (TEMP3)
scalar x temp3*temp4*3*-4.58	Multiplies TEMP3 by -4.58 (TEMP4)
transform x mpd*temp5*2	Takes ln of MPD (TEMP5)
scalar x temp5*temp6*3*2.87	Multiplies TEMP5 by 2.87 (TEMP6)
overlay x 3*length*n*temp7	Multiplies LENGTH and N (TEMP7)
scalar x temp7*temp8*3*1.47	Multiplies TEMP7 by 1.47 (TEMP8)
overlay x 3*length*theta*temp9	Multiplies LENGTH and THETA (TEMP9)
scalar x temp9*temp10*3*-1.63	Multiplies TEMP9 by -1.63 (TEMP10)
scalar x temp1*temp11*2*10.14	Subtracts 10.14 from TEMP1 (TEMP11)
overlay x 1*temp11*temp2*temp12	Adds TEMP11 and TEMP2 (TEMP12)
overlay x 1*temp12*temp4*temp13	Adds TEMP12 and TEMP4 (TEMP13)
overlay x 1*temp13*temp6*temp14	Adds TEMP13 and TEMP6 (TEMP14)
overlay x 1*temp14*temp8*temp15	Adds TEMP14 and TEMP8 (TEMP15)
overlay x 1*temp15*temp10*temp16	Adds TEMP15 and TEMP10 (TEMP16)
transform x temp16*temp17*3	Takes natural antilog of TEMP16 (TEMP17)

scalar x temp17*temp18*1*1	Adds 1 to TEMP17 (TEMP18)
transform x temp18*temp19*1	Takes reciprocal of TEMP18. Calculation of the TN trapped according to the formula is completed at this point (TEMP19)
scalar x temp19*temp20*3*100	Multiplies TEMP19 by 100 to convert range of values from 0-1 to 0-100 (TEMP20).

The following lines describe conversion of trapping efficiencies into delivery ratios:

scalar x temp20*temp21*3*-1	Multiplies previous image by -1 (TEMP21).
scalar x temp21*temp22*1*100	Adds 100 to the previous image (TEMP22).
overlay x 3*temp22*tcmask*tnraw	Final image TNRAW is produced via overlay of previous image with TCMASK. The value of 0 is assigned to cells outside the study area.

#### TCTP:IML

scalar x length*temp2*3*-0.416	Multiplies LENGTH by -0.416 (TEMP2)
scalar x sqrd*temp3*3*0.012	Multiplies SQRD by 0.012 (TEMP3)
scalar x p*temp4*3*0.296	Multiplies P by 0.296 (TEMP4)
scalar x n*temp5*3*-5.74	Multiplies N by -5.74 (TEMP5)
scalar x temp2*temp6*1*1.47	Adds 1.47 to TEMP2 (TEMP6)
overlay x 1*temp6*temp3*temp7	Adds TEMP6 and TEMP3 (TEMP7)
overlay x 1*temp7*temp4*temp8	Adds TEMP7 and TEMP4 (TEMP8)
overlay x 1*temp8*temp5*temp9	Adds TEMP8 and TEMP5 (TEMP9)
transform x temp9*temp10*3	Takes natural antilog of TEMP9 (TEMP10)
scalar x temp10*temp11*1*1	Adds 1 to TEMP10 (TEMP11)
transform x temp11*temp12*1	Takes reciprocal of TEMP11. Calculation of the TN trapped according to the formula is completed at this point (TEMP12).
scalar x temp12*temp13*3*100	Multiplies TEMP12 by 100 to convert range of values from 0-1 to 0-100 (TEMP13).
The following lines describe conversion of trapping efficiencies into delivery ratios:	
scalar x temp13*temp14*3*-1	Multiplies TEMP13 by -1 (TEMP14).
scalar x temp14*temp15*1*100	Adds 100 to TEMP14 (TEMP15).

overlay x 3 temp15*tcmask*tpraw	Final imageTPRAW is produced via overlay of TEMP15 with TCMASK. The value of 0 is assigned to the cells outside the study area.
---------------------------------	---

#### TCTS.IML

scalar x length*temp2*3*-0.33	Multiplies LENGTH by -0.33 (TEMP2)
scalar x sqrd*temp3*3*0.011	Multiplies SQRD by 0.011 (TEMP3)
scalar x theta*temp4*3*22.82	Multiplies THETA by 22.82 (TEMP4)
scalar x p*temp5*3*0.73	Multiplies P by 0.73 (TEMP5)
scalar x temp2*temp6*2*3.57	Subtracts 3.57 from TEMP2 (TEMP6)
overlay x 1*temp6*temp3*temp7	Adds TEMP6 and TEMP3 (TEMP7)
overlay x 1*temp7*temp4*temp8	Adds TEMP7 and TEMP4 (TEMP8)
overlay x 1*temp8*temp5*temp9	Adds TEMP8 and TEMP5 (TEMP9)
transform x temp9*temp10*3	Takes natural antilog of TEMP9 (TEMP10)
scalar x temp10*temp11*1*1	Adds 1 to TEMP10 (TEMP11)
transform x temp11*temp12*1	Takes reciprocal of TEMP11. Calculation of the TS trapped according to the formula is completed at this point (TEMP12).
scalar x temp12*temp13*3*100	Multiplies TEMP12 by 100 to convert range of values from 0-1 to 0-100 (TEMP13).
The following lines describe conversion of trapping efficiencies into delivery ratios:	
scalar x temp13*temp14*3*-1	Multiplies TEMP13 by -1 (TEMP14).
scalar x temp14*temp15*1*100	Adds 100 to TEMP14 (TEMP15).
overlay x 3*temp15*tcmask*tsraw	Final imageTSSRAW is produced via overlay of TEMP15 with TCMASK. The value of 0 is assigned to the cells outside the study area.